

tekstilec

1/2025 • vol. 68 • 1–100

ISSN 0351-3386 (tiskano/printed)

ISSN 2350-3696 (elektronsko/online)

UDK 677 + 687 (05)

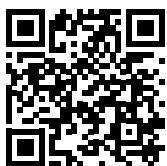


UNIVERZA
V LJUBLJANI

NTF

Naravoslovnotehniška
fakulteta





Časopisni svet/*Publishing Council*
Barbara Simončič, predsednica/*President*
Katja Burger Kovič, Univerza v Ljubljani
Manja Kurečič, Univerza v Mariboru
Tatjana Kreže, Univerza v Mariboru
Gasper Lesjak, Predilnica Litija, d. o. o.
Nataša Peršuh, Univerza v Ljubljani
Petra Prebil Bašin, Gospodarska zbornica Slovenije
Melita Rebič, Odeja, d. o. o.
Tatjana Rijavec, Univerza v Ljubljani
Simona Strnad, Maribor, SI
Helena Zidarič Kožar, Lisca, d. o. o.
Vera Žlabravec, Predilnica Litija, d. o. o.

Glavna in odgovorna urednica/
Editor-in-Chief
Tatjana Rijavec

Namestnica glavne in odgovorne
urednice/*Assistant Editor*
Tatjana Kreže

Področni uredniki/*Associate Editors*
Matejka Bizjak, Katja Burger Kovič, Andrej Demšar, Mateja Kos Koklič, Alenka Pavko Čuden, Andreja Rudolf, Barbara Simončič, Dunja Šajn Gorjanc, Sonja Šterman, Brigita Tomšič

Izvršna urednica za podatkovne baze/
Executive Editor for Databases
Irena Sajovic

Mednarodni uredniški odbor/
International Editorial Board
Matej Bračič, Maribor, SI
Snježana Brnada, Zagreb, HR
Andrea Ehrmann, Bielefeld, DE
Petra Forte Tavčer, Ljubljana, SI
Jelka Geršak, Maribor, SI
Marija Gorjanc, Ljubljana, SI
Lubos Hes, Moka, MU
Aleš Hladnik, Ljubljana, SI
Svetlana Janjič, Banja Luka, BA
Mateja Kert, Ljubljana, SI
Dragana Kopitar, Zagreb, HR
Yordan Kostadinov Kyoshev, Dresden, DE
Petra Komarkova, Liberec, CZ
Mateja Kos Koklič, Ljubljana, SI
Mirjana Kostić, Beograd, RS
Manja Kurečič, Maribor, SI
Boris Mahlrig, Niederrhein, DE
Subhankar Maity, Kanpur, IN
Małgorzata Matusiak, Łódź, PL
Ida Nuramdhani, Bandung, ID
Alenka Ojstršek, Maribor, SI
Roshan Paul, Aachen, DE
Tanja Pušić, Zagreb, HR
Ivana Salopek Čubrić, Zagreb, HR
Snežana Stanković, Beograd, RS
Jovan Stepanović, Leskovac, RS
Dunja Šajn Gorjanc, Ljubljana, SI
Mohammad Tajul Islam, Dhaka, BD
Antoneta Tomljenović, Zagreb, HR

tekstilec (ISSN: 0351-3386 tiskano, 2350-3696 elektronsko) je znanstvena revija, ki podaja temeljne in aplikativne znanstvene informacije v fizikalni, kemijski in tehnološki znanosti, vezani na tekstilno in oblačilno tehnologijo, oblikovanje in trženje tekstilij in oblačil. V prilogah so v slovenskem jeziku objavljeni strokovni članki in prispevki o novostih v tekstilni tehnologiji iz Slovenije in sveta, prispevki s področja oblikovanja tekstilij in oblačil, informacije o raziskovalnih projektih ipd.

tekstilec (ISSN: 0351-3386 printed, 2350-3696 online) the scientific journal gives fundamental and applied scientific information in the physical, chemical and engineering sciences related to the textile and clothing industry, design and marketing. In the appendices written in Slovene language, are published technical and short articles about the textile-technology novelties from Slovenia and the world, articles on textile and clothing design, information about research projects etc.

Dosegljivo na svetovnem spletu/*Available Online at*
<https://journals.uni-lj.si/tekstilec>



Tekstilec je indeksiran v naslednjih bazah/*Tekstilec is indexed in*
Emerging Sources Citation Index – ESCI (by Clarivate Analytics):

Journal Impact Factor (JIF) for 2023 = 0.7

Journal Citation Indicator (JCI) for 2023 = 0.2

Category Quartile for 2023 : Q3

Leiden University's Center for Science & Technology Studies:

Source-Normalized Impact per Paper (SNIP) for 2023 = 0.632

SCOPUS/Elsevier:

Q3, SJR for 2023 = 0.22

Cite Score for 2023 = 1.3

H-Index for 2023 = 15

Ei Compendex

DOAJ

WTI Frankfurt/TEMA® Technology and Management/TOGA® Textile Database

World Textiles/EBSCO Information Services

Textile Technology Complete/EBSCO Information Services

Textile Technology Index/EBSCO Information Services

Chemical Abstracts/ACS

ULRICHWEB – global serials directory

LIBRARY OF THE TECHNICAL UNIVERSITY OF LODZ

dLIB

SICRIS za 2022: 1A3 (Z, A⁺, A1/2); Scopus (d)

tekstilec

Ustanovitelj / Founded by

- Zveza inženirjev in tehnikov tekstilcev Slovenije /
Association of Slovene Textile Engineers and Technicians
- Gospodarska zbornica Slovenije – Združenje za tekstilno,
oblačilno in usnjarsko predelovalno industrijo /
*Chamber of Commerce and Industry of Slovenia – Textiles,
Clothing and Leather Processing Association*

Revijo sofinancirajo / Journal is Financially Supported

- Javna agencija za raziskovalno dejavnost Republike Slovenije /
Slovenian Research Agency
- Univerza v Ljubljani, Naravoslovnotehniška fakulteta /
University of Ljubljana, Faculty of Natural Sciences and Engineering
- Univerza v Mariboru, Fakulteta za strojništvo /
University of Maribor, Faculty for Mechanical Engineering

Sponzor / Sponsor

Predilnica Litija, d. o. o.

Izdajatelj / Publisher

Univerza v Ljubljani, Naravoslovnotehniška fakulteta /
University of Ljubljana, Faculty of Natural Sciences and Engineering

Revija Tekstilec izhaja pod okriljem Založbe Univerze v Ljubljani /
The journal Tekstilec is published by the University of Ljubljana Press

Revija Tekstilec izhaja šestkrat letno
(štirje znanstveni zvezki in dve strokovni prilogi)

*Journal Tekstilec appears six times a year (four
scientific issues and two professional supplements)*

Revija je pri Ministrstvu za kulturo vpisana v
razvid medijev pod številko 583.
Letna naročnina za člane Društev inženirjev in
tehnikov tekstilcev je vključena v članarino.

Letna naročnina za posameznike 38 € za

- študente 22 €
- za mala podjetja 90 € za velika podjetja 180 €
- za tujino 110 €

Cena posamezne številke 10 €

Na podlagi Zakona o davku na dodano vrednost
sodi revija Tekstilec med proizvode, od katerih se
obračunava DDV po stopnji 5 %.

Imetnik računa / *Account holder:*
Univerza v Ljubljani,
Naravoslovnotehniška fakulteta,
Askerceva 12, 1000 Ljubljana, SI-Slovenija

Transakcijski račun / *Bank Account:*
SI56 01100–6030708186, Banka Slovenije,
Slovenska 35, 1000 Ljubljana, SI-Slovenija
SWIFT / *SWIFT Code:* BSLJSI2X

Naslov uredništva / Editorial Office Address:

Uredništvo Tekstilec, Snežniška 5, SI–1000 Ljubljana
Tel. / *Tel.:* + 386 1 200 32 00, +386 1 200 32 24
Faks / *Fax:* + 386 1 200 32 70

E-pošta / *E-mail:* revija.tekstilec@ntf.uni-lj.si
Spletni naslov / *Internet page:* <https://journals.uni-lj.si/tekstilec>

Lektor za slovenščino / *Slovenian Language Editor* Milojka Mansoor
Lektor za angleščino / *English Language Editor*
Glen Champagne, Barbara Luštek Preskar

Oblikovanje platnice / *Design of the Cover* Tanja Nuša Kočevar
Oblikovanje / *Design* ENOOKI Kraft, Mitja Knapič s.p

Tisk / *Printed by* DEMAT d.o.o.

Copyright © 2025 by Univerza v Ljubljani, Naravoslovnotehniška fakulteta,
Oddelek za tekstilstvo, grafiko in oblikovanje

Revija Tekstilec objavlja članke v skladu z načeli odprtega dostopa pod pogoji
licence Creative Commons Attribution 4.0 International License (CC BY 4.0).
Uporabnikom je dovoljeno nekomercialno in komercialno reproduciranje, dis-
tribuiranje, dajanje v najem, javna priobčitev in predelava avtorskega dela, pod
pogojem, da navedejo avtorja izvirnega dela. / *Creative Commons Attribution CC
BY 4.0 licence Journal Tekstilec is published under licence Creative Commons CC
BY 4.0. This license enables reusers to distribute, remix, adapt, and build upon the
material in any medium or format, so long as attribution is given to the creator. The
license allows for commercial use.*



SCIENTIFIC ARTICLES/

Znanstveni članki

- 4 *Petra Forte Tavčer*
Digital Printing Knitted Fabrics made of Polyamide, Cotton and Blends thereof
Digitalni tisk poliamida in mešanic bombaž-poliamid
- 14 *Emilija Zdraveva, Zenun Skenderi, Ivana Salopek Čubrić, Budimir Mijovic*
Effects of Morphology, Structure and Altering Layers on the Composite Heat Resistance of Electrospun PS/PU
Vpliv morfologije, strukture in razporeditve elektropredenih plasti iz PS/PU na toplotni upor kompozitaj
- 31 *Scolastica Manyim, Ambrose K. Kiprop, Josphat I. Mwasiagi, Cleophas M. Achisa M., Mark P. Otero*
Evaluation of Antioxidant, Antibacterial and Fastness Properties of Erythrina abyssinica Extracts on Cotton Fabric Using Biomordants
Vrednotenje antioksidativnih in protibakterijskih lastnosti ter barvnih obstojnosti izvlečkov Erythrina Abyssinica na bombažni tkanini z uporabo biočimž
- 42 *Hafsa Ibrahim, Mumtaz Hasan Malik, Ahmad Fraz, Imran Ahmad Khan*
From Waste to Weave: Recycling Industrial and Consumer Cotton Waste for Sustainable and Cost-Effective Terry Fabric Production
Od odpadkov do tkanja: recikliranje industrijskih in potrošniških bombažnih odpadkov za trajnostno in stroškovno učinkovito proizvodnjo frotirja
- 57 *Sultan Ullah, Arvydas Palevicius, Giedrius Janusas, Zeeshan Ul Hasan*
Impact Properties of Composite Materials: The Significance of Glass Microspheres
Odpornost kompozitnih materialov proti udarcem: pomen steklenih mikrokroglic
- 70 *Sofien Benltoufa, Hind Algamdy*
Breathability and Dynamic Evaporative Cooling Heat Flow of a Ripstop Defence Fabric
Dihalnost in hladilni dinamični izparilni toplotni tok zaščitne tkanine ripstop
- 82 *Brigita Tomšič, Maja Blagojevič, Nuša Klančar, Erik Makoter, Klara Močenik, Nika Pirš, Sebastijan Šmid, Marija Veskova, Marija Gorjanc, Mateja Kert, Barbara Simončič*
Multifunctional Properties of Cotton Fabric Tailored via Green Synthesis of TiO₂/Curcumin Composite
Večfunkcionalne lastnosti bombažne tkanine, pripravljene z zeleno sintezo kompozita TiO₂/kurkuminu

Petra Forte Tavčer

University of Ljubljana, Faculty of Natural Sciences and Engineering, Aškerčeva 12, 1000 Ljubljana

Digital Printing Knitted Fabrics made of Polyamide, Cotton and Blends thereof

Digitalni tisk poliamida in mešanic bombaž-poliamid

Original scientific article/Izvirni znanstveni članek

Received/Prispelo 6–2024 • Accepted/Sprejeto 12–2024

Corresponding author/Korespondenčna avtorica:

Prof. Dr. Petra Forte Tavčer

E-mail: petra.forte@ntf.uni-lj.si

ORCID iD: 0009-0006-3621-9014

Abstract

Knitted fabrics with different compositions, i.e. 100% cotton (CO), 100% polyamide (PA), and a blend of 50% cotton and 50% polyamide (CO/PA), were digitally printed with reactive dyes. The cotton fabric was pretreated with a conventional alkaline solution of alginate thickener, sodium carbonate and urea. The polyamide fabric was pretreated with an acidic solution of galactomannan thickener. The CO/PA blend was pretreated once with the alginate and once with the galactomannan preparation. The aim of the study was to determine whether the proposed preparation is suitable for printing polyamide with reactive dyes and which preparation is more suitable for printing the cotton-polyamide blend. The CIE $L^*a^*b^*$ colour values, the colour depth (K/S) and the dye penetration of the printed samples were compared. It was determined that under the same printing conditions, the highest colour depth was achieved on cotton, while a lower depth was recorded on polyamide. The colour depth on the cotton-polyamide blend was lower than on the two pure fabrics. For some colours, the colour depth was higher with the alginate thickener preparation, for others with the galactomannan thickener, so that no definitive preference for one preparation over the other can be given for printing blends. The colour fastness of the prints to dry rubbing (crock test), light and washing at 40 °C was acceptable for all samples.

Keywords: digital printing, reactive dyes, polyamide, cotton, preparations

Izvilleček

Pletivo z različno surovinsko sestavo: 100-odstotni bombaž (CO), 100-odstotni poliamid (PA) in mešanica 50 % bombaža in 50 % poliamida (CO/PA) je bilo digitalno tiskano z reaktivnimi barvili. Bombažno blago je bilo pred tiskanjem impregnirano s alkalno raztopino alginatnega zgostila, natrijevega karbonata in sečnine. Poliamidno blago je bilo impregnirano s kislno raztopino galaktomananskega zgostila. Mešanica CO/PA je bila impregnirana ali z alginatno ali z galaktomanansko apreturo. Namen raziskave je bil ugotoviti, ali je predlagana apretura primerna za digitalno tiskanje poliamida z reaktivnimi barvili in katera apretura je bolj primerna za tiskanje mešanice iz bombaža in poliamida. Na vzorcih, potiskanih s cian, magenta, rumeno in črno, so bili izmerjeni CIE $L^*a^*b^*$ barvne vrednosti, globina barvnih tonov (K/S) in pretisk barvila na hrbtno stran blaga. Ugotovljeno je bilo, da se pri istih pogojih tiskanja dosežejo najvišje K/S vrednosti na bombažu in nižje na poliamidu. Globina barve na mešanicah je bila nižja kot na obeh čistih pletivih. Za nekatere barve so bile K/S -vrednosti višje ob impregnaciji z alginatnim zgostilom, za nekatere



Content from this work may be used under the terms of the Creative Commons Attribution CC BY 4.0 licence (<https://creativecommons.org/licenses/by/4.0/>). Authors retain ownership of the copyright for their content, but allow anyone to download, reuse, reprint, modify, distribute and/or copy the content as long as the original authors and source are cited. No permission is required from the authors or the publisher. This journal does not charge APCs or submission charges.

z galaktomananskim zgostilom, tako da za nobeno apreturo ne moremo reči, da je primernejša za tiskanje mešanic bombaž/poliamid. Barvne obstojnosti tiskov na suho drgnjenje (crock test), svetlobo in pranje pri 40 °C so bile ustrezne pri vseh vzorcih.

Ključne besede: digitalni tisk, reaktivna barvila, poliamid, bombaž, mešanica, impregnacija

1 Introduction

Digital printing is the latest, but already fully established textile printing technology. Dyes in the form of tiny droplets of dye solutions (ink) are sprayed onto the fabric through numerous micrometre-sized nozzles [1].

Reactive, disperse, acid and pigment dyes in the form of ink are used for digital textile printing. The dyes must match the textile substrate, bond physically and chemically with the fibres, fix sufficiently and have the required fastness properties.

Reactive dyes are a group of dyes with brilliant shades and good fastness properties that chemically bind to textile fibres. They are most commonly used for printing on cellulose fibres and are also suitable for printing on silk, wool and polyamide [2]. They are anionic, as one or more sulphonate groups are bound to the dye molecule (dye-SO₃⁻). Reactive dyes can bind to the hydroxyl groups of cellulose via the reactive system and form covalent bonds under alkaline conditions, usually through nucleophilic bimolecular substitution or nucleophilic addition mechanisms [3]. Reactive dyes also react with water molecules, a process known as hydrolysis. The hydrolysed dye is no longer reactive and can no longer chemically bond with the fibres. It must be removed from the fabric in subsequent treatments [1].

Polyamides contain an amide functional group (–CO–NH–) in their backbone. The polyamide chain ends on one side with an amino group (–NH₂) and on the other side with a carboxyl group (–COOH). The amino end group is basic and can be protonated to an ammonium ion (–NH₃⁺) under acidic conditions. The carboxyl end group is acidic and can release a proton under basic conditions to form a carboxylate ion (–COO⁻). Reactive dyes can bind

covalently to the amino group of polyamide fibres (–NH₂). Under acidic conditions, the protonation of the amino groups in the polyamide increases the affinity of the anionic dyes to the polyamide. At high pH values, the polyamide is anionic and essentially no fixation occurs due to electrostatic repulsion between the strongly anionic dye and the anionic fibre, although the concentration of –NH₂ groups, the active nucleophilic species that react with the electrophilic groups of the dye, is high. The pH value is one of the key parameters influencing the degree of exhaustion and thus the final fixation of reactive dyes to polyamide [2]. The optimum pH value for good prints has determined to be 4–5 [2–6].

The textile material to be printed must be prepared accordingly before printing, and the dye must be fixed, washed and dried after printing. Absorption and capillary forces in the fibres cause spreading and deteriorate the contour quality. Therefore, the fabric must be impregnated with a thickening agent and suitable fixing agents before printing. The composition of the impregnating bath and the steaming time have a significant impact on the adsorption and fixation of reactive dye on both materials, cotton [7, 8] and polyamide [9].

For printing on cotton, low-viscosity alginate thickeners in low concentrations are used, in which auxiliaries, oxidizing agents and alkalis are dissolved [10, 11]. Various pretreatments have been investigated for polyamide: impregnation with hydroxypropyl methylcellulose [10], impregnation with sodium alginate with alpha-olefin sulfonate [12], O₂ plasma treatment [13] and non-thermal plasma in combination with sublimation printing [14]. Several authors suggested low-viscosity polygalactomannan ethers as thickening agents for polyamide printing [3, 6, 15].

After printing and drying, the dyes are fixed on

the textile. During fixation, the dyes diffuse from the thickening film into the interior of the fibre and bind there. The most common fixation process is one-step normal steaming at 100–103 °C.

Fixation is followed by post-treatments that give the prints their final appearance and improve wet fastness, handle and rub fastness. Non-fixed dyes, thickeners and chemical additives must be removed. Generally, the prints are first washed with cold water and then with hotter wash baths, sometimes with the addition of dispersion soap [1].

The aim of this study was to investigate whether polyamide and blends thereof can be successfully printed digitally with reactive dyes, and which preparation is best suited for this purpose. Four

basic colours were printed on fabrics made of cotton, polyamide and a blend of cotton and polyamide. The CIE $L^*a^*b^*$ colour values, the colour depth (K/S) and the dye penetration (P) were compared on different materials printed under the same conditions. The colour fastness of the prints to rubbing (crock test), light and washing was measured.

2 Experimental

2.1 Materials

Knitted fabrics from the manufacturer Inplet Pletiva d.o.o., Slovenia, were used. Fabric data are presented in Table 1.

Table 1: Knitted fabric data

Material	Label	Horizontal density (stiches/cm)	Vertical density (course/cm)	Mass per unit area (g/m ²)
100% cotton	CO	18	24	149.1
50% cotton/50% polyamide	CO/PA	15	17	217.6
100% polyamide	PA	13	18	100.8

2.2 Preparation of textiles for printing

The fabrics were pretreated with an alginate thickening preparation (A) or a galactomannan thickening preparation (GM). The recipes are presented in Tables 2 and 3.

The following chemicals were used: CHT alginate EHV (Bezema, Switzerland), alginate thickener; Prisulon DCA 130 (Bezema, Switzerland), polygalactomannan ether; sodium hydrogen carbonate (NaHCO_3) (Kemika, Zagreb, Croatia); urea ($\text{CO}(\text{NH}_2)_2$) (J.T. Baker, Netherlands), hydrotropic agent, Rapidoprint XR (Bezema, Switzerland), sodium m-nitrobenzenesulfonate, oxidising agent; and citric acid ($\text{C}_6\text{H}_8\text{O}_7$) (Kemika, Zagreb, Croatia).

The fabrics were impregnated using a laboratory two-roller padder (Mathis, Switzerland) with an impregnation effect of 88%. The alginate thickening preparation was applied to cotton and cotton-polyamide blended fabrics. The galactomannan thickening preparation was applied to polyamide and

cotton-polyamide blended fabrics. The impregnated samples were air dried at room temperature.

Table 2: Recipe for the preparation of the alginate thickener

Additive	Amount (g)
CHT-alginat EHV 4%	400
Distilled H_2O	525
NaHCO_3	15
$\text{CO}(\text{NH}_2)_2$	50
Rapidoprint XR	10
Total	1000

Table 3: Recipe for the preparation of galactomannan thickener

Additive	Amount (g)
Prisulon DCA 130. 8%	910
Citric Acid 0.2%	90
Total	1000

2.3 Printing, fixation and after-treatment

Printing was performed using a digital piezo DOD printer TextileJet Tx2-1600 from Mimaki with a resolution of 720 dpi and reactive dyes Jettex R (DyStar, England). The patterns were pre-processed as squares in Adobe Photoshop. 100% cyan, 100% yellow, 100% magenta and 100% black were printed.

The printed fabrics were fixed in a laboratory steamer DHE 20675 (Werner Mathis AG, Switzerland) in 90% saturated steam at 102 °C. Cotton was steamed for 10 minutes and polyamide for 20 minutes, while the blends were steamed depending on the preparation: 10 minutes for the alginate preparation and 20 minutes for the galactomannan preparation.

After fixation, the fabric was first rinsed with cold water to remove residual thickeners, chemicals and some unfixed dyes, then with warm water and finally with hot water. The next step was soaping for five minutes at 100 °C with 1 g/l CIBAPON R detergent (CIBA, Switzerland) to remove all remaining dye residues. After soaping, the samples were rinsed with warm and cold water and air-dried at room temperature.

2.4 Analyses

The colour coordinates CIE $L^*a^*b^*$ and the reflectance R (%) of the printed samples were measured using a SF 600 PLUS-CT spectrophotometer (Datacolor International, Switzerland). Ten measurements were taken for each colour on each print. The measurements were taken on the front and back of the printed fabric. The measurement conditions were: standard light D65, standard observer 10°, device geometry d/8°, measuring range 400–700 nm, four fabric layers and a measuring aperture of 20 mm.

The colour difference (ΔE^*) was calculated from the CIE colour coordinates $L^*a^*b^*$ according to equation 1 [16]:

$$\Delta E_{ab}^* = \sqrt{(\Delta L^*)^2 + (\Delta a^*)^2 + (\Delta b^*)^2} \quad (1)$$

where ΔL^* represents the difference in lightness, Δa^* represents the difference on the red-green axis

and Δb^* represents the difference on the yellow-blue axis.

The colour depth values (K/S) of the prints were calculated from the reflectance measurements using equation 2 [16]:

$$\frac{K}{S} = \frac{(1-R)^2}{2R} \quad (2)$$

where K represents the absorption coefficient (depending on the dye concentration), S represents the scattering coefficient and R represents the reflectance of the sample at a specific wavelength ($R = 0 - 1$).

The penetration coefficient, P , indicates the amount of dye that has reached the back of the fabric. It was calculated according to equation 3 [1]:

$$P = \frac{K/S_{(back)}}{(0.5 \times [K/S_{(front)} + K/S_{(back)}])} \times 100 (\%) \quad (3)$$

where $K/S_{(front)}$ represents the colour depth on the front side of the sample and $K/S_{(back)}$ represents the colour depth on the back side of the sample.

Rub fastness was determined according to the standard SIST EN ISO 105-X12:2002 – Colour fastness to rubbing. Rubbing was carried out using a Crockmeter (Electronic Crockmeter; SDL Atlas, USA).

Light fastness was determined according to the standard SIST EN ISO 105-B02:2014 – Colour fastness to artificial light: Xenon arc lamp test on a Xenotest Alpha (Atlas, USA).

Colour fastness to washing was determined according to the standard ISO 105-C01:1989 – Textiles – Colour fastness tests – Part C01: Colour fastness to washing: Test 1. Depending on the raw material composition of the sample, one accompanying fabric was made of cotton and another of polyamide. The 10 x 4 cm samples were washed with the accompanying fabrics in a Launder-ometer LDH-HT B-S (Atlas Electric Devices, USA).

3 Results and discussion

Table 4 presents the results of the CIE $L^*a^*b^*$ colour values of CMYK prints on cotton, polyamide and cotton-polyamide blended fabrics impregnated with different preparations. For all colours except magenta, the CIE L^* value is lowest on cotton, indicating

that prints on cotton are darker than on polyamide and cotton-polyamide blended fabrics, regardless of the preparation used. The calculated colour differences, ΔE^* , show that the colours printed on various materials differ significantly. The differences are smallest for magenta, but even here they are greater than 1 and therefore visible to the naked eye.

Table 4: CIE $L^*a^*b^*$ values on cotton (CO), polyamide (PA) and blended fabrics (CO/PA) impregnated with alginate (A) or galactomannan (GM) as thickener, and colour differences (ΔE^*) between prints on CO and other materials

Colour	Material	L^*	a^*	b^*	ΔE^*
C	CO	53.14	-30.31	-28.11	-
	CO/PA (A)	69.10	-11.41	-26.97	24.76
	PA	69.61	-13.56	-26.64	23.54
	CO/PA (GM)	75.05	-10.68	-24.82	29.60
M	CO	53.37	54.58	-3.05	-
	CO/PA (A)	53.49	58.73	-10.66	8.67
	PA	51.63	58.55	-6.92	5.81
	CO/PA (GM)	57.22	56.23	-11.99	9.87
Y	CO	79.07	5.77	87.53	-
	CO/PA (A)	86.52	-1.26	43.65	45.06
	PA	85.93	-3.78	75.52	16.81
	CO/PA (GM)	87.89	-8.25	70.19	23.98
K	CO	18.95	-2.14	-0.01	-
	CO/PA (A)	45.88	16.80	-1.63	32.96
	PA	33.02	23.25	4.56	29.39
	CO/PA (GM)	33.60	24.78	6.24	31.28

Figure 1 shows the spectra of the K/S values as a function of the wavelength (360 nm to 700 nm). The colour depth (K/S) is highest for cyan, yellow and black on CO, which again indicates that prints on CO are darker than prints on PA and blends, regardless of the preparation used. The K/S values are similar for all fabrics for magenta.

CO/PA blends have lower K/S values than CO and PA, regardless of the preparation used. The differences in the K/S values between the blends are small, so that the current measurements cannot confirm the superiority of one preparation over another. From this it can be deduced that the dye binds to CO and not to PA in the alkaline preparation

with alginate thickener. Conversely, the dye binds to PA and not to CO in the acidic preparation with galactomannan thickener. The blends are therefore printed in lighter shades.

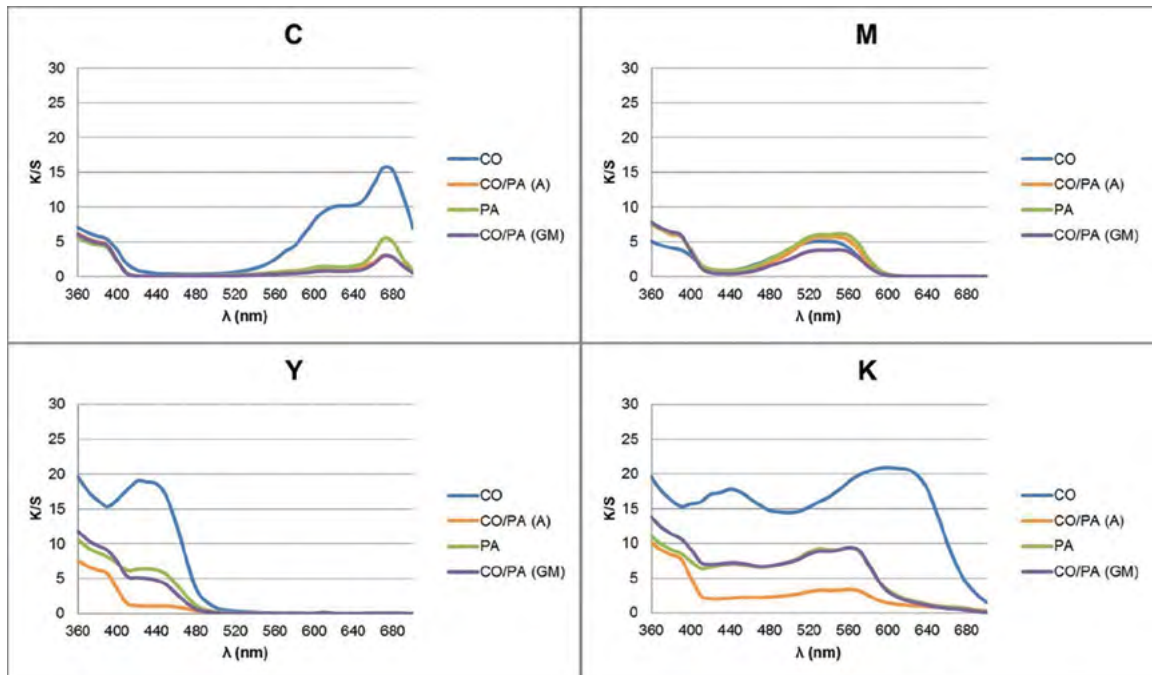


Figure 1: K/S values of CMYK prints on cotton (CO), polyamide (PA) and blended fabrics (CO/PA) impregnated with alginate (A) or galactomannan (GM) as a thickening agent

Figure 2 shows the degree of penetration of the CMYK colours. The lowest penetration can be seen with CO. PA has a higher penetration than CO, which means that the dye solution migrates more to the back of the fabric. This can be explained by the fact that polyamide fibres are hydrophobic and absorb much less water than cellulose fibres, which leads to slower dye diffusion into the fibres and more difficult access to the available amino groups.

The highest penetration is observed with blends, especially with CO/PA(A). The high penetration is one reason for the low K/S values on the front side of the fabric. Dye that is transferred to the back of the fabric and binds there is less visible, resulting in a lower colour depth. Comparing the effects of preparation, the prints on CO/PA (A) generally have higher penetration than on CO/PA (GM).

Table 5 presents the colour fastness values of the prints for dry and wet rubbing according to the grey scale. The results show that all prints have good fastness to dry rubbing, with very high values of 4–5.

The values for wet rubbing vary. The highest wet rubbing fastness is achieved for PA (grade 4) with

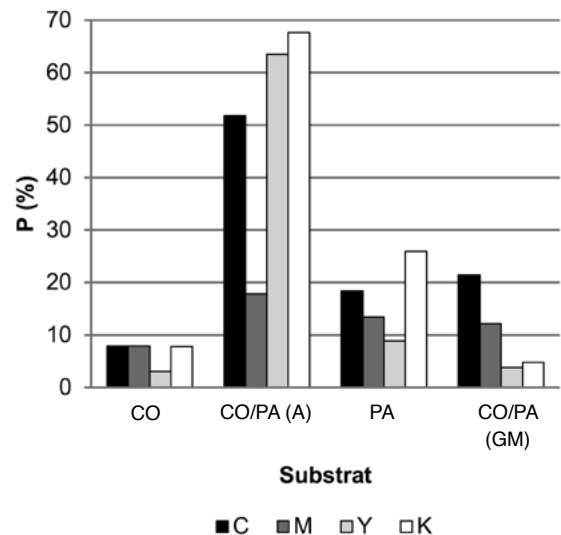


Figure 2: Penetration degree (P) of CMYK prints on cotton (CO), polyamide (PA) and blended fabrics impregnated with alginate (CO/PA(A)) or galactomannan (CO/PA(GM)) as a thickening agent

cyan, magenta and black, and for the blend CO/PA (GM) with magenta and black. The values are lower for CO and CO/PA (A), with the lowest rub fastness being achieved for CO with cyan (score 1), and for

the CO/PA (A) blend with cyan, yellow and black. This can be explained by the fact that the absorption of the dyes by the cotton is higher than their fixation. Cotton also absorbs hydrolysed dye, which cannot react with the fibres. Hydrolysed dye that was not removed in final rinsing steps becomes visible during wet rubbing. PA, as a less absorbent material, absorbs less hydrolysed dye, and this can also be removed more easily during rinsing. The wet rubbing results are therefore better for PA.

As the highest wet rubbing fastness applies to PA, this is also the case with the CO/PA (GM) blend, as the dyes in this case are predominantly bound to PA and not to CO.

Table 5: Colour fastness values to rubbing on cotton (CO), polyamide (PA) and blended fabrics (CO/PA) impregnated with alginate (A) or galactomannan (GM) as thickening agents

Colour	Material	Dry rubbing	Wet rubbing
C	CO	4	1
	CO/PA (A)	4	1
	PA	5	4
	CO/PA (GM)	5	3
M	CO	5	2
	CO/PA (A)	5	2
	PA	5	4
	CO/PA (GM)	4	4
Y	CO	5	2
	CO/PA (A)	4	1
	PA	4	3
	CO/PA (GM)	4	3
K	CO	4	3
	CO/PA (A)	5	1
	PA	4	4
	CO/PA (GM)	4	4

Table 6 presents the colour fastness values of the samples to light. From this it can be concluded that light fastness depends primarily on the dye and less on the fabric on which they are printed. Regardless of the fabric, the highest light fastness is for yellow, lower for magenta and black, and the lowest for

cyan. Within the individual dyes, the values are better for CO and PA, and worse for blends, regardless of the preparation used. The reason for this is that less dye is bound in blends, so that the dyes are more accessible to light and the discoloration is therefore more visible. The highest rating is 7 for yellow on PA, while the lowest is 1 for cyan on the blend CO/PA (GM).

Table 6: Light fastness values of samples on cotton (CO), polyamide (PA) and blended fabrics (CO/PA) impregnated with alginate (A) or galactomannan (GM) as thickening agent

Colour	Material	Light fastness
C	CO	5
	CO/PA (A)	2
	PA	2
	CO/PA (GM)	1
M	CO	2
	CO/PA (A)	3
	PA	4
	CO/PA (GM)	3
Y	CO	6
	CO/PA (A)	3
	PA	7
	CO/PA (GM)	4
K	CO	4
	CO/PA (A)	2
	PA	3
	CO/PA (GM)	2

Table 7 shows the colour fastness values of the prints when washed at 40 °C. The 100% CO and 100% PA fabrics recorded the best values for colour change, although they are not excellent, which means that some of the dye (hydrolysed dye) is removed during washing. The values are lower for blended fabrics. The reason for this is the same as for light fastness. Less dye is bound on blended fabrics than on CO and PA fabrics, so the reduction in the amount of dye on the fibres due to washing is more visible.

The ratings for dye transfer to cotton and polyamide adjacent fabric are similar for all dyes and

fabrics. The ratings range from 3 to 4–5. Staining on the adjacent fabrics is relatively low, indicating that the washed-out dye does not stain the adjacent fabrics.

Table 7: Wash fastness values at 40 °C of cotton (CO), polyamide (PA) and blended fabrics (CO/PA) impregnated with alginate (A) or galactomannan (GM) as a thickening agent

Colour	Material	Washing fastness		
		Colour change	Staining of CO	Staining of PA
C	CO	4–5	4	4–5
	CO/PA (A)	2	3–4	4
	PA	4	3–4	4
	CO/PA (GM)	3	4	4
M	CO	3–4	4–5	3–4
	CO/PA (A)	3	4	3
	PA	4	3–4	4
	CO/PA (GM)	2	4	4
Y	CO	3–4	4–5	4
	CO/PA (A)	2	4	3–4
	PA	4	3–4	4–5
	CO/PA (GM)	2–3	4	3–4
K	CO	4	4	4
	CO/PA (A)	2–3	3–4	4
	PA	4–5	3	4
	CO/PA (GM)	4–5	4	3

4 Conclusion

The colour depth of prints is highest on cotton, lowest on polyamide and even lower on blended fabrics for all colours. The lightness values (CIE L*) are consequently lowest for cotton, slightly higher for polyamide and highest for blended fabrics. Visually, the colours appear intense and bright on cotton and polyamide, while they are significantly lighter and less intense on blended fabrics.

Reactive dyes adhere well to cotton with the alkaline alginate preparation (pH 9) and to polyamide with the acidic galactomannan preparation (pH 5.5). Good colour values were achieved in both cases. In blends, the colours are lighter and the colour values lower because the pH value of the preparation is only suitable for one component in the blend. In the alkaline alginate preparation, the reactive dye binds well to cotton but poorly to polyamide. In the acidic

galactomannan preparation, the dye binds well to polyamide but poorly to cotton. This means that one component of the blend is dyed poorly or not at all.

The degree of dye penetration also influences the K/S values. If the dye is transferred to the back side of the fabric, it is not visible on the front side. In our cases, polyamide is more hydrophobic and therefore absorbs less dye than cotton, so more dye is transferred to the back and penetration is high. In blends, one component is polyamide, which transfers the dye to the back, while the other component does not bind the dye due to the unsuitable pH value. The penetration is therefore even higher. The highest percentage of dye on the back of the fabric, is found for all colours on the cotton/polyamide blend impregnated with alginate thickener, and the lowest on the 100% cotton fabric.

All prints exhibit good fastness to dry rubbing, while the fastness values to wet rubbing are moderate. The best fastnesses to wet rubbing value were

recorded on polyamide and the cotton-polyamide blend impregnated with galactomannan thickener, as these fabrics absorb less hydrolysed dye. Light fastness is best for 100% cotton and 100% polyamide and worse for blends, regardless of the preparation used. Wash fastness is good for 100% cotton and 100% polyamide and worse for blends, regardless of the preparation used.

In summary, polyamide fabrics impregnated with acidic galactomannan thickener can be successfully printed digitally with reactive dyes, although the colour tones achieved are slightly lower than those obtained with cotton fabrics impregnated with alkaline alginate thickener. The light fastness, wash fastness and fastness to rubbing are acceptable. Cotton/polyamide blends can also be digitally printed with reactive dyes, although the colour tones are even lower than those of polyamide and cotton and the fastness properties are poorer. The superiority of the alkaline alginate preparation or the acidic galactomannan preparation cannot be confirmed on the basis of the current measurements. The results are similar for both. Lower K/S values are related to less favourable pH conditions for the binding of the dye to one component of the blend and a high penetration of the dye to the back of the fabric.

This research was funded by the Slovenian Research and Innovation Agency (Program P2-0213; Infra-structural Centre RIC UL-NTF).

References

1. UJIIE, H. *Digital Printing of Textiles*. Cambridge : Woodhead Publishing, 2006.
2. SOLEIMANI-GORGANI, A., TAYLOR, J.A. Dyeing of nylon with reactive dyes. Part 1. The effect of changes in dye structure on the dyeing of nylon with reactive dyes. *Dyes and Pigments*, 2006, **68**(2–3), 109–117, doi: 10.1016/j.dyepig.2005.01.014.
3. ŠOSTAR, S., SCHNEIDER, R. Guar gum as an environment-friendly alternative thickener in printing with reactive dyes. *Dyes and Pigments*, 1998, **39**(4), 211–221, doi: 10.1016/S0143-7208(97)00111-3.
4. SOLEIMANI-GORGANI, A., TAYLOR, J.A. Dyeing of nylon with reactive dyes. Part 2. The effect of changes in level of dye sulphonation on the dyeing of nylon with reactive dyes. *Dyes and Pigments*, 2006, **68**(2–3), 119–127, doi: 10.1016/j.dyepig.2005.01.012.
5. BURKINSHAW, S.M., CHEVLI, S.N., MARFELL, D.J. Printing of nylon 6,6 with reactive dyes part 1: preliminary studies. *Dyes and Pigments*, 2000, **45**(3), 235–242, doi: 10.1016/S0143-7208(00)00022-X.
6. SHEN-KUNG, L., HUO-YUAN, C. Ink-jet printing of nylon fabric using reactive dyestuff. *Coloration Technology*, 2011, **127**(6), 390–395, doi: 10.1111/j.1478-4408.2011.00335.x.
7. YUEN, C.W.M., KU, S.K.A., CHOI, P.S.R., KAN, C.W. Factors affecting the color yield of an ink-jet printed cotton fabric. *Textile Research Journal*, 2005, **75**(4), 319–325, doi: 10.1177/0040517505054733.
8. YANG, Y., NAARANI, V. Effect of steaming conditions on colour and consistency of ink-jet printed cotton using reactive dyes. *Coloration Technology*, 2004, **120**(3), 127–131, doi: 10.1111/j.1478-4408.2004.tb00218.x.
9. LIAO, S.K., CHEN, H.Y. Ink-jet printing of nylon fabric using reactive dyestuff. *Coloration Technology*, 2011, **127**(6), 390–395, doi: 10.1111/j.1478-4408.2011.00335.x.
10. QIAO, X., FANG, K., LIU, X., GONG, J., ZHANG, S., WANG, J., ZHANG, M. Different influences of hydroxypropyl methyl cellulose pretreatment on surface properties of cotton and polyamide in inkjet printing. *Progress in Organic Coatings*, 2022, **165**, 1–9, doi: 10.1016/j.porgcoat.2022.106746.

11. ESER, B., ÖZGÜNEY, A.T., ÖZERDEM, A.
Investigation of the usage of different thickening agents in ink-jet printing with reactive dyes. *Industria Textila*, 2012, **63**(2), 85–90.
12. LI, C., FANG, L., FANG, K., LIU, X., AN, F., LIANG, Y., LIU, H., ZHANG, S., QIAO, X.
Synergistic effects of alpha olefin sulfonate and sodium alginate on inkjet printing of cotton/polyamide fabrics. *Langmuir*, 2021, **37**(2), 683–692, doi: 10.1021/acs.langmuir.0c02723.
13. HOSSAIN, M.A., CHEN, W., ZHENG, J., ZHANG, Y., WANG, C., JIN, S., WU, H.
The effect of O₂ plasma treatment and PA 6 coating on digital ink-jet printing of PET nonwoven fabric. *The Journal of The Textile Institute*, 2020, **111**(8), 1184–1190, doi: 10.1080/00405000.2019.1688902
14. SILVA, M.C., PETRACONI, G., CECCI, R.R.R., PASSOS, A.A., DO VALLE, W.F., BRAITE, B., LOURENÇO, S.R., GASI, F. Digital sublimation printing on knitted polyamide 6.6 fabric treated with non-thermal plasma. *Polymers*, 2021, **13**(12), 1–15, doi: 10.3390/polym13121969
15. MARIE, M.M., SALEM, A.A., EL ZAIRY, E.M.R.
A novel printing method to enhance the fixation of reactive dyes on wool–polyamide fabrics. *The Journal of The Textile Institute*, 2011, **102**(9), 790–800, doi: 10.1080/00405000.2010.522049.
16. BERGER-SCHUNN, A. *Practical Color Measurement : a Primer for the Beginner, A Reminder for the Expert*. New York : Wiley-Interscience, 1994, p. 179.

Emilija Zdraveva,¹ Zenun Skenderi,² Ivana Salopek Čubrić,² Budimir Mijovic¹

¹ University of Zagreb Faculty of Textile Technology, Department of Fundamental Natural and Engineering Sciences, Prilaz b. Filipovića 28a, Zagreb, Croatia

² University of Zagreb Faculty of Textile Technology, Department of Textile Design and Management, Prilaz b. Filipovića 28a, Zagreb, Croatia

Effects of Morphology, Structure and Altering Layers on the Composite Heat Resistance of Electrospun PS/PU

Vpliv morfologije, strukture in razporeditve elektropredenih plasti iz PS/PU na toplotni upor kompozita

Original scientific article/Izvirni znanstveni članek

Received/Prispelo 7–2024 • Accepted/Sprejeto 12–2024

Corresponding author/Korespondenčna avtorica:

Assist. Prof. Emilija Zdraveva, PhD

Tel: +38513712557

E-mail: emilija.zdraveva@ttf.unizg.hr

ORCID iD: 0000-0003-2845-8630

Abstract

Thermal insulating materials are of paramount importance in many application areas, including building construction, electronics, aerospace engineering, the automobile industry and the clothing industry. Electrospun materials are light weight with a well-controlled fibre diameter/morphology and a highly interconnected porous structure that facilitates the trapping of air and breathability. When combined with other conventional materials, they enhance the thermal insulating property of a composite structure. This study focused on electrospun single polyurethane (PU), polystyrene (PS) and layered composites thereof, in terms of heat resistance and its dependence on fibre diameter, pore area, number, thickness (solution volume) and the position of electrospun layers. It thus contributes to the field by addressing the effects of multiple parameters effect on a composite material's heat resistance. The fibre diameter for both electrospun polymers increased significantly by increasing the concentration, while there was a generally opposite effect from increasing electrical voltage. The 10 wt% PU and 30 wt% PS used to produce the layered composites demonstrated the highest reduction of the fibre mean diameter, from (443 ± 224) nm to (328 ± 148) nm, and from (2711 ± 307) nm to (2098 ± 290) nm, respectively. Thicker PS fibres resulted in the greatest mean pore areas of $(13 \pm 9) \mu\text{m}^2$, while the PU mean pore areas were in the range of $(2 \pm 1) \mu\text{m}^2$ to $(4 \pm 2) \mu\text{m}^2$. Although all single and PS/PU composites demonstrated a porosity greater than 97%, their configuration in terms of number of layers, total thickness and PS and PU positioning (includes fibre diameter and pore area) affected the measured heat resistance. Single electrospun PS demonstrated a reduction in heat resistance of $0.0219 \text{ m}^2\text{K/W}$ (compared to electrospun PU) due to its thicker fibres and larger pore areas, and thus looser structure. Combining the two electrospun layers improved heat resistance up to $0.0341 \text{ m}^2\text{K/W}$. The total heat resistance of the layered PU/PS composite was increased (up to $0.1063 \text{ m}^2\text{K/W}$ for the electrospun PS/PS/PU/PU) by increasing the number and volume of each electrospun layer solution, and by spinning the PU layer on top of the system, which resisted the heat flow due to its smaller pore areas and



Content from this work may be used under the terms of the Creative Commons Attribution CC BY 4.0 licence (<https://creativecommons.org/licenses/by/4.0/>). Authors retain ownership of the copyright for their content, but allow anyone to download, reuse, reprint, modify, distribute and/or copy the content as long as the original authors and source are cited. No permission is required from the authors or the publisher. This journal does not charge APCs or submission charges.

compact structure. These results prove that by optimizing process/structure parameters, a multi-layered material with good thermal performance can be designed to meet the requirements of a thermal insulating product. Keywords: polyurethane, polystyrene, fibre diameter, pore area, thermal resistance

Izvilleček

Toplotnoizolacijski materiali so izjemno pomembni na številnih področjih uporabe, vključno z gradbeništvom, elektroniko, vesoljskim inženiringom, avtomobilsko in oblačilno industrijo. Elektropredeni materiali so lahki, iz vlaken enakomerne debeline/morfologije in visoke medsebojne povezanosti v porozno strukturo, ki zagotavlja zadrževanje zraka in dihalnost. S kombiniranjem elektropredenih s klasičnimi materiali v kompozitne strukture se izboljša toplotna izolativnost. V raziskavi sta proučevana vpliv premera vlaken in površine por na toplotni upor enoplastnih poliuretanskih (PU) in polistirenskih (PS) elektropredenih materialov in vpliv števila, debeline (volumna raztopine) in položaja elektropredenih plasti v večplastnih kompozitnih strukturah, saj vsi omenjeni parametri vplivajo na toplotni upor kompozitnega materiala. Pri obeh elektropredenih polimernih materialih se je debelina vlaken znatno povečala z naraščajočo koncentracijo predilne raztopine, pri čemer je zviševanje električne napetosti na splošno vplivalo na zmanjševanje debeline vlaken. Pri večplastnih kompozitnih materialih, izdelanih z uporabo raztopin 10 ut.% PU in 30 ut.% PS, je bilo z naraščajočo električno napetostjo zmanjšanje povprečne debeline vlaken najbolj izrazito, s (443 ± 224) nm na (328 ± 148) nm in z (2711 ± 307) nm na (2098 ± 290) nm. Materiali iz najdebelejših vlaken iz PS so imeli največje povprečne površine por $(13 \pm 9) \mu\text{m}^2$, medtem ko so bile povprečne površine por materialov iz PU v razponu od $(2 \pm 1) \mu\text{m}^2$ do $(4 \pm 2) \mu\text{m}^2$. Čeprav so vsi enoplastni in večplastni PS/PU-kompoziti dosegli več kot 97-odstotno poroznost, pa je njihova konfiguracija – število plasti, skupna debelina in položaj PS in PU (vključuje premer vlaken in površino por) – vplivala na izmerjeni toplotni upor. V primerjavi z elektropredenim PU je enoplastni elektropredeni PS material zaradi debelejših vlaken in večje površine por dosegel za $0,0219 \text{ m}^2\text{K/W}$ nižji toplotni upor, imel je bolj zrahljano strukturo. Kombinacija dveh elektropredenih plasti je izboljšala toplotni upor do $0,0341 \text{ m}^2\text{K/W}$. Skupni toplotni upor večplastnega PU/PS-kompozita se je povečal – na $0,1063 \text{ m}^2\text{K/W}$ za elektropredeni PS/PS/PU/PU – s povečanjem števila plasti in uporabljenega volumna predilnih raztopin ter s PU-plastjo na zunanji strani kompozita, ki je zaradi manjše površine por in kompaktnejše strukture imela višji toplotni upor. Ti rezultati dokazujejo, da je mogoče z optimizacijo procesnih in strukturnih parametrov oblikovati večplastni kompozitni material z lastnostmi, ki ustrezajo zahtevam toplotnoizolacijskega izdelka.

Ključne besede: poliuretan, polistiren, premer vlakna, površina pore, toplotni upor

1 Introduction

Thermal insulation is extremely important in many applications that require a balance of temperature or protection against temperature fluctuations. There are many natural materials (e.g. wool, fur, feathers, wood fibres, expanded cork, cotton, flex, hemp and reed), [1–3] that are good thermal insulators with a high heat resistance used in the areas of building construction [4], electronics, aerospace engineering, the automobile industry [5] and the clothing industry [6]. Besides natural, frequently used artificial

insulating materials include asbestos, rock wool, fibre-glass, expanded clay, perlite and plastic foams (i.e. polystyrene, polyurethane, polyester) [7]. Today, advanced materials and the associated technologies have become a prerequisite in the development of thermally insulating materials that will fulfil the requirements of a modern product. These include low thermal conductivity, chemical and physical stability at high operating temperatures, mechanical integrity, non-toxicity and more, specifically, fire, water and pest resistance, lightweight, porous structure, durability, cost-effectiveness and sustainability. High-per-

formance materials for thermal insulation do not necessarily mean the use of manmade materials, such as plastics or composites thereof (i.e. with organic or inorganic based additives), but also natural-based materials from renewable resources, such as by-products or waste (e.g. seagrass, palm fibres, cornstalks and rice husks) from agriculture or other industries [3]. Recent advanced technologies that have emerged as promising in this field include 3D printing [8] and various nanostructure fabrication techniques (e.g. electrospinning) [9]. The 3D printing technique offers versatility in material composition (e.g. polymers, ceramics and metals), flexibility in design, and custom shaping with complex cellular geometries and dimensions [10]. The technique of electrospinning facilitates the fabrication of lightweight nanofibrous materials with a large surface area, high porosity and interconnected pores with the ability to entrap a large quantity of air in between as an extremely important property in thermal performance. The process utilizes electrostatic forces that stretch a viscoelastic polymer solution to form ultrathin fibres that are solidified as the jet reaches a collector after organic solvent evaporation [11]. Fibre diameter, morphology and the pore sizes of electrospun materials are very well-controlled through the adjustment of a polymer solution's properties, processing parameters and ambient conditions. The crucial parameter that affects fibre uniformity is the polymer solution concentration, which is directly related to its viscosity, while higher solution viscosity results in thicker fibres [12]. Increasing a solution's concentration prevents partial jet break up due to higher viscoelastic force, as well as increased polymer chain entanglement, that results in the formation of smooth, uniform fibres [13]. The most dominant processing parameter that affects fibre diameter and morphology is electrical voltage. Generally, increasing electrical voltage reduces fibre diameter due to an increase in the stretching force. Opposite observations have also been reported, as well as no significant changes in fibre diameter [14–16]. Among the many application areas that are well-known for these materials (e.g. biomedicine, electronics, energy

storage and conversion, environmental protection, chemistry and functional textiles [11]), the field of thermal insulation is explored to a lesser extent. The advantages of electrospun materials over conventional materials include their light weight, the ability to control fibre diameter/morphology, and their highly porous structure, which facilitates the trapping of air and breathability. These materials perform better in terms of heat resistance when combined with other conventional materials, i.e. in a composite structure. Some of the first reported studies concern a comparison of electrospun polyacrylonitrile (PAN) thermal performance to commercially available insulation materials, such as waterfowl down and wool, high-loft polyester (artificial down, Primaloft), meltblown pitch carbon fibre and silica aerogel-impregnated flexible fibrous insulation. The authors concluded that electrospun PAN may be used in hybrid battings, meaning nanofibers can be incorporated into existing insulating materials to improve thermal insulation, while microfibers are needed for durability and compression recovery [9]. Major factors influencing thermal insulation efficiency also include fibre diameter, added particles and structures density in a thermal insulating composite. Single nozzle and co-axial electrospinning were performed for the fabrication of PAN/silica aerogel laminated composites, where the latter showed a reduction in thermal conductivity by 12.5%. When a spacer layer of hollow glass microspheres were inserted in the composite structure, insulation improved by 20% [17]. More complex electrospun structures were prepared using modified twisting yarn electrospinning. Continuous hollow yarns with phase changeability were fabricated from hydroxypropyl cellulose-based mixed esters and poly (m-phenylene isophthalamide) (HPCMEs/PMIA). The yarns demonstrated a heat storage capacity of 20–30 kJ/kg and an air coupling ability, and can thus be used in thermal regulation and thermal insulation applications [18]. Polystyrene (PS) and polyurethane (PU) are frequently used polymers in the building insulation market, as they are low in cost and have low thermal conductivities due to

their foam microstructures [19]. Improved super-insulating materials (with greatly reduced thermal conductivity) are usually obtained when the same are combined with nanofillers in a composite system [20].

To best of our knowledge, few studies address the heat resistance properties of electrospun materials and the measurement thereof using a sweating guarded hot plate. In fact, we report here on only one study (found in available literature) where a sweating hotplate device was used to measure the heat resistance of multi-jet electrospun polystyrene/polyamide 6 (PS/PA 6). The material demonstrated lowered thermal resistance due to the higher thermal conductivity and lowered air content of the compact PA 6. When electrospun in a higher humidity environment, PS generated more pores and a rougher surface, and thus demonstrated higher heat resistance. It has been suggested that the system be used as thermally comfortable textile [21]. Other authors reported on the water vapour resistance evaluation of electrospun polyacrylonitrile (PAN) using the Permetest skin model. The study showed an exponential correlation between water vapour resistance and the membrane ratio: varying the morphology of the electrospun PAN resulted in a water vapour permeability value of between 0.1 Pam²/W and greater than 10 Pam²/W [22]. This study considered electrospun single and composite PS/PU microporous materials to be used in thermal protective applications (i.e. protective clothing or aids). The effect of the processing parameters (electrical voltage and polymer solution concentration) on fibre morphology, the number of electrospun layers, thickness (solution

volume) and their consecutive position on the composite heat resistance were examined.

2 Experimental part

2.1 Materials and methods

The polymers used in this study were polyurethane (PU), DESMOPAN 588E produced by Bayer, Germany, and polystyrene (PS) 678E, produced by Dioki, Croatia, and organic solvents N,N-dimethylformamide (DMF) and tetrahydrofuran (THF), produced by Sigma Aldrich. The textile substrate used to support the electrospun material was a commercially available fine woven net textile (polyamide tulle). The PU was of extrusion and injection moulding grade with improved microbial and hydrolysis resistance and a density of 1.15 g/cm³. The PS was general purpose, transparent, with excellent optical properties, processability, high melt flow rate and a density of 1.05 g/cm³. The two polymers were dissolved in DMF/THF and DMF (weight ratio of 2:3) to prepare two separate ranges of solutions 10–16 wt% and 24–30 wt% for the PU and PS, respectively. Electrospun materials were produced by electrospinning device type NT-ESS-300, NTSEE Co. Ltd., South Korea. The processing conditions, electrical voltage U (kV), needle tip to collector distance x (cm) and volume flow rate v (mL/h) are presented in Table 1, while the collector rotation speed was 90 rpm and the collector horizontal migration was 0.206 m/min. These conditions refer to electrospun materials used to evaluate a material's morphology and porosity.

Table 1: Electrospinning process conditions

Polymer	Parameters			
	c^a (wt%)	U^b (kV)	v^c (mL/h)	x^d (cm)
Polyurethane	10, 12, 14, 16	10, 12, 14, 16, 18	1	12
Polystyrene	24, 26, 28, 30	10, 12, 14, 16, 18, 20	1–4	12

^{a)} concentration, ^{b)} voltage, ^{c)} volume flow rate, ^{d)} needle tip to collector distance

For the purpose of heat resistance evaluation, the materials were fabricated (dimensions of 30

cm x 30 cm) using a single or combined PS and PU electrospinning solution on a net textile substrate

(NTS). PS/PU composite materials were electrospun continuously in a layer-by-layer manner. The electrospinning conditions chosen for the PU were 10 wt%, 18 kV, 12 cm and 1 mL/h, while the conditions

for PS were 30 wt%, 18 kV, 12 cm and 4 mL/h. The configurations of the electrospun materials in terms of polymer solution volume and layer alteration are given in Table 2.

Table 2: Electrospun single and composite materials configurations

Sample ID	A	B	C
	V = const (4 mL (total))	V ≠ const (4 mL each layer)	V ≠ const (4 mL each layer)
1	PU; one layer (A = B = C)		
2	PS; one layer (A = B = C)		
3	PS/PU two layers	PS/PU two layers (B = C)	
4	PS/PU/PS/PU four layers	PS/PU/PS/PU four layers	PS/PS/PU/PU four layers
5	PS/PU/PS/PU/PS/PU six layers	/	/

In case of equal polymer layering, electrospinning was continued after one hour of drying at room temperature. Figure 1 illustrates the configurations of the three types (A, B and C) of single and PS/PU composite materials. “A” stands for materials/composites made from one, two, four or six PS and PU alternating layers with a total polymer solution volume of 4 mL. Materials in group A were made from one layer (PS or PU), two layers electrospun one by one (PS/PU), four (PS/PU/PS/PU) or six alternating layers PS/PU/PS/PU/PS/PU. The difference between group A and B was in the polymer solution volume.

stands for materials/composites made from one, two or four PS and PU repeating layers with a polymer solution of 4 mL for each single layer. The difference between group B and C is in the electrospinning order of the polymers, as seen in Figure 1. For all composites, the top layer of each configuration was PU, as it facilitates better adherence, due to faster solvent evaporation, in contrast to the high PS concentration solution system. To ensure composites compactness, each of the configurations was electrospun on a net textile substrate.

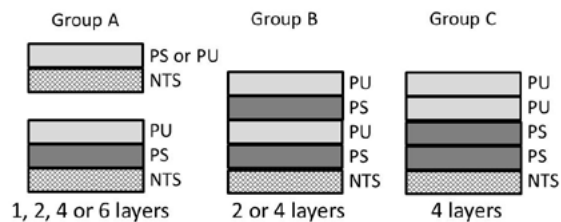


Figure 1: Scheme of the electrospun PS and PU alternating layers

“B” stands for materials/composites made from one, two or four PS and PU alternating layers with a polymer solution of 4 mL for each single layer. “C”

2.1.1 SEM analysis and porosity calculation

The morphology of the electrospun materials was observed using a SEM MIRA3 TESCAN scanning electron microscope, with palladium/gold coating beforehand. The fibre diameter and pore area were measured using randomly selected 100 fibres, while areas between the fibres were measured using *ImageJ* software. A statistical analysis of the collected data was performed using OriginLab software. ANOVA and Tukey tests were conducted taking into account comparisons that were statistically significant at $p < 0.05$.

The thickness of the electrospun materials was measured on a reconstructed universal measuring

microscope with a laser interferometer connected to a computer, Carl Zeiss (resolution of 0.0001 mm), University of Zagreb Faculty of Mechanical Engineering and Naval Architecture. The porosity P (%) of the single (P_s) and composite (P_c) electrospun materials was estimated using equations 1 and 2, respectively [23].

$$P_s = \left(1 - \frac{\frac{m}{A \cdot h}}{\rho_p}\right) \cdot 100\% \quad (1)$$

$$P_c = \left(1 - \frac{\frac{m_{c1}}{\rho_{c1}} + \frac{m_{c2}}{\rho_{c2}}}{V_c}\right) \cdot 100\% \quad (2)$$

where, m (g) represents the sample mass, A (cm²) represents the area and h (cm) represents the thickness, ρ (g/cm³) represents the density of the polymer and V_c (cm³) represents the composite material volume. The subscripts c_1 and c_2 refer to each of the components in the electrospun composite material.

2.1.2 Heat resistance measurement

The heat resistance of the electrospun materials was measured on a sweating guarded hotplate (SGHP) device placed in an air conditioned chamber. The hotplate simulated the transfer of heat from the skin, through the material, to the environment by maintaining a temperature of (35 ± 0.1) °C at its surface (i.e. the human skin temperature). The conditions of the chamber were as follows: temperature of 20 °C, relative humidity of 65% and airflow velocity of 1 m/s [24]. The heat resistance (R_{ct} , m²K/W) of the electrospun materials was calculated according to equation 3 [25].

$$R_{ct} = \frac{(T_m - T_a) \cdot A}{H} \quad (3)$$

where, T_m (K) represents the plate temperature, T_a (K) represents the air temperature, and H/A (W/m²) represents the heat flux.

3 Results and discussion

Figures 2–4 show the SEM images of the single electrospun PU (10–16 wt%) and PS (24–30 wt%) materials, PS/PU composite materials, and the associated textile substrate in the composite configurations. The PU electrospun fibres showed variations in the thicknesses along their lengths with random beads, especially in the case of 10 and 12 wt% solutions (Figure 2a–2b). An increase in the PU polymer concentrations (above 10 wt%; see Figure 2b–2d), resulted in an increase in the fibres' uniform morphology, i.e. the fibres had circular cross sections, no deformations along the length and smooth surfaces.

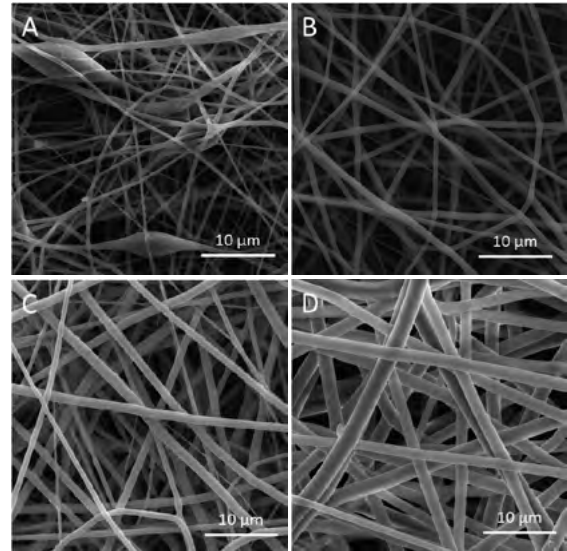


Figure 2: Electrospun single PU in concentrations of: a) 10 wt%, b) 12 wt%, c) 14 wt% and d) 16 wt% (supplemental SEM images of electrospun PU under all processing conditions presented in Table 1)

In case of the electrospun PS materials (Figure 3a–3d), the fibres demonstrated uniformity for all concentration ranges, as the latter were initially high (above 24 wt%). Thus, at higher concentrations, the solidification process of the fibres was faster because solution viscosity was predominant over surface tension, which resulted in fewer beads or in beadless fibres [26]. The SEM images clearly show the difference in the PU and PS fibres thicknesses, and

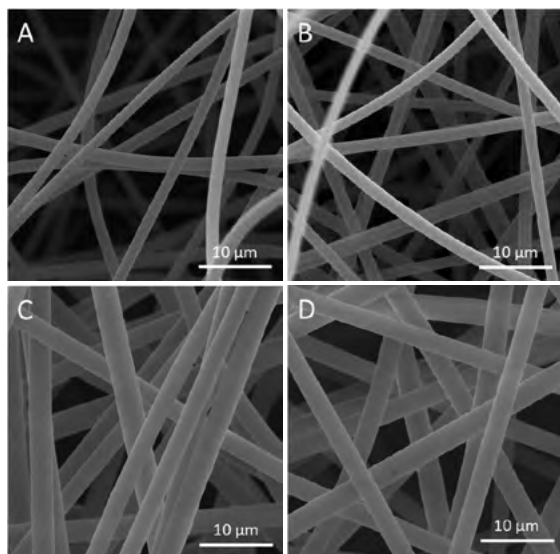


Figure 3: Electrospun single PS in concentrations of: a) 24 wt%, b) 26 wt%, c) 28 wt% and d) 30 wt% (supplemental SEM images of electrospun PS under all processing conditions presented in Table 1)

thus the composite structure (Figure 4a) illustrates the composite system with thinner PU and thicker PS fibres. Such nano/micro fibrous structures are of paramount importance in the field of biomedicine as such structures will provide cells penetration (micro pores) and free delivery, and the diffusion of nutrients as well as waste products (nano fibres) [27]. Layered systems (combining electrospun materials and conventional fabrics) will attain barrier/transport properties with different levels of thermal comfort and protection not achievable with existing personal protective materials [28]. In this study the bottom layer of the composites was a net textile substrate (Figure 4b) that will only mechanically support the electrospun materials due to its high open structure.

Figure 5 and 6 illustrate the dependence of the fibre diameter of single electrospun PU and PS on the electrical voltage and polymer solution concentrations. Generally, an increase in the electrical voltage from 10 kV to 20 kV resulted in a reduction of the fibre diameter in both polymers, which is in line with other reported studies [29]. Thinner fibres

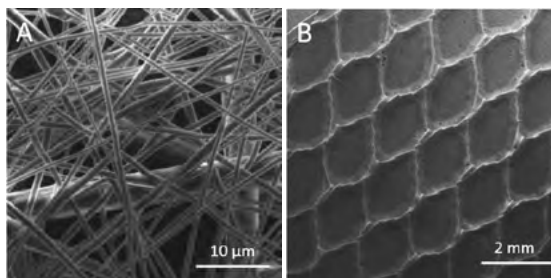


Figure 4: Electrospun materials: a) PS/PU configuration – top layer and b) PS/PU configuration – bottom layer or net textile substrate

are formed due to the increase in the charge density on the jet surface and increase in the repulsive force [30]. An opposite effect was observed in the case of the electrospun 24 wt% and 26 wt% PS at the critical voltages of 20 kV and 12 kV (Figure 6). This was also reported in the case of electrospun PU, where the diameter demonstrated a sigmoidal increase with an increase in voltage [31]. Jet traveling time was affected by an increase in electrical voltage, which then resulted in an increase in fibre diameter [32]. The concentration of 16 wt% PU was not spinnable at the voltages of 16 kV and 18 kV, while the concentration of 14 wt% PU was not spinnable at 18 kV. In the case of the electrospun PS, fibre formation was not possible in the case of the concentrations of 26 wt% and 30 wt% at the voltages of 14–20 kV and 18–20 kV, respectively. Spinnability mainly depends on the solution concentration. Thus at higher concentrations, the solvent evaporates at the tip of the needle with no possibility of the solution jet being stretched up to the collector to form the fibres. An excessively high polymer concentration and excessively high voltage will also result in a difficult spinning process [30]. The reduction of the 10 wt% PU fibre diameter with an increase in the electrical voltage was significant at voltages of 10 kV, 12 kV, 14 kV and 18 kV, and at 14 kV and 16 kV, with the highest reduction of (443 ± 224) nm to (328 ± 148) nm (Figure 5). In the case of the 12 wt% PU, the fibres were significantly thinner (highest reduction of almost 50%) for all U (kV) increases, except at 16 kV and 18 kV (Figure 5).

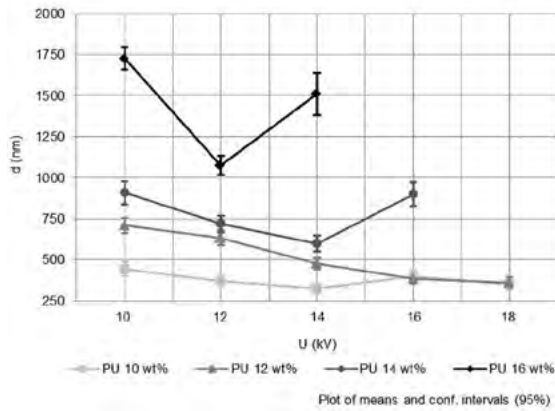


Figure 5: Effect of the concentration and electrical voltage on the electrospun PU fibre diameter

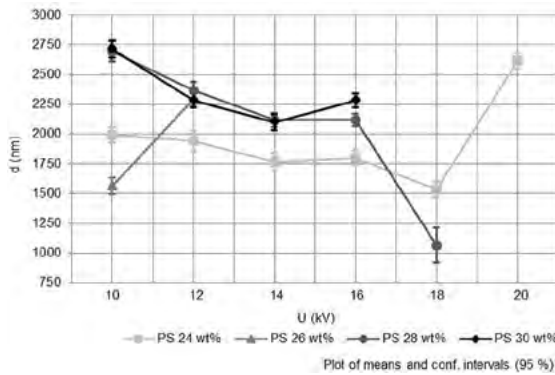


Figure 6: Effect of the concentration and electrical voltage on the electrospun PS fibre diameter

Similarly, no significant difference in the reduced fibre diameter was recorded for the 14 wt% PU at a voltage of between 10 kV and 16 kV, with the highest reduction of (908 ± 356) nm to (598 ± 238) nm. For the 16 wt% PU, a significant fibre reduction was present at all U (kV) levels, with the most significant reduction of more than 650 nm. Significant increases in fibre diameters were observed for the 14 wt% and 16 wt% PU, from (598 ± 238) nm to (898 ± 368) nm (14 kV to 16 kV), and (1075 ± 294) nm to (1511 ± 653) nm (12 to 14 kV), respectively (Figure 5). The trend of PS fibre diameter reduction was significant for all polymer concentrations at all increasing electrical voltage levels, except at 12 kV and 16 kV (24 and 30 wt% PS), 14 kV and 16 kV (24 wt% and 28 wt% PS). The most significant reduction in the PS

fibre diameter was from (2694 ± 367) nm to (1065 ± 622) nm in case of the 28 wt% PS at the 18 kV, while the highest increase was from (1534 ± 278) nm to (2614 ± 282) nm, at the highest electrical voltage level of 20 kV for the 24 wt% PS (Figure 6). A significant increase in fibre diameter was also observed for the 26 wt% PS from (1564 ± 290) nm to (2295 ± 259) nm (10 kV to 12 kV; see Figure 6). The greatest fibre mean diameter was observed in the case of the 30 wt% PS, while the most significant reduction for that sample was from (2711 ± 307) nm to (2098 ± 290) nm at 18 kV. Figure 7 and 8 show the dependence of the single electrospun PU and PS pore area on the electrical voltage and polymer solution concentrations. Although a general reduction in the pore areas was observed with an increase in the electrical voltage, the opposite effect was also seen at certain concentrations and U (kV) levels. There was a higher variation of the measured values as compared to the measured fibre diameters. Studies report on the broader fibres distribution, which may influence broader pore size distribution due to enhanced jet instability caused by the high electrical voltage [33]. A reduction in fibre diameters usually results in a decrease in pore areas as well, as the pore size and its distribution depends on the fibre diameter [34].

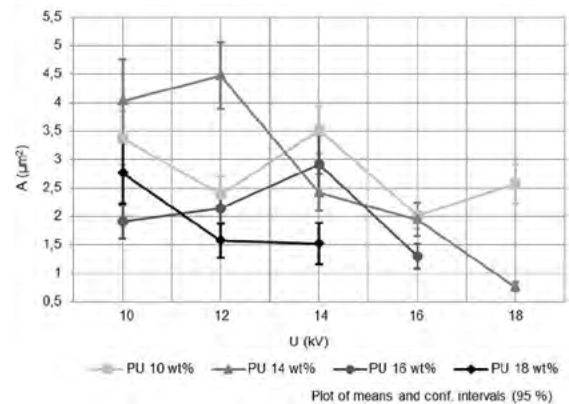


Figure 7: Effect of the concentration and electrical voltage on the electrospun PU pore area

The reduction of the 10 wt% PU pore areas with an increase of the electrical voltage was significant at voltages of 10 kV, 12 kV, 16 kV and 18 kV, 12 kV and

14 kV (pores were increased by $1.13 \mu\text{m}^2$), and at 14 kV, 16 kV and 18 kV (pores were increased by $0.55 \mu\text{m}^2$ from 16 kV to 18 kV), with the highest reduction of $(3.37 \pm 2.43) \mu\text{m}^2$ to $(2.02 \pm 1.16) \mu\text{m}^2$ (Figure 7). In the case of the 12 wt% PU, the pore areas were significantly smaller (highest reduction of almost $3.71 \mu\text{m}^2$) for all U (kV) increases, except at 10 and 12 kV (pores were increased by $0.44 \mu\text{m}^2$), and at 14 kV and 16 kV (Figure 7).

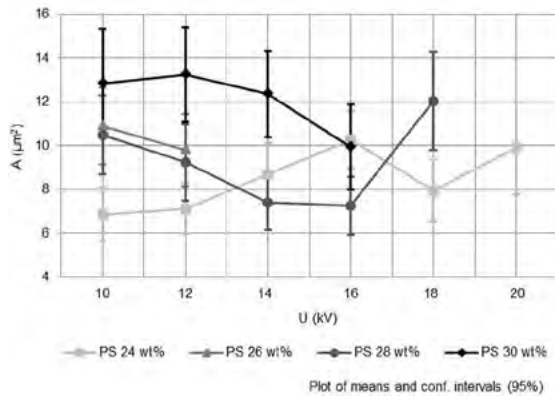


Figure 8: Effect of the concentration and electrical voltage on the electrospun PS pore area

The reduction of the pore areas in the case of the 14 and 16 wt% was only insignificant at voltages of 10 kV, 12 kV and 16 kV, and at 12 kV and 14 kV, respectively. The highest observed reductions of the pore areas were 55% (for the 14 wt% PU) and 45% (for the 16 wt% PU; see Figure 7). The variations of the measured pore areas were greater for the electrospun PS than for the electrospun PU. Thus a significant increase or reduction in pore areas was only observed in the case of the 24 wt% at voltages of 10 kV and 16 kV, and at 12 kV and 16 kV, and in the case of the 28 wt% at voltages of 14 kV and 18 kV, and at 16 kV and 18 kV (Figure 8). The most significant increase in the pore areas in the case of the 24 wt% was from $(6.85 \pm 5.98) \mu\text{m}^2$ to $(10.27 \pm 6.63) \mu\text{m}^2$, and from $(7.26 \pm 5.87) \mu\text{m}^2$ to $(12.03 \pm 9.63) \mu\text{m}^2$ in the case of the 28 wt% PS (Figure 8). In the case of the 30 wt% PS, the ranges of the mean pore areas were between $(9.94 \pm 8.21) \mu\text{m}^2$ and $(13.23 \pm 9.30) \mu\text{m}^2$, with the highest value observed.

Table 3 presents the electrospun materials' mass per surface area m (g/cm^2), thickness h (mm) and calculated total porosity P (%). The mass per surface area and the thicknesses of the electrospun materials increased with an increase in the number of electrospun layers in the composite systems. There was no significant difference between the composite materials in terms of calculated porosity, as all of the listed materials showed porosities higher than 97%, which is quite high and beneficial, and will thus contribute to their excellent moisture vapor transport properties [35].

Table 3: Calculated porosity of electrospun materials

Sample	m (* $10^{-3} \text{g}/\text{cm}^2$)	h (mm)	P (%)
TS	1.08	0.1900	/
A1	0.24	0.3104	99.1
A2	0.78	0.2749	99.2
A3	0.57	0.4866	97.2
A4	0.69	0.5454	98.6
A5	0.89	0.5564	98.4
B3	1.17	0.9364	98.7
B4	2.62	0.7200	99.9
C4	2.43	1.1817	98.0

Figure 9 illustrates the heat resistance vs. thickness and vs. total porosity of single electrospun PS and PU (on the NTS), as well as the associated PU/PS/NTS composite systems with a varying number and position of layers. When observing group A of the electrospun materials, it can be easily concluded that the single electrospun PS (A2) showed reduced heat resistance (for $0.0219 \text{ m}^2\text{K}/\text{W}$) compared to the single electrospun PU (A1) material due to thicker fibres and greater pore areas, meaning a looser structure. When the two were combined into two to six layers, the heat resistance increased up to $0.0557 \text{ m}^2\text{K}/\text{W}$ for the electrospun A5 or PS/PU/PS/PU/PS/PU material. In group B, an increase in the polymer solution volume (4 mL) in each of the consecutive layers drastically increased the composites' heat resistance to 0.0834 (B3 two layers) and $0.102 \text{ m}^2\text{K}/\text{W}$ (B4 four layers).

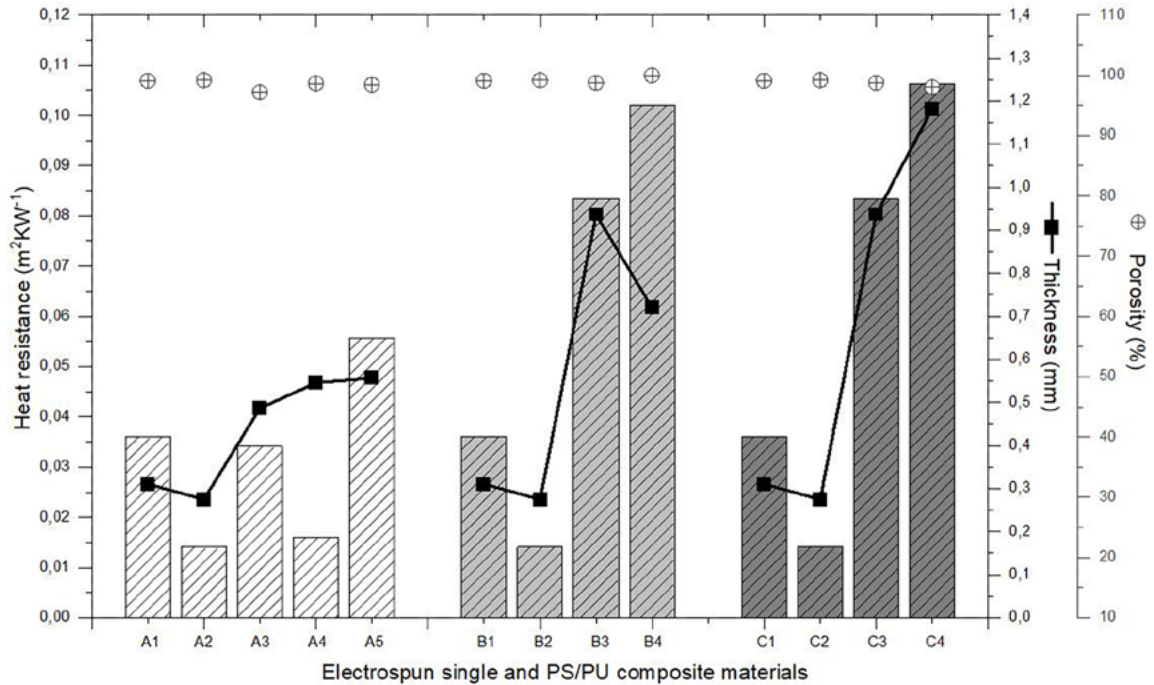


Figure 9: Heat resistance of the three groups (A, B and C) of electrospun composite materials vs. thickness and vs. porosity

The highest heat resistance of $0.1063 \text{ m}^2\text{K/W}$ was measured for the four layered PS/PS/PU/PU (C4) composite material. When compared to the four layered B4 composite, it can be concluded that the position of the PU layer in C4 contributed to an increase in heat resistance. Two of the PU layers were electrospun as the top layers (after the two PS layers), while the reason for the increase was their small pore areas and compact structure resisting the heat flow. A previous study reported on the fabrication of a multi-layered fabric combining cotton and lyocell fabrics, and a PU nanofibrous coating to improve wind-resistance and comfort properties of knitted structures [36]. Similarly, when electrospun polyacrylonitrile (PAN) was placed between polyethylene (PE) nonwoven layers, PAN with thinner fibres (108 nm) and a higher surface density (5 g/m^2) resulted in a reduction in thermal conductivity and improved water vapor transfer by 28% [37]. When these results are correlated to the calculated total porosity, there is no trend to be

followed, as the changes in the porosities among all materials were insignificant. In the case of the thickness relation, one general observation is that higher heat resistances is the result of an increase in the composite thickness (i.e. from 0.5454 mm for A4, to 0.7200 mm for B4, to 1.1817 mm for C4). A linear relationship between a fabric's heat resistance and its corresponding thickness was reported in a study of polyester knitted fabrics to provide thermal comfort in clothing design. As explained, the still air entrapped between the fibre spaces increases the heat resistance value [38]. In this study, there was the opposite effect of increasing thickness, as well. If one observes material A3 and A4, it is evident that, despite the increase in the thickness by 0.0588 mm, the heat resistance of the thicker material A4 was reduced by $0.0181 \text{ m}^2\text{K/W}$. This may suggest that an increase in the number of PS layers that have a looser structure or larger pore areas facilitate the pass through of heat, resulting in reduced thermal insulation. The same effect can be

seen for the B3 and B4 materials. A study reported on the evaluation of the heat resistance of different twill woven fabrics used in sportswear. The thicknesses of the fabrics were in the ranges of 0.17 mm to 0.28 mm. The measured thermal resistances were between 0.0059 m²K/W to 0.0142 m²K/W [39]. The single electrospun PS material in our study, with a thickness of 0.2749 mm, was comparable with the reported twill woven fabric, with a thickness of 0.28 mm. However, in terms of R_{ct} , the heat resistance of our material was 0.0139 m²K/W higher. Similarly, another study reported the heat resistances of single jersey knitted fabrics (cotton, or cotton + elastane, grey or finished) in the ranges of ~0.015 m²K/W to ~0.02 m²K/W [40]. Comparing the results, one can observe the similarity of the knitted fabrics with some of those from the current study's group A materials, while increasing solution volume (material thickness), the number of layers, and the electrospinning order thereof (groups B and C) resulted in more than 0.05 m²K/W R_{ct} (i.e. material C4, PS/PS/PU/PU, 1.1817 mm, 0.1063 m²K/W). This suggests that the layering configuration of the electrospun materials is beneficial for thermal performance and thus would imply a combination with other conventional materials, as well. Their light weight would still not be compromised in the case of a greater number of electrospun layers, which would contribute to total comfort in terms of freedom of movement.

4 Conclusion

Among the many application areas of the electrospun materials, the field of thermal protective fabrics has been explored very little. This study deals with this topic by first investigating the effect of the electrical voltage and polymer concentrations on fibre diameter and pore area, and then by correlating the two parameters with heat resistance properties. Heat resistance, which is directly related to the material heat insulation, was measured to determine a change in heat resistance in terms of the number, thickness

(solution volume) and position of electrospun layers variation in a PU/PS/NTS composite system. Generally, the higher the electrical voltage was, the thinner the PU and PS fibres were, with a few opposite effects indicating polymer jet instabilities. The electrospun PS demonstrated thicker fibres (> 1000 nm to ~2700 nm) and larger pore areas (> 6 µm² to ~13 µm²), resulting in a looser structure and, as expected, in a lower heat resistance of 0.0141 m²K/W compared to the PU of 0.036 m²K/W. The compact structure of the electrospun PU was the result of its thinner fibres (~300 nm to ~1700 nm) and smaller pore areas (0.75 µm² to 4.5 µm²), and thus improved the heat resistance of PU/PS composites. Increasing the number of electrospun layers from one to six and the volume of each electrospun layer solution, and adding a PU layer on top of the system increased the total heat resistance of the multi-layered composites, with the highest value (0.1063 m²K/W) recorded for the group C.

Acknowledgement

This work was supported by the University of Zagreb, Faculty of Textile Technology under short-term financial support for research for 2023, TP20-23, PI: Emilija Zdraveva.

Conflict of interest statement

The authors declare there were no conflicts of interest.

References

1. FAN, M., FU, F. Introduction: a perspective–natural fibre composites in construction. In *Advanced High Strength Natural Fibre Composites in Construction*. Edited by M. Fan and F. Fu. Cambridge : Elsevier, 2017, 1–20, doi: 10.1016/B978-0-08-100411-1.00001-7.

2. KORJENIC, A., PETRÁNEK, V., ZACH, J., HROUDOVÁ, J. Development and performance evaluation of natural thermal-insulation materials composed of renewable resources. *Energy and Buildings*, 2011, **43**(9), 2518–2523, doi: 10.1016/j.enbuild.2011.06.012.
3. BOZSAKY, D. Nature-based thermal insulation materials from renewable resources. A state-of-the-art review. *Slovak Journal of Civil Engineering*, 2019, **27**(1), 52–59, doi: 10.2478/sjce-2019-0008.
4. CETINER, I., SHEA, A.D. Wood waste as an alternative thermal insulation for buildings. *Energy and Buildings*, 2018, **168**, 374–384, doi: 10.1016/j.enbuild.2018.03.019.
5. CAI, Z., AL FARUQUE, M.A., KIZILTAS, A., MIELEWSKI, D., NAEBE, M. Sustainable lightweight insulation materials from textile-based waste for the automobile industry. *Materials*, 2021, **14**(5), 1–20, doi: 10.3390/ma14051241.
6. SALOPEK ČUBRIĆ, I., SKENDERI, Z. Impact of cellulose materials finishing on heat and water vapour resistance. *Fibres & Textiles in Eastern Europe*, 2013, **97**(1), 61–66.
7. BOZSAKY, D. The historical development of thermal insulation materials. *Periodica Polytechnica Architecture*, 2010, **41**(2), 49–56, doi: 10.3311/pp.ar.2010-2.02.
8. DHANGAR, M., CHATURVEDI, K., MILI, M., PATEL, S. S., KHAN, M. A., BHARGAW, H. N. SRIVASTAVA, A. K., VERMA, S. Emerging 3D printed thermal insulating materials for sustainable approach: A review and a way forward. *Polymers for Advanced Technologies*, 2023, **34**(5), 1425–1434, doi: 10.1002/pat.5989.
9. GIBSON, P. W., LEE, C., KO, F., RENEKER, D. Application of nanofiber technology to nonwoven thermal insulation. *Journal of Engineered Fibers and Fabrics*, 2007, **2**(2), 32–40, doi: 10.1177/155892500700200204.
10. GRABOWSKA, B., KASPERSKI, J. The thermal conductivity of 3D printed plastic insulation materials – the effect of optimizing the regular structure of closures. *Materials*, 2020, **13**(19), 1–15, doi: 10.3390/ma13194400.
11. ZDRAVEVA, E., FANG, J., MIJOVIĆ, B., LIN, T. Electrospun nanofibers. In *Structure and Properties of High-performance Fibers*. Edited by Gajanan Bhat. Cambridge : Woodhead Publishing, 2017, 267–300, doi: 10.1016/B978-0-08-100550-7.00011-5.
12. SUKIGARA, S., GANDHI, M., AYUTSEDE, J., MICKLUS, M., KO, F. Regeneration of *Bombyx mori* silk by electrospinning – part I: processing parameters and geometric properties. *Polymer*, 2003, **44**(19), 5721–5727, doi: 10.1016/S0032-3861(03)00532-9.
13. MIT-UPPATHAM, C., NITHITANAKUL, M., SUPAPHOL., P. Ultrafine electrospun polyamide-6 fibers: effect of solution conditions on morphology and average fiber diameter. *Macromolecular Chemistry and Physics*, 2004, **205**(17), 2327–2338, doi: 10.1002/macp.200400225.
14. BUCHKO, C.J., CHEN, L.C., SHEN, Y., MARTIN, D.C. Processing and microstructural characterization of porous biocompatible protein polymer thin films. *Polymer*, 1999, **40**(26), 7397–7407, doi: 10.1016/S0032-3861(98)00866-0.
15. YUAN, X., ZHANG, Y., DONG, C., SHENG, C. Morphology of ultrafine polysulfone fibers prepared by electrospinning. *Polymer International*, 2004, **53**(11), 1704–1710, doi: 10.1002/pi.1538.
16. TAN, S.-H., INAI, R., KOTAKI, M., RAMAKRISHNA, S. Systematic parameter study for ultra-fine fiber fabrication via electrospinning process. *Polymer*, 2005, **46**(16), 6128–6134, doi: 10.1016/j.polymer.2005.05.068.
17. LEE, D., JUNG, J., LEE, G. H., LEE, W. I. Electrospun nanofiber composites with micro-/nano-particles for thermal insulation. *Advanced Composite Materials*, 2019, **28**(2), 193–202, doi: 10.1080/09243046.2018.1478607.
18. CHEN, W., FU, M., WENG, W. Electrospinning of continuous nanofiber hollow yarns for thermal storage and insulation by a multi-step twisting method. *Textile Research Journal*, 2020, **90**(9–10), 1045–1056, doi: 10.1177/0040517519886023.

19. BAE, M., AHN, H., KANG, J., CHOI, G., CHOI, H. Determination of the long-term thermal performance of foam insulation materials through heat and slicing acceleration. *Polymers*, 2022, **14**(22), 1–18, doi: 10.3390/polym14224926.
20. MERILLAS, B., VILLAFANE, F., RODRÍGUEZ-PÉREZ, M.Á. Improving the insulating capacity of polyurethane foams through polyurethane aerogel inclusion: from insulation to superinsulation. *Nanomaterials*, 2022, **12**(13), 1–19, doi: 10.3390/nano12132232.
21. YOON, J.W., PARK, Y., KIM, J., PARK, C.H. Multi-jet electrospinning of polystyrene/polyamide 6 blend: thermal and mechanical properties. *Fashion and Textiles*, 2017, **4**(9), 1–12, doi: 10.1186/s40691-017-0090-4.
22. SABANTINA, L., HES, L., MIRASOL, J.R., CORDERO, T., EHRMANN, A. Water vapor permeability through PAN nanofiber mat with varying membrane-like areas. *Fibres & Textiles in Eastern Europe*, 2019, **1**(133), 12–15, doi: 10.5604/01.3001.0012.7502.
23. YAMAGUCHI, T., KUROKI, H., MIYATA, F. DMFC performances using a pore-filling polymer electrolyte membrane for portable usages. *Electrochemistry Communications*, 2005, **7**(7), 730–734, doi: 10.1016/j.elecom.2005.04.030.
24. ISO 11092:1993 Textiles – physiological effects – measurement of thermal and water-vapour resistance under steady-state conditions (sweating guarded-hotplate test). Geneva : International Organization for Standardization, 1993, 1–10.
25. SALOPEK ČUBRIĆ, I., SKENDERI, Z., MIHELIĆ-BOGDANIĆ, A., ANDRASSY, M. Experimental study of thermal resistance of knitted fabrics. *Experimental Thermal and Fluid Science*, 2012, **38**, 223–228, doi: 10.1016/j.expthermflusc.2011.12.010.
26. KIM, G.-T., HWANG, Y.-J., AHN, Y.-C., SHIN, H.-S., LEE, J.-K., SUNG, C.-M. The morphology of electrospun polystyrene fibers. *Korean Journal of Chemical Engineering*, 2005, **22**, 147–153, doi: 10.1007/BF02701477.
27. ANJUM, S., RAHMAN, F., PANDEY, P., ARYA, D.K., ALAM, M., RAJINIKANTH, P.S., AO, Q. Electrospun biomimetic nanofibrous scaffolds: a promising prospect for bone tissue engineering and regenerative medicine. *International Journal of Molecular Sciences*, 2022, **23**(16), 1–33, doi: 10.3390/ijms23169206.
28. LEE, S., OBENDORF, S.K. Transport properties of layered fabric systems based on electrospun nanofibers. *Fibers and Polymers*, 2007, **8**, 501–506, doi: 10.1007/BF02875872.
29. ZDRAVEVA, E., MIJOVIĆ, B. Parameters dependence of fibers diameter and pores area in electrospinning. *Advanced Engineering Forum*, 2018, **26**, 67–73, doi: 10.4028/www.scientific.net/AEF.26.67.
30. CAO, X., CHEN, W., ZHAO, P., YANG, Y., YU, D.-G. Electrospun porous nanofibers: pore-forming mechanisms and applications for photocatalytic degradation of organic pollutants in wastewater. *Polymers*, 2022, **14**(19), 1–25, doi: 10.3390/polym14193990.
31. DEMIR, M.M., YILGOR, I., YILGOR, E., ERMAN, B. Electrospinning of polyurethane fibers. *Polymer*, 2002, **43**(11), 3303–3309, doi: 10.1016/S0032-3861(02)00136-2.
32. SENCADAS, V., CORREIA, D.M., AREIAS, A., BOTELHO, G., FONSECA, A., NEVES, I., RIBELLES, J. G., MENDEZ, S. L. Determination of the parameters affecting electrospun chitosan fiber size distribution and morphology. *Carbohydrate Polymers*, 2012, **87**(2), 1295–1301, doi: 10.1016/j.carbpol.2011.09.017.
33. RIBEIRO, C., SENCADAS, V., COSTA, C. M., RIBELLES, J.L.G., LANCEROS-MÉNDEZ, S. Tailoring the morphology and crystallinity of poly (L-lactide acid) electrospun membranes. *Science and Technology of Advanced Materials*, 2011, **12**(1), 1–10, doi: 10.1088/1468-6996/12/1/11660947.

34. TORNELLO, P.R.C., CARACCIOLO, P.C., ROSELLÓ, J.I.I., ABRAHAM, G.A. Electrospun scaffolds with enlarged pore size: porosimetry analysis. *Materials Letters*, 2018, **227**, 191–193, doi: 10.1016/j.matlet.2018.05.072.
35. SCHREUDER-GIBSON, H., GIBSON, P., SEN-ECAL, K., SENNETT, M., WALKER, J., YEO-MANS, W. Protective textile materials based on electrospun nanofibers. *Journal of Advanced Materials*, 2002, **34**(3), 44–55.
36. OĞLAKCIOĞLU, N., AKDUMAN, C., SARI, B. Investigation of thermal comfort properties of electrospun thermoplastic polyurethane fiber coated knitted fabrics for wind-resistant clothing. *Polymer Engineering & Science*, 2021, **61**(3), 669–679, doi: 10.1002/pen.25607.
37. NASOURI, K., SHOUSHARI, A.M., HAJI, A. The role of nanofibers diameter in the enhanced thermal conductivity of electrospun nanofibers. In *Proceedings of the The 6th TEX TEH International Conference, Bucharest, Romania*, 2013, 1–9.
38. ÖZKAN, E.T., KAPLANGIRAY, B.M. Investigating thermophysiological comfort properties of polyester knitted fabrics. *Journal of Textile Engineering & Fashion Technology*, 2019, **5**(1), 50–56, doi: 10.15406/jteft.2019.05.00180.
39. LU, X., WU, S. Thermo-physiological comfort properties of different woven fabrics used in sportswear for outdoor activities. *Thermal Science*, 2022, **26**(3B), 2707–2712, doi: 10.2298/TSCI2203707L.
40. MIJOVIĆ, B., SKENDERI, Z., SALOPEK ČUBRIĆ, I. Measurement of thermal parameters of skin-fabric environment. *Periodicum Biologorum*, 2010, **112**(1), 69–73.

Appendix

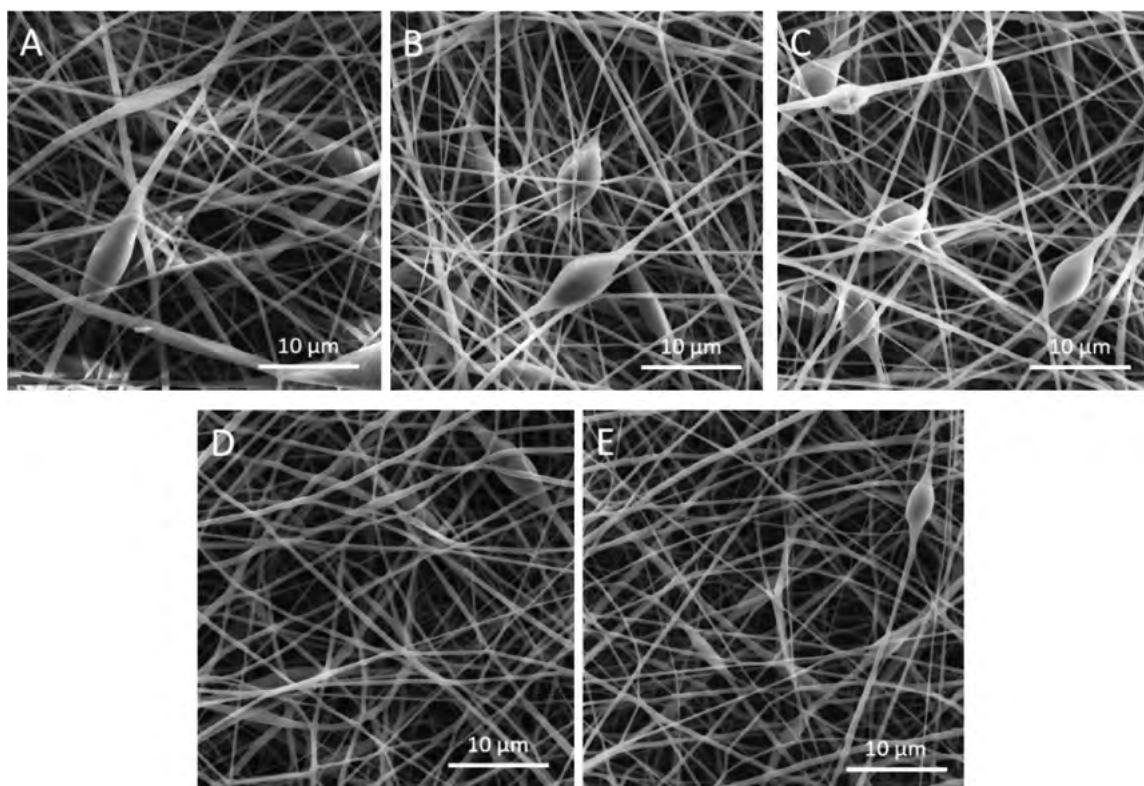


Figure A1: Electrospun 10 wt% PU at the electrical voltages of: a) 10 kV, b) 12 kV, c) 14 kV, d) 16 kV and e) 18 kV

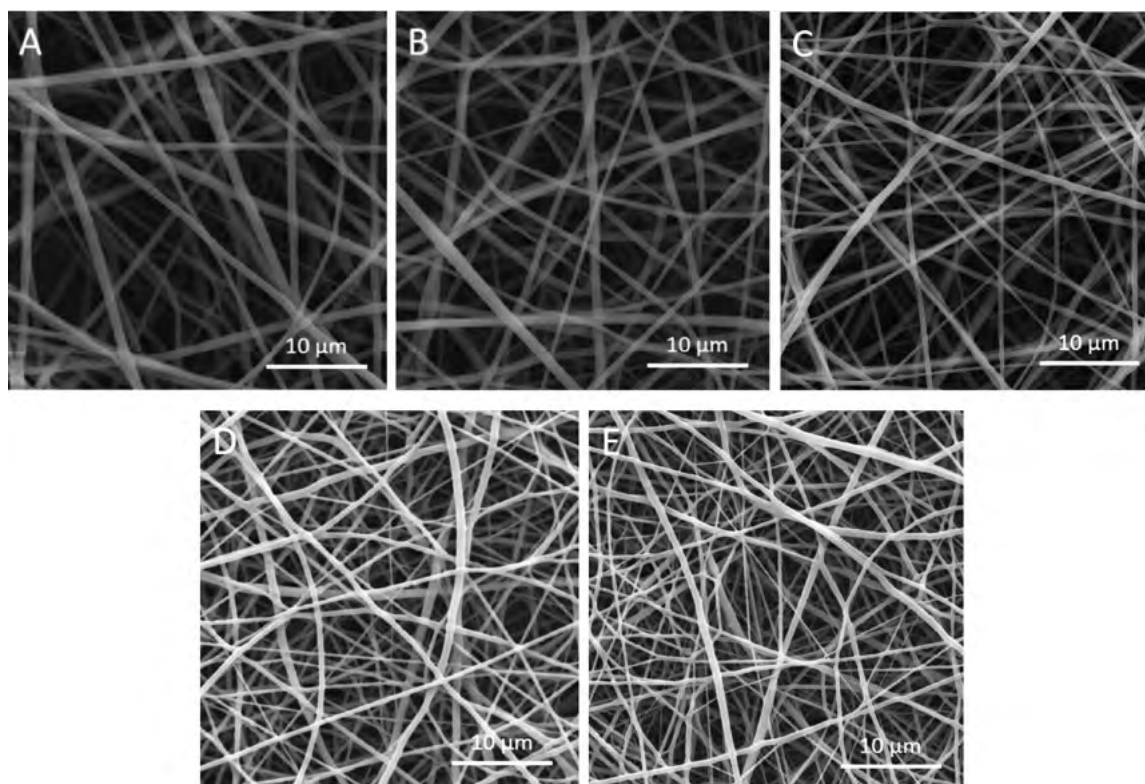


Figure A2: Electrospun 12 wt% PU at the electrical voltages of: a) 10 kV, b) 12 kV, c) 14 kV, d) 16 kV and e) 18 kV

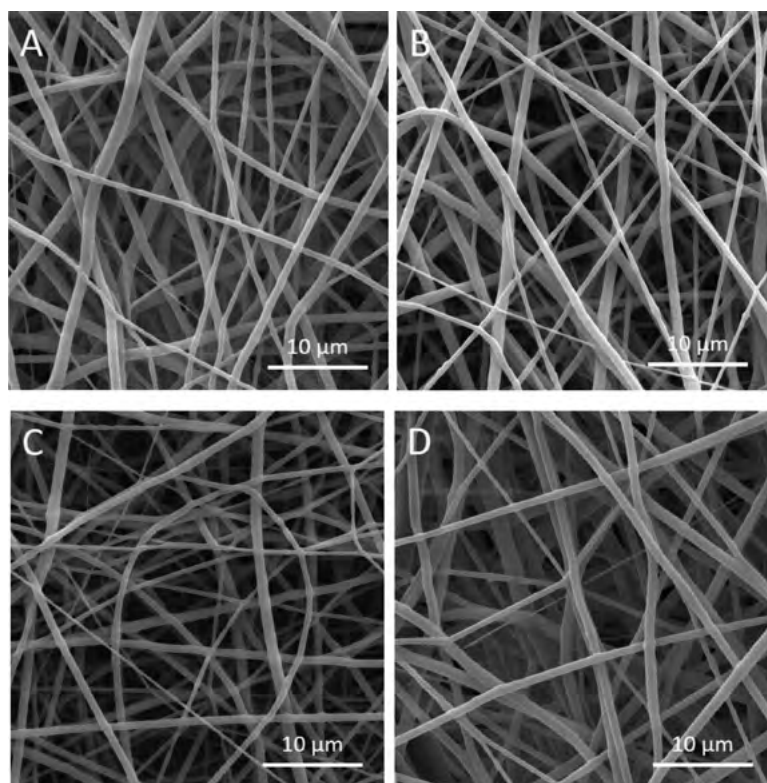


Figure A3: Electrospun 14 wt% PU at the electrical voltages of: a) 10 kV, b) 12 kV, c) 14 kV and d) 16 kV

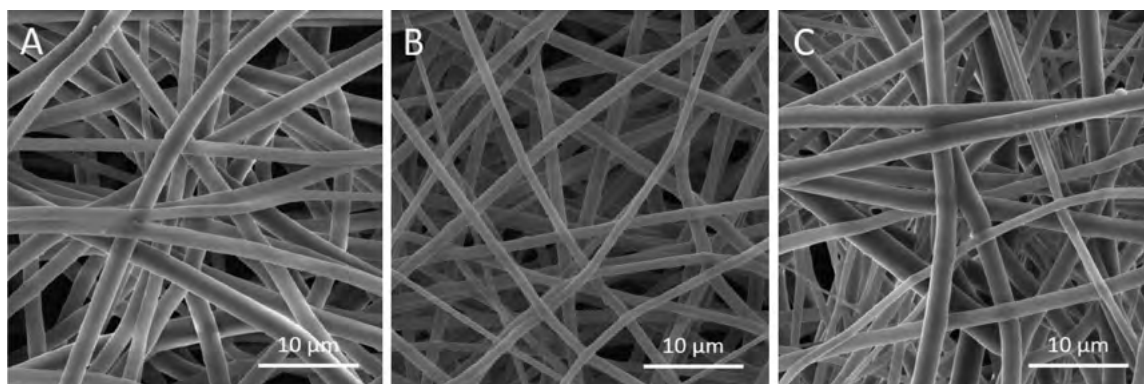


Figure A4: Electrospun 16 wt% PU at the electrical voltages of: a) 10 kV, b) 12 kV and c) 14 kV

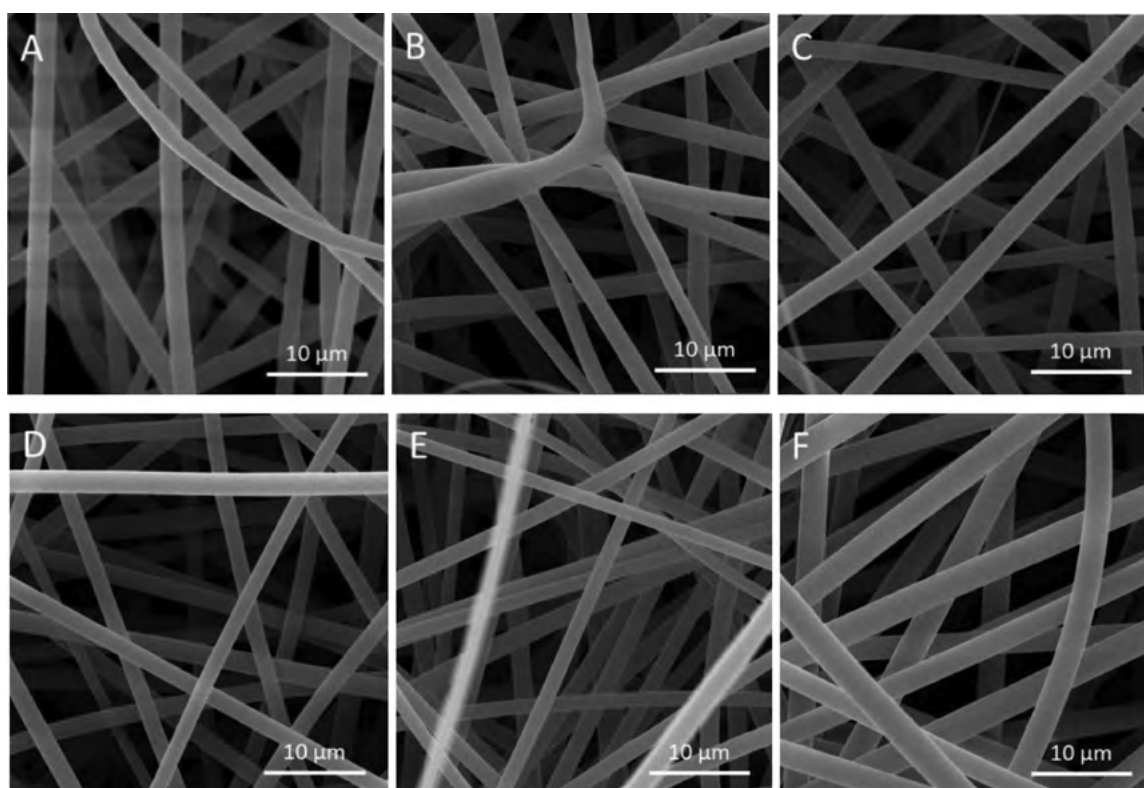


Figure A5: Electrospun 24 wt% PS at the electrical voltages of: a) 10 kV, b) 12 kV, c) 14 kV, d) 16 kV, e) 18 kV and f) 20 kV

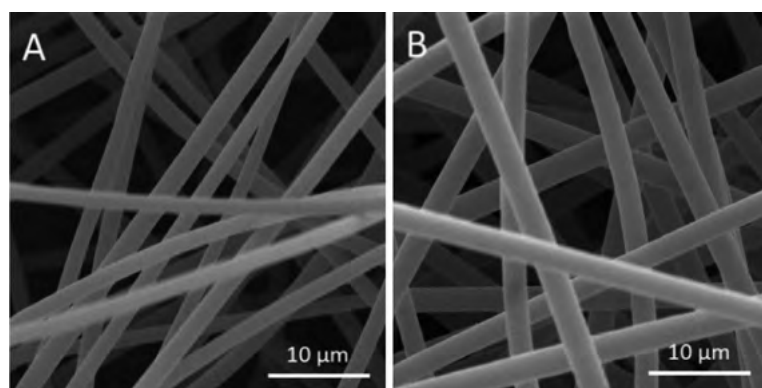


Figure A6: Electrospun 26 wt% PS at the electrical voltages of: a) 10 kV and b) 12 kV

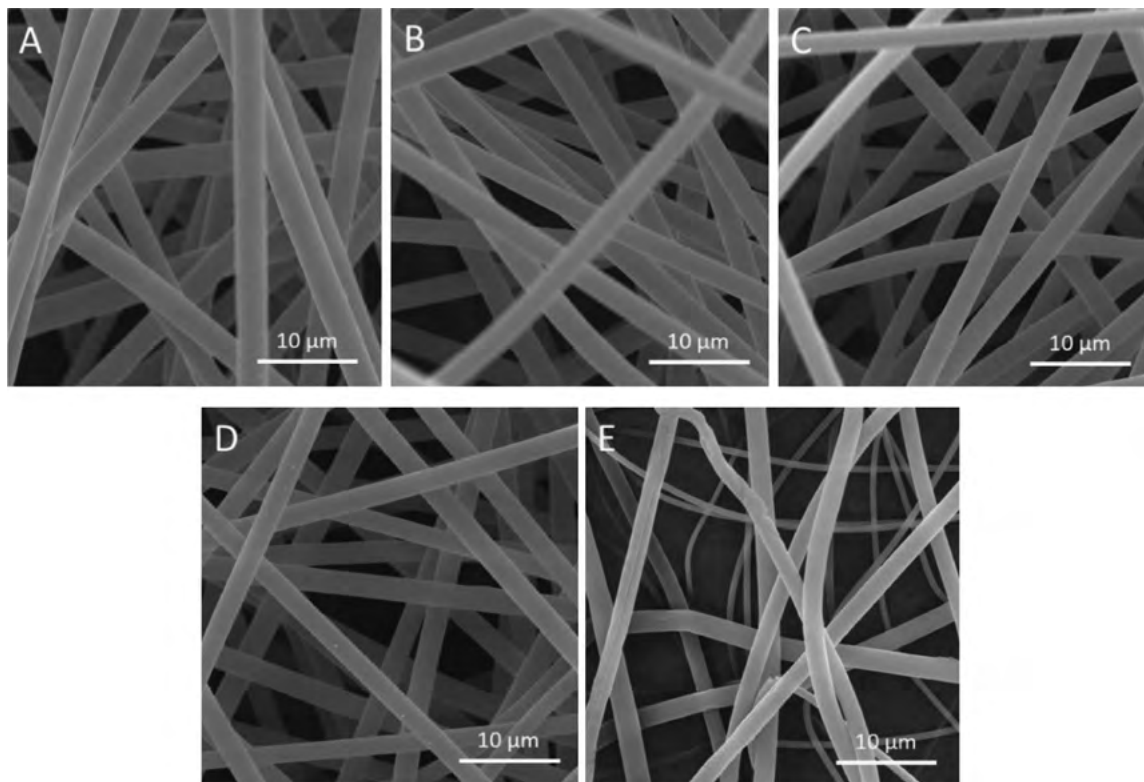


Figure A7: Electrospun 28 wt% PS at the electrical voltages of: a) 10 kV, b) 12 kV, c) 14 kV, d) 16 kV and e) 18 kV

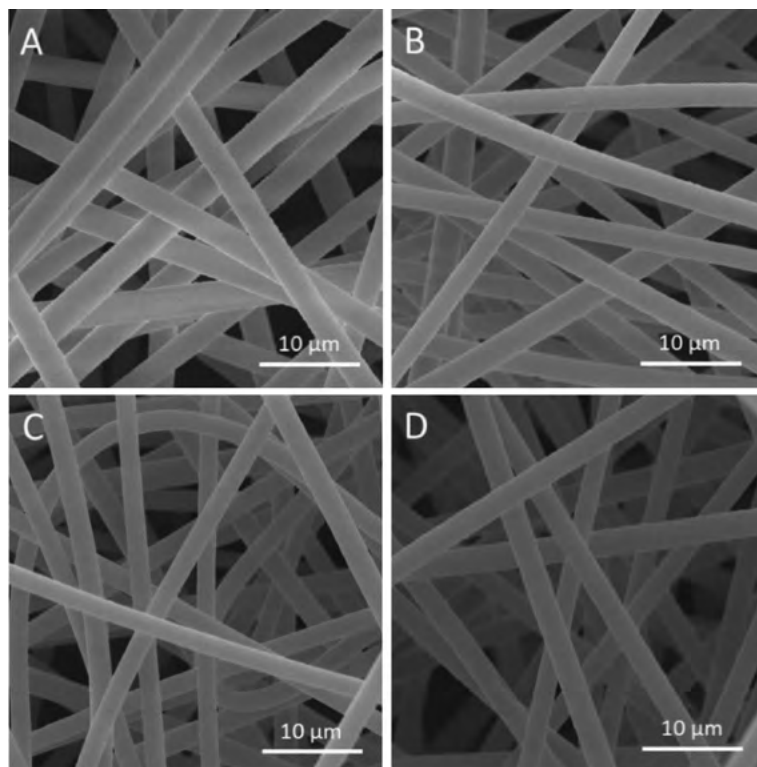


Figure A8: Electrospun 30 wt% PS at the electrical voltages of: a) 10 kV, b) 12 kV, c) 14 kV and d) 16 kV

Scolastica Manyim,^{1,2} Ambrose K. Kiprop,^{1,2} Josphat I. Mwasiagi,^{2,3} Cleophas M. Achisa M.,^{2,4} Mark P. Odero⁵

¹ Department of Chemistry and Biochemistry, Moi University, Kenia

² Africa Center of Excellence in Phytochemicals, Textile and Renewable Energy, Moi University, Kenia

³ Department of Manufacturing, Industrial and Textile Engineering, Moi University, Kenia

⁴ Department of Chemical and Process Engineering, Moi University, Kenia

⁵ Department of Applied Science Rift Valley Technical Training Institute, Kenia

Evaluation of Antioxidant, Antibacterial and Fastness Properties of Erythrina abyssinica Extracts on Cotton Fabric Using Biomordants

Vrednotenje antioksidativnih in protibakterijskih lastnosti ter barvnih obstojnosti izvlečkov Erythrina Abyssinica na bombažni tkanini z uporabo biočimž

Original scientific article/Izvirni znanstveni članek

Received/Prispelo 7–2024 • Accepted/Sprejeto 1–2025

Corresponding author/Korespondenčna avtorica:

Scolastica Manyim

Tel: +92-3139374141

E-mail: smanyim@gmail.com

ORCID iD: 0000-0001-9639-9877

Abstract

Due to the toxicity of synthetic dyes, natural dyes have been touted as possible alternatives owing to their eco-friendliness and ability to impart bio-functional properties, such as antibacterial, antifungal and antioxidant properties, especially when natural dyes are mordanted using with biomordants. The aim of the study was to evaluate the effects of using biomordants on the natural dyeing properties of Erythrina abyssinica dye extract, and to evaluate their antioxidant and antimicrobial biofunctionalization properties on cotton fabric. The biomordants used in this study were from mango bark and rosemary extracts. The antioxidant activity of the dyed cotton fabric was established using the 2,2-diphenyl-1-picrylhydrazyl radical (DPPH) method, while the antimicrobial activity of cotton fabric was measured against the Escherichia coli and Staphylococcus aureus strains of bacteria using the direct absorbance method. The use of biomordants in dyeing led to an increase in colour strengths from 0.601 to 0.762 and 0.692 for rosemary and mango biomordants, respectively. Cotton dyed using E. abyssinica demonstrated an antioxidant activity of up to 78.6 1%. The dye imparted a microbial reduction ability of up to 69.11% and 70.06% against E. coli and S. aureus, respectively, to the fabric. Dyeing properties, such as wash fastness, light fastness, colour fastness and perspiration, improved after biomordanting. It can thus be concluded that E. abyssinica dye extracts are suitable for textile dyeing and biofunctionalization

Keywords: natural dyes, antioxidant activity, antimicrobial activity, biomordants, dye fastness



Content from this work may be used under the terms of the Creative Commons Attribution CC BY 4.0 licence (<https://creativecommons.org/licenses/by/4.0/>). Authors retain ownership of the copyright for their content, but allow anyone to download, reuse, reprint, modify, distribute and/or copy the content as long as the original authors and source are cited. No permission is required from the authors or the publisher. This journal does not charge APCs or submission charges.

Izvleček

Zaradi toksičnosti sintetičnih barvil naravna barvila vse bolj pridobivajo na pomenu kot okolju prijazna zamenjava, ki lahko poleg obarvanja vlaken zagotavlja tudi biofunkcionalne protibakterijske, protiglivične in antioksidativne lastnosti, še zlasti takrat, ko se uporabljajo skupaj z biočimžami. Cilj raziskave je bil ovrednotiti učinke uporabe biočimž na obarvljivost bombažnih tkanin z izvlečkom barvila *Erythrina abyssinica* ter proučiti antioksidativne in protimikrobne biofunkcionalne lastnosti tako obarvane bombažne tkanine. Biočimži, uporabljeni v tej raziskavi, sta bili pridobljeni iz lubja manga in izvlečkov rožmarina. Antioksidativno delovanje obarvane bombažne tkanine je bilo ocenjeno z metodo lovljenja prostih radikalov 2,2-difenil-1-pikrilhidrazila (DPPH), protimikrobna aktivnost pa ocenjena proti bakterijama *Escherichia coli* in *Staphylococcus aureus* z metodo neposredne absorpcije. Uporaba biočimž pri barvanju je privedla do povečanja intenzitete obarvanja (K/S) od vrednosti 0,601 na vrednost 0,762 in 0,692 za biočimži iz rožmarina oziroma manga. Bombaž, obarvan z *E. abyssinica*, je dosegel do 78,61-odstotno antioksidativno aktivnost in dobro protimikrobno aktivnost z 69,11-% in 70,06-% redukcijo rasti bakterij *E. coli* in *S. aureus*. Z uporabo biočimž so se izboljšale obstojnosti barve pri pranju, svetlobi in znoju. Rezultati potrjujejo, da je izvleček barvila *E. abyssinica* v kombinaciji z biočimžami primeren za barvanje in doseganje biofunkcionalnih lastnosti bombaža.

Ključne besede: naravna barvila, protioksidativno delovanje, protimikrobno delovanje, biočimže, obstojnost barvila

1 Introduction

Due to increased environmental concerns, the use of natural dyes in textile, food and leather has been discouraged because of their potential environmental toxicity [1]. Currently, between 15–40% of dyes are released as textile effluents into the environment, leading to adverse effects such as water coloration, toxicity, carcinogenicity and allergic effects [2]. Because of their high solubility, the process of removing most synthetic dyes is both expensive and difficult. For this reasons, natural dyes have often been touted as possible alternatives to their poisonous counterparts [3, 4]. Natural dyes comprise colorants derived from plants and mineral origins, with their main advantages being that they result in unique, soft and attractive shades with additional properties such as antimicrobial, antifungal, UV protective, skin friendly, etc. [5, 6].

Despite the fact that natural dyes have a many advantages, most of them have low colour fastness, meaning that they easily lose their shade, as they lack a good affinity to most fibres. For this reason, natural dyes are often combined with synthetic mordants to

help bind the dyes to fabric. Most synthetic mordants are polyvalent metallic salts that work by chelating to dye molecules, resulting in a complex link formation between the dye structure and the fibre. Currently, the most common mordants are copper sulfate, the potassium dichromate salts of iron, such as iron sulphate, and the salts of tin, such as tin chloride. [7]. Research shows that during the dyeing process, a fraction of the applied metallic mordant is absorbed by the fabric while a vast amount finds its way into the environment [8].

Conversely, there is equal concern that, despite most natural dyes being environmentally friendly, the amount of synthetic mordants dispelled into the environment still make it environmentally unfriendly. For this reason, natural or biomordants have been suggested. Studies have shown that biomordants generally improve both the colour strengths and fastness characteristics of natural dye in a similar way that has been observed with metallic mordants [9, 10]. This can be attributed to the diversity of phytochemical compounds present specifically in plants that are rich in compounds, such as tannins, which

have specifically been identified as excellent biomordants in the dyeing of linen and woollen fabric, using kapok flower extract in tandem with tannin-based natural mordant [11].

Apart from additional shades, natural dyeing and biomordanting, when combined, often lead to the biofunctionalization of textiles. This includes UV-protective properties, antioxidant, antibacterial, antifungal and deodorizing effects. Apart from these properties, natural textile materials, such as cotton and silk, are susceptible to different microbial attacks because they naturally provide suitable conditions, such as temperature and moisture, that enhance growth and the multiplication of microbes. Thus,

textiles that have been finished with antibacterial properties are currently preferred by most contemporary consumers [12–14].

The aim of this research was to determine the effects of biomordants from rosemary plant and mango bark on the dyeing properties of *E. abyssinica* natural dye extracts, and to evaluate the antioxidant, fastness and antimicrobial potentials of the natural dye on cotton fabric. The *E. abyssinica* plant, has been found to be rich in several phytochemicals such as flavonoids, isoflavonoids, alkaloids and chalcones. Some of the chemical structures of the compounds that have been isolated from this plant are as shown in Figure 1 [15–17].

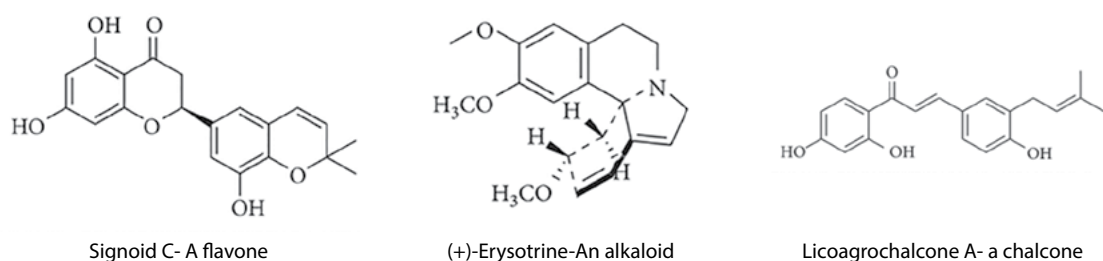


Figure 1: Compounds that have previously been isolated from *Erythrina Abyssinica*

2 Materials and methods

2.1 Materials

The stem bark of the *E. abyssinica* plant was harvested from the Nandi hills (0°07'36.8"N and 35°10'29.7"E) in Nandi County in Kenya. Plain woven and commercially bleached cotton fabrics (20 ends/cm, 13 picks/cm, 17.34 tex and 97.1 g/m²) were obtained from Rivatex East Africa, the textile facility of Moi University, and subsequently used for dyeing.

2.2 Extraction of the natural dye

The plant samples were first cleaned with tap water for the removal of impurities and dust particles. The cleaned samples were subsequently in the shade until there was no change in masses. They were then ground to fine powder to increase the extraction of surface area to volume ratio. The aqueous extraction

method was used to extract the dye, which was then filtered using filter paper.

2.3 Cotton pre-treatment

The wetting of 1g of cotton was carried out using 5 g/L of a non-ionic soap detergent for thirty minutes (Rivatex EA). The pretreatment of the fabric to increase its absorption ability was performed according to the method prescribed by [1]. The fabric was dipped in a 4% tannic acid (Loba Chemie, India) solution and pretreated for two hours, and subsequently washed and dried.

2.4 Dyeing experiments and biomordanting

The extraction of mango bark biomordant was performed as described by [18]. Extraction was done for one hour at a temperature of 90 °C using 75 g/L of the sample dissolved in distilled water. *Rosmarinus*

officinalis, commonly referred to as rosemary plant, was purchased from the Eldoret local market, dried under in the shade and subsequently ground to powder. A total of 20 g/L of the powder was dissolved in distilled water at 100 °C for 60 minutes. The biomordanting process was carried out using pre-mordanting, simultaneous/meta-mordanting and the post-mordanting methods.

The fabric was reduced into equal sizes of 1g each. The fabric was wetted with 5 g/L of non-ionic soap detergent for half an hour before dyeing with *E. abyssinica* aqueous dye extract. After the dyeing process, the dye bath (material to liquor ratio of 1:40) was left to cool and the subsequently dyed samples rinsed with cold water for the removal of any unfixed dyes. They were then subjected to soaping using 2 g/L of soap solution, followed by washing with distilled water and then air dried.

2.5 Colorimetric measurements

The colour characteristics of the dyed fabric samples were then measured using a Spectro -Flash X-rite SP62 spectrophotometer device with a D65 light source coupled with a 10° observer. The CIELAB coordinates that were measured in this study were a reddish-greenish colour that ranged between the points (+a* = red, -a* = green), a yellowish-bluish colour in the range (+b* = yellow, -b* = blue), with the light or brightness denoted as (L*), and the colour saturation (C) and hues (H*) with a plain undyed cotton fabric acting as the fabric blank.

The colour strengths denoted by the (K/S) values were determined using the Kubelka–Munk equation [19] as shown in equation 1.

$$\frac{K}{S} = \frac{(1-R)^2}{2R} \quad (1)$$

where *K* represents the coefficient of absorption, *S* represents the coefficient of scattering and *R* represents the minimum reflectance of the dye sample.

2.6 Fastness tests

Colour fastness was determined as follows: the dyed fabric were paired with another piece of the same material (cotton), and the two stitched together following the specifications of the ISO 105-C06:1994 standard. This combined fabric was then immersed in a solution containing 5 g/L of non-ionic detergent, maintaining a material-to-liquor ratio of 1:50, and processed at 50 °C for 45 minutes using an SDL Atlas Launder-o-meter. The samples were evaluated for colour loss, with differences assessed using the grey scale method according to the ISO 105-A02:1993 standard for colour change [20, 21].

For fastness to light, thin fabric strips, approximately 1 cm by 8 cm, were placed in test tubes and suspended on an exposure rack. The samples were then exposed to illumination for 4 hours using a 500 W SDL ATLAS light fastness tester. The loss of shade depth was subsequently evaluated using the grey scale method according to the ISO 105-A02:1993 [22–24] standard.

Rub fastness was tested using a Crock-meter (AATCC Model M238AA SDATLAS) according to the ISO 105-X12:2001 standard. The dyed fabric was mounted on the Crock-meter panel and rubbed ten times in both wet and dry conditions. The extent of staining was then evaluated on the specialised white fabric [22–24].

2.7 Antioxidant activity

The antioxidant activity of the undyed and dyed fabrics was calculated using the DPPH radical scavenging assay according to [13]. Pure and dyed cotton fabric measuring 2.54 cm² was separately immersed in a test tube containing a 50mL solution of DPPH that was diluted in methanol (0.15 mM). Afterwards, the samples were incubated at room temperature inside a dark room for half an hour. The solution's absorbance was then measured using a Beckman Coulter 720 (USA) UV-Vis device at a wavelength of 517 nm, and the percentage antioxidant activity calculated using the equation 2:

$$A = \frac{A_{control} - A_{sample}}{A_{control}} \times 100 (\%) \quad (2)$$

where A represents the calculated percentage antioxidant activity, $A_{control}$ represents the initial absorbance and A_{sample} represents the absorbance of DPPH remaining after incubation with the sample.

2.8 Antibacterial activity

The antibacterial properties of both dyed and biomordanted fabric were assessed using the absorbance technique as described by [13]. A piece of fabric, measuring 1.27 cm², was dipped into a 25 mL solution of nutrient broth that had been inoculated with *E. coli* and *S. aureus*. The broth was again incubated in an automated incubator (Unitronic – J.P. Selector) at 37 °C for exactly 24 hours and the absorbance of the bacteria culture media evaluated at 595 nm using a UV-Visible Beckman Coulter 720 (USA) spectrometer. The reduction percentages of the bacterial growths were the calculated using equation 3:

$$R = \frac{B-A}{B} \times 100 (\%) \quad (3)$$

where R represents the percentage reduction in antimicrobial activity and B represents the absorbance of media that has been inoculated with the microbe

and subsequently introduced in the undyed cotton fabric. A represents the absorbance of media inoculated with microbes and introduced in the dyed cotton fabric.

2.9 Percentage durability of antibacterial finishing to washing cycles

The antibacterial and antioxidant durability on the cotton fabric was evaluated after the fabric was subjected to several wash cycles, namely after the 1st, 5th and 10th wash cycles according to [25, 26]. This was done by washing the samples in a washing solution of 2 g/L commercial detergent with a material to liquor ration of 1.50.

2.10 UV-VIS analysis of dye








Extracts of *E. Abyssinica* were analysed using a UV-Visible Beckman Coulter 720 (USA) device in the ranges of 200–800 nm.

3 Results and discussion

3.1 Colorimetric analysis of biomordanted cotton fabric

The colorimetric analysis of the fabric dyed with *E. abyssinica* was evaluated and the results are presented in Table 1.

Table 1: Colorimetric values of *E. abyssinica* dyed fabric

Mordanting method	Mordant	L*	a*	b*	C*	H°	K/S	Fabric
-	None	87.9	-0.8	+20.1	18.7	92.7	0.601	
Pre-mordanting	Mango bark	86.1	+1.4	+15.1	15.2	84.5	0.692	
	Rosemary	86.0	+0.6	+26.2	23.1	88.3	0.762	
Meta-mordanting	Mango bark	87.5	+2.0	+14.7	23.9	88.4	0.618	
	Rosemary	86.7	+0.4	+25.2	23.0	88.4	0.663	
Post-mordanting	Mango bark	87.9	+2.2	+14.5	23.5	88.3	0.611	
	Rosemary	85.9	+0.9	+27.2	22.9	88.1	0.630	

All the dyed fabric resulted in different shades of brown with the introduction of mordants, leading to the brightening of the shades of brown. This can be concluded from the *L* values, where the cotton fabric dyed without the mordant and the one post-mordanted with Mango had the highest *L* value of 87.9, while the others had lower values [27]. Equally, the results suggest that the use of biomordants successfully improved the colour strengths (*K/S*) of the dye

from 0.601 to a high of 0.7620 for rosemary and 0.692 for mango biomordants [28, 29]. Moreover, the highest colour strengths were achieved when fabric dyeing was performed using pre-mordanting in both cases.

3.2 Fastness properties of dyed fabric

The colour, wash, rub, light and perspiration fastness were evaluated and the reports presented in Table 2.

Table 2: Colour fastness properties of dyed cotton fabric using different mordanting techniques

Method	Mordant	Washing fastness		Rubbing fastness		Perspiration fastness		Light fastness
		Colour change	Colour staining	Dry	Wet	Colour change	Colour staining	
-	Without	2.5	2.5	3.0	3.0	4	4	3.0
Pre	Mango bark	4.5	4.5	5	5	4.5	4.5	4.5
	Rosemary	4.5	4.5	4.5	4.5	5	5	4
Meta	Mango bark	4	4.5	4	4	4.5	4	4
	Rosemary	4	4.5	4	4	4.5	4.5	4
Post	Mango bark	4	4.5	4	4	4.5	4.5	4
	Rosemary	4	4.5	4	4	4.5	4.5	4

The wash fastness of the fabric dyed without any mordant was average before the introduction of mordants. After mordants were used, there was a significant improvement in the wash properties from an average of (2.5) to excellent (4.5). This shows that the mordants successfully improved the fixation of the dye to the fabric [30]. Similar results have also been reported with other natural dyes, where the introduction of mordants and biomordants, significantly improved dye wash fastness properties [31–33].

It can also be concluded from the table that biomordanting improved the rubbing, perspiration and light fastness of the fabric [28]. In general, the pre-mordanting technique of dyeing achieved the best overall results, as it significantly improved the wash, rub, perspiration and light fastness compared with other methods.

3.3 Antibacterial activity of the dyed cotton fabric

The antibacterial activity of the biomordanted fabric was evaluated using the absorbance method and the results are presented in Figure 2. Previous literature

indicates that most natural dyes extracts of *E. abyssinica* demonstrate antimicrobial activity [16].

It is evident from Figure 2 that the dyeing of cotton with biomordants increased bacterial reduction abilities from 61.3%, when unmordanted, to 68.6% and 69.1%, respectively, when mordanted with mango and rosemary in *E. coli*. Moreover, for *S. Aureus*, the bacterial reduction percentage also increased from 64.3%, when unmordanted, to 68.9% and 70.1%, respectively. These results are similar to other results reported in literature, where biomordants not only improved fabrics fastness but also introduced bacterial reduction properties [12].

Fabric biomordanted with rosemary extracts demonstrated a higher bacterial reduction efficacy than fabric biomordanted with mango bark extracts. This could be attributed to the presence of additional phenolic hydroxyl groups from the rosemary biomordant extracts, which enhance the bacterial inhibition ability of the dye [28].

3.4 Antibacterial activity after wash cycles

The laundering durability of the dyed samples was assessed and the results presented in Figure 2.

Percentage bacteria reduction refers to the percentage decrease in the bacteria population [6]. It is evident from the results above that antibacterial activity decreased continuously as the number of washes increased. Similar results have also been observed in literature, where antimicrobial inhibition activities decrease with an increase in the number of

washes [4, 11, 12].

In this case, it was observed that the decrease in antimicrobial efficacy was negligible for mordanted fabric compared with unmordanted fabric. The ability to retain the antimicrobial activity of the dyed fabric in some cases above 50% even after the 10th successive wash proved that the *E. divinorum* dye extract was good for the development of antimicrobial functionalized textile fabric [4].

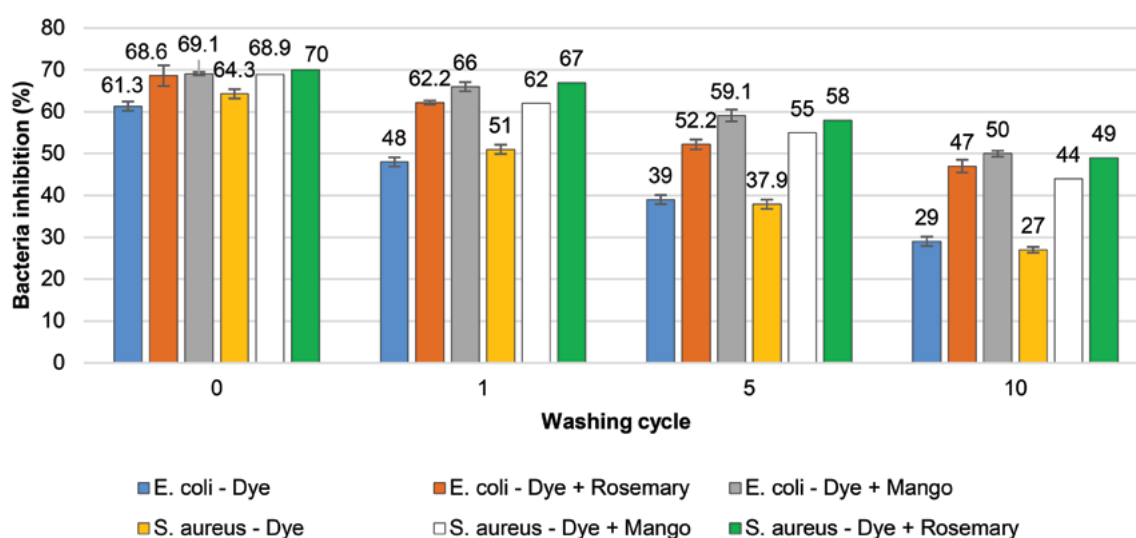


Figure 2: Bacteria reduction of fabric against *E. coli* and *S. aureus* after washing cycles

3.5 Percentage antioxidant activity of the dyed fabric before and after wash cycles

The antioxidant activity of the dyed cotton fabric is shown in Figure 3. It can be concluded from Figure 3 that the mordanting of fabric with biomordants increased the antioxidant activity of the fabric from a low of 26.9, without mordant, to a high of 78.6 when dyed with rosemary mordant [34]. This result is similar to others which suggest that both mango and rosemary extract biomordants increase the antioxidant properties of fabric due the high number of polyphenols present in them [34–36].

In addition, the antioxidant activity was examined after the 1st, 5th and 10th wash cycles as seen in Figure 3. A reduction in the antioxidant activity was observed as the number of washes increased, as has

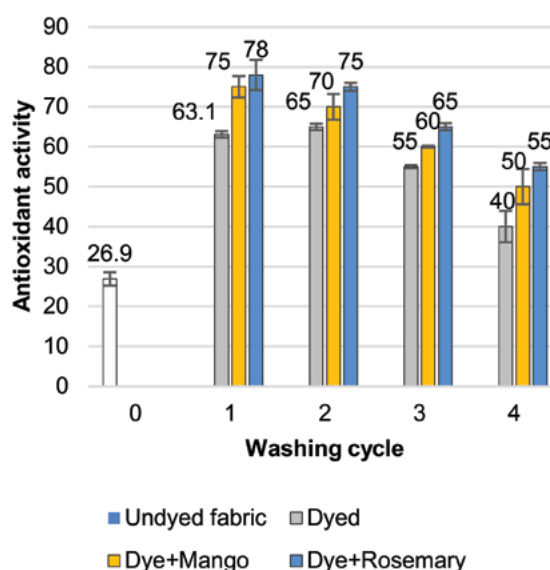


Figure 3: Antioxidant activity after wash cycles

been recorded in similar studies [37]. Overall, the rosemary mordanted fabric had higher antioxidant activities even after 10 wash cycles.

3.6 UV VIS spectroscopy analysis

A UV-Visible analysis of the *E. abyssinica* dye extracts (Figure 4) showed that the dye contained a mixture. This is not unique to these extracts, as other natural dyes have also been discovered to be a mixture of compounds as previously discussed by [38, 39].

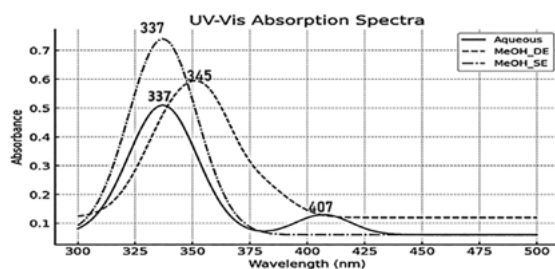


Figure 4: UV-Visible spectra of *E. abyssinica* extracts

The extracts showed several peaks at 407 nm, 345 nm and 337 nm. These peaks have previously been proven to belong to flavonoids that are usually yellowish in colour. It can thus be suggested that *E. Abyssinica* dyes are flavonoid rich [40].

4 Conclusion

Dyeing cotton fabric with extracts of *E. abyssinica* in the presence of biomordants enhanced the colour strength of the dyes from 0.601 to 0.762 and 0.692 for rosemary and mango biomordants, respectively. The *E. abyssinica* dye extract imparted an antimicrobial activity to a maximum of 69.11% and 70.06% against *E. coli* and *S. aureus*, respectively. The antimicrobial and antioxidant activities were increased when biomordants were used. Dyeing properties, such as wash fastness, light fastness, colour fastness and perspiration, were examined before and after biomordanting, with the results indicating that the biomordants improved the dyeing properties of *E. Abyssinnica* dye. As a result, it can be concluded that

E. Abyssinica dye extracts are suitable for use and the development of biofunctionalized textile fabric.

Author contributions: conceptualization – Scolastica Manyim and Ambrose Kiprop; methodology – Scolastica Manyim, Ambrose Kiprop, Josephat Mwasiagi, Cleophas Achisa and Mark Odero; formal analysis – Scolastica Manyim and Mark Odero; investigation – Scolastica Manyim and Josephat Mwasiagi; writing (original draft preparation) – Scolastica Manyim and Mark Odero; writing (review and editing) – Ambrose Kiprop, Josephat Mwasiagi and Cleophas Achisa; visualization – Scolastica Manyim; supervision – Ambrose Kiprop, Josephat Mwasiagi and Cleophas Achisa. All authors have read the manuscript and have approved it for publication.

Conflicts of interest: The authors declare that there is no conflict of interest.

Acknowledgements: This research was supported by the Africa Centre of Excellence II in Phytochemicals, Textile and Renewable Energy (ACEII-PTRE,) a World Bank funded project. We acknowledge support from Rivatex East Africa Limited (the textile facility of Moi University) and the Department of Chemistry and Biochemistry of Moi University.

References

1. ODERO, M.P., KIPROP, A.K., K'OWINO, I.O., ARIMI, M., MANYIM, S. Evaluation of dyeing properties of natural dyes extracted from the heartwood of *Prosopis juliflora* on cotton fabric. *Research Journal of Textile and Apparel*, 2021, 25(1), 19–30, doi: 10.1108/RJTA-06-2020-0058.
2. GURU, R., RANI, J. Dyeing tencel fabric with azadirachta indica leaves and mordanting with potassium aluminium sulphate and *Citrus limon* extract for enhanced fastness properties. *Textile & Leather Review*, 2023, 6, 498–516, doi: 10.31881/TLR.2023.104.

3. ADEEL, S., ZIA, K. M., ABDULLAH, M., REHMAN, F. U., SALMAN, M., ZUBER, M. Ultrasonic assisted improved extraction and dyeing of mordanted silk fabric using neem bark as source of natural colourant. *Natural Product Research*, 2019, **33**(14), 2060–2072, doi: 10.1080/14786419.2018.1484466.
4. MANYIM, S., KIPROP, A. K., MWASIAGI, J.I., MECHA, A.C. Cleaner production of bio-active and coloured cotton fabric using euclea divinatorum dye extract with bio-mordants. *Tekstilec*, 2023, **66**(1), 38–46, doi: 10.14502/tekstilec.66.2022072.
5. KAMBOJ, A., JOSE, S., SINGH, A. Antimicrobial activity of natural dyes—a comprehensive review. *Journal of Natural Fibers*, 2022, **19**(13), 5380–5394, doi: 10.1080/15440478.2021.1875378.
6. SHAHID, M., AHMAD, A., YUSUF, M., KHAN, M. I., KHAN, S. A., MANZOOR, N., MOHAMMAD, F. Dyeing, fastness and antimicrobial properties of woolen yarns dyed with gallnut (*Quercus infectoria* Oliv.) extract. *Dyes and Pigments*, 2012, **95**(1), 53–61, doi: 10.1016/j.dyepig.2012.03.029.
7. HAAR, S., SCHRADER, E., GATEWOOD, B.M. Comparison of aluminum mordants on the colorfastness of natural dyes on cotton. *Clothing and Textiles Research Journal*, 2013, **31**(2), 97–108, doi: 10.1177/0887302X13480846.
8. VANKAR, P. S., SHUKLA, D. *New Trends in Natural Dyes for Textiles*. Woodhead Publishing, 2019, 139–158, doi: 10.1016/B978-0-08-102686-1.00003-2.
9. PINHEIRO, L., KOHAN, L., DUARTE, L. O., GARAVELLO, M.E.D.P.E., ARUQUE-RAMOS, J. Biomordants and new alternatives to the sustainable natural fiber dyeings. *SN Applied Sciences*, 2019, **1**, 1–8, doi: 10.1007/s42452-019-1384-5.
10. İŞMAL, Ö. E., YILDIRIM, L. Metal mordants and biomordants. In *The Impact and Prospects of Green Chemistry for Textile Technology*. Edited by Shahid-ul-Islam and B.S. Butola. Woodhead Publishing, 2019, 57–82, doi: 10.1016/B978-0-08-102491-1.00003-4.
11. KETEMA, A., WORKU, A. Antibacterial finishing of cotton fabric using stinging nettle (*Urtica dioica* L.) plant leaf extract. *Journal of Chemistry*, 2020, **2020**, 1–10, doi: 10.1155/2020/4049273.
12. PRABHU, K.H., TELI, M.D. Eco-dyeing using *Tamarindus indica* L. seed coat tannin as a natural mordant for textiles with antibacterial activity. *Journal of Saudi Chemical Society*, 2014, **18**(6), 864–872, doi: 10.1016/j.jscs.2011.10.014.
13. RATHER, L.J., AZAM, M., SHABBIR, M., BUKHARI, M.N., SHAHID, M., KHAN, M.A., HAQUE, Q.M.R., MOHAMMAD, F. Antimicrobial and fluorescence finishing of woolen yarn with *Terminalia arjuna* natural dye as an ecofriendly substitute to synthetic antibacterial agents. *RSC Advances*, 2016, **6**(45), 39080–39094, doi: 10.1039/c6ra02717b.
14. BAAKA, N., MAHFOUDHI, A., HADDAR, W., MHENNI, M. F., MIGHRI, Z. Green dyeing process of modified cotton fibres using natural dyes extracted from *Tamarix aphylla* (L.) Karst. leaves. *Natural Product Research*, 2017, **31**(1), 22–31, doi: 10.1080/14786419.2016.1207072.
15. CHITOPPOA, W., MUCHACHAA, I., MANGOYI, R. Evaluation of the antimicrobial activity of *Erythrina abyssinica* leaf extract. *Journal of Microbial & Biochemical Technology*, 2019, **11**(2), 1–4, doi: 10.4172/1948-5948.1000413.
16. OBAKIRO, S.B., KIPROP, A., KIGONDU, E., K'OWINO, I., ODERO, M.P., MANYIM, S., OMARA, T., NAMUKOBE, J., OWOR, R.O., GAVAMUKULYA, Y., BUNALEMA, L. Traditional medicinal uses, phytoconstituents, bioactivities, and toxicities of *Erythrina abyssinica* Lam. ex DC.(fabaceae): a systematic review. *Evidence-Based Complementary and Alternative Medicine*, 2021, **2021**, 1–43, doi: 10.1155/2021/5513484.
17. MUTHUKRISHNAN, S., PALANISAMY, S., SUBRAMANIAN, S., SELVARAJ, S., MARI, K.R., KUPPULINGAM, R. Phytochemical profile of *Erythrina variegata* by using high-performance

- liquid chromatography and gas chromatography-mass spectroscopy analyses. *Journal of Acupuncture and Meridian Studies*, 2016, **9**(4), 207–212, doi: 10.1016/j.jams.2016.06.001.
18. WANGATIA, L.M., TADESSE, K., MOYO, S., WANGATIA, L.M., TADESSE, K., MOYO, S. Mango bark mordant for dyeing cotton with natural dye: fully eco-friendly natural dyeing. *International Journal of Textile Science*, 2015, **4**(2), 36–41, doi: 10.5923/j.textile.20150402.02.
 19. BAAKA, N., HADDAR, W., BEN TICHA, M., MHENNI, M.F. Eco-friendly dyeing of modified cotton fabrics with grape pomace colorant: optimization using full factorial design approach. *Journal of Natural Fibers*, 2019, **16**(5), 652–661, doi: 10.1080/15440478.2018.1431997.
 20. ZUBAIRU, A., MSHELIA, Y.M. Effects of selected mordants on the application of natural dye from onion skin (*Allium cepa*). *Science and Technology*, 2015, **5**(2), 26–32, doi: 10.5923/j.scit.20150502.02.
 21. YUSUF, M., MOHAMMAD, F., SHABBIR, M. Eco-friendly and effective dyeing of wool with anthraquinone colorants extracted from *Rubia cordifolia* roots: optimization, colorimetric and fastness assay. *Journal of King Saud University-Science*, 2017, **29**(2), 137–144, doi: 10.1016/j.jksus.2016.06.005.
 22. JIHAD, R. Dyeing of silk using natural dyes extracted from local plants. *International Journal of Scientific & Engineering Research*, 2014, **5**(11), 809–818.
 23. KUMARESAN, M. Dyeing of silk fabric with eco-friendly natural dye obtained from flower of *Thespesia populnea* using single mordants. *International Journal of ChemTech Research*, 2018, **11**(2), 161–167, doi: 10.20902/IJC-TR.2018.110220.
 24. KUMARESAN, M., PALANISAMY, P.N., KUMAR, P.E. Application of ecofriendly natural dye on silk using combination of mordants. *International Journal of Chemistry Research*, 2011, **2**(1), 11–14, <https://ijcr.info/index.php/journal/article/view/21>.
 25. LI, Y. D., GUAN, J.P., TANG, R.C., QIAO, Y.F. Application of natural flavonoids to impart antioxidant and antibacterial activities to polyamide fiber for health care applications. *Antioxidants*, 2019, **8**(8), 1–15, doi: 10.3390/antiox8080301.
 26. BUTOLA, B. S. A synergistic combination of shrimp shell derived chitosan polysaccharide with *Citrus sinensis* peel extract for the development of colourful and bioactive cellulosic textile. *International Journal of Biological Macromolecules*, 2020, **158**, 94–103, doi: 10.1016/j.ijbiomac.2020.04.209.
 27. YUSUF, M., SHAHID, M., KHAN, M. I., KHAN, S.A., KHAN, M.A., MOHAMMAD, F. Dyeing studies with henna and madder: a research on effect of tin (II) chloride mordant. *Journal of Saudi Chemical Society*, 2015, **19**(1), 64–72, doi: 10.1016/j.jscs.2011.12.020.
 28. İŞMAL, Ö. E., YILDIRIM, L., ÖZDOĞAN, E. Use of almond shell extracts plus biomordants as effective textile dye. *Journal of Cleaner Production*, 2014, **70**, 61–67, doi: 10.1016/j.jclepro.2014.01.055.
 29. BUKHARI, M.N., SHABBIR, M., RATHER, L.J., SHAHID, M., SINGH, U., KHAN, M.A., MOHAMMAD, F. Dyeing studies and fastness properties of brown naphthoquinone colorant extracted from *Juglans regia* L on natural protein fiber using different metal salt mordants. *Textiles and Clothing Sustainability*, 2017, **3**, 1–9, doi: 10.1186/s40689-016-0025-2.
 30. SINGH, G., MATHUR, P., SINGH, N., SHEIKH, J. Functionalization of wool fabric using kapok flower and bio-mordant. *Sustainable Chemistry and Pharmacy*, 2019, **14**, 1–6, doi: 10.1016/j.scp.2019.100184.
 31. KUMBHAR, S., HANKARE, P., SABALE, S., KUMBHAR, R. Eco-friendly dyeing of cotton with brown natural dye extracted from *Ficus amplissima* Smith leaves. *Environmental Chemistry Letters*, 2019, **17**(2), 1161–1166, doi: 10.1007/s10311-018-00854-w.

32. LOHTANDER, T., AROLA, S., LAAKSONEN, P. Biomordanting willow bark dye on cellulosic materials. *Coloration Technology*, 2020, **136**(1), 3–14, doi: 10.1111/cote.12442.
33. BONET, M.Á., BOU, E., MONTAVA, I., DIAZ, P. Dyeing cotton with *Eisenia Bicyclis* as natural dye using different biomordants. *Annals of the University of Oradea. Fascicle of Textiles, Leatherwork*, 2015, **16**(2), 9–12.
34. SULTANA, B., HUSSAIN, Z., ASIF, M., MUNIR, A. Investigation on the antioxidant activity of leaves, peels, stems bark, and kernel of mango (*Mangifera indica* L.). *Journal of Food Science*, 2012, **77**(8), C849–C852, doi: 10.1111/j.1750-3841.2012.02807.x.
35. COELHO, E.M., DE SOUZA, M.E.A.O., CORRÊA, L.C., VIANA, A.C., DE AZEVEDO, L.C., DOS SANTOS LIMA, M. Bioactive compounds and antioxidant activity of mango peel liqueurs (*Mangifera indica* L.) produced by different methods of maceration. *Antioxidants*, 2019, **8**(4), 1–11, doi: 10.3390/antiox8040102.
36. CHRAIBI, M., FARAH, A., ELAMIN, O., IRAQUI, H.M., FIKRI-BENBRAHIM, K. Characterization, antioxidant, antimycobacterial, antimicrobial effects of Moroccan rosemary essential oil, and its synergistic antimicrobial potential with carvacrol. *Journal of Advanced Pharmaceutical Technology & Research*, 2020, **11**(1), 25–29, doi: 10.4103/japtr.JAPTR_74_19.
37. SHEIKH, J., BRAMHECHA, I. Multifunctional modification of linen fabric using chitosan-based formulations. *International Journal of Biological Macromolecules*, 2018, **118**, 896–902, doi: 10.1016/j.ijbiomac.2018.06.150.
38. SELVAM, R.M., ATHINARAYANAN, G., NANTHINI, A.U.R., SINGH, A.R., KALIRAJAN, K., SELVAKUMAR, P.M. Extraction of natural dyes from *Curcuma longa*, *Trigonella foenum graecum* and *Nerium oleander*, plants and their application in antimicrobial fabric. *Industrial Crops and Products*, 2015, **70**, 84–90, doi: 10.1016/j.indcrop.2015.03.008.
39. KAUR, V., ARJUNAN, S., NANAIAH, I. Extraction of dyes from plant sources and their application on cotton and wool using mordants. *Current Trends in Biotechnology and Pharmacy*, 2021, **15**(5), 503–506, doi: 10.5530/ctbp.2021.3s.46.
40. WAN, Y.W.A., RAHIM, R., AHMAD, M.R., KADIR, M.I.A., MISNON, M.I. The application of Gluta aptera wood (Rengas) as natural dye on silk and cotton fabrics. *Universal Journal of Environmental Research and Technology*, 2011, **1**, 545–551.

Hafsa Ibrahim, Mumtaz Hasan Malik, Ahmad Fraz, Imran Ahmad Khan

Department of Textile and Apparel Science, University of Management and Technology, Lahore-54470, Pakistan

From Waste to Weave: Recycling Industrial and Consumer Cotton Waste for Sustainable and Cost-Effective Terry Fabric Production

Od odpadkov do tkanja: recikliranje industrijskih in potrošniških bombažnih odpadkov za trajnostno in stroškovno učinkovito proizvodnjo frotirja

Original scientific article/Izvirni znanstveni članek

Received/Prispelo 9–2024 • Accepted/Sprejeto 1–2025

Corresponding author/Korespondenčni avtor:

Imran Ahmad Khan

Tel: +92-3139374141

E-mail: enggimran110@gmail.com

ORCID iD: 0000-0002-7127-5509

Abstract

The textile sector is a major source of global pollution and resource depletion, generating waste at every stage of production, from spinning to garment manufacturing. This study addresses the critical need for sustainability in the textile industry by exploring the recycling of pre- and post-consumer textile waste to produce terry fabric. This research emphasizes a sustainable approach to recycling, utilizing pre-consumer waste, such as blowroom and carding waste, alongside post-consumer waste from discarded garments. These recycled fibres were spun into yarn and woven into terry fabric, and their properties compared to those of virgin cotton terry. While virgin cotton terry exhibited minor advantages in visual and tactile qualities, other properties remained consistent across all samples. A cost analysis further demonstrated the feasibility of producing medium to high-quality terry fabric from recycled yarn, providing a cost-effective alternative to virgin cotton. The research work contributes to the advancement of sustainable textile production, underscoring the potential of recycling to mitigate the environmental impact of the textile industry.

Keywords: recycling; sustainability; cotton waste; terry fabric; cost-effectiveness

Graphical abstract



Content from this work may be used under the terms of the Creative Commons Attribution CC BY 4.0 licence (<https://creativecommons.org/licenses/by/4.0/>). Authors retain ownership of the copyright for their content, but allow anyone to download, reuse, reprint, modify, distribute and/or copy the content as long as the original authors and source are cited. No permission is required from the authors or the publisher. This journal does not charge APCs or submission charges.

Izvleček

Tekstilni sektor je z ustvarjanjem odpadkov na vseh stopnjah proizvodnje, od predenja do izdelave oblačil, velik vir globalnega onesnaževanja in izčrpavanja virov. Ta raziskava obravnava nujno potrebo po trajnosti v tekstilni industriji z vidika recikliranja industrijskih in popotrošnih odpadkov za proizvodnjo frotirja. V raziskavi je poudarjen trajnostni pristop k recikliranju industrijskih odpadkov, kot so odpadki pri rahljanju in mikanju vlaken, ter zavrženih oblačil. Reciklirana vlakna so bila predelana v prejo in frotir, ki je bil primerjan s frotirjem iz nerekiciranega bombaža. Frotir iz recikliranega bombaža je bil za malenkost slabšega videza in otipa kot frotir iz nerekiciranega bombaža, druge lastnosti pa so se pokazale kot zelo ponovljive. Analiza stroškov je potrdila izvedljivost proizvodnje srednje- do visokokakovostnega frotirja iz reciklirane preje, ki lahko zagotavlja stroškovno učinkovito zamenjavo nerekiciranega bombaža. Raziskava pripomore k napredku trajnostne proizvodnje tekstilij in poudarja potencial recikliranja za ublažitev vpliva tekstilne industrije na okolje.

Ključne besede: recikliranje, trajnost, bombažni odpadki, frotirna tkanina, stroškovna učinkovitost

1 Introduction

Sustainability has become one of the most critical discussions of today, and is driven by the need to extend the lifecycle of products and reduce waste before those products are discarded. Sustainability encompasses three key aspects: environmental, economic and societal [1]. Embracing these principles requires a commitment to the 3R (reduce, reuse and recycle) or the expanded 4R (reduce, reuse, recycle and rebuy) concepts, with the latter broadening the scope of sustainable practices by encouraging consumers to repurchase recycled goods. The economic, social and environmental benefits of recycling are significant [2]. Recycling contributes to waste reduction and plays a crucial role in the preservation of natural resources [3]. Economically, recycling is often more cost-effective than producing new products from raw materials in some cases, as it conserves energy, reduces production costs and minimizes the financial burden associated with waste disposal facilities. Socially, recycling initiatives create job opportunities and support small business ventures focused on producing recycled goods, thereby enhancing community welfare [4–6].

The global production of textile fibres has risen dramatically, from 23.9 million metric tons (Mt) in 1975 to 98.5 Mt in 2017, driven by increasing fashion

demand. This growth has led to significant waste generation, with approximately 26 Mt of garments dumped annually and only 3.5 Mt recycled in 2017. In China, textile waste ranges from 20 to 26 Mt per year, with the recycling rate remaining critically low, while around 45% of produced textiles are wasted. In 2010, textile waste accounted for 13.2 Mt or 5.3% of global municipal solid waste (MSW). Addressing this issue through recycling practices, such as converting textile waste into usable yarns, supports sustainability by reducing landfill use, conserving energy and reducing environmental impacts, in line with circular economy principles [7].

Textile waste presents a significant environmental challenge due to its substantial volume and slow decomposition rate [8]. The fashion industry's rapid cycles and consumer trends contribute to the overconsumption of clothing, leading to increased textile waste generation [9]. The global recycling rates for textile waste remain low, with only 10% of generated clothing waste being recycled, 8% reused and the majority either landfilled or incinerated [10]. Textile waste can be categorized into pre-consumer and post-consumer waste [11]. Pre-consumer waste refers to the waste generated during the production process, from fibre generation to garment manufacturing, and is often recycled into low-grade yarns or used as filling materials for automotive, building

insulation and furnishings [12]. Approximately 75% of pre-consumer waste is recycled in this manner. Post-consumer waste, which consists of discarded clothing and textile products, presents a greater challenge, with only 15% being recycled [13]. While thermoplastic polymer-based fibres are commonly recycled due to their ease of processing and ability to be reshaped, natural fibres pose a greater challenge, as recycling processes can compromise their quality [14].

Cotton, a natural fibre known for its softness, absorbency, comfort, breathability and hypoallergenic properties, is highly regarded by consumers, particularly in cotton and cotton-blend apparel [15]. Currently, cotton constitutes 25% of all fibres utilized in textiles, with its consumption steadily increasing in response to global population growth and the gradual recovery from the impacts of COVID-19 in major cotton-consuming nations such as China, Bangladesh, Pakistan, India and Mexico [16]. Additionally, global cotton prices have been on an upward trajectory since July 2021, driven by rising demand [17]. Given the increasing demand for cotton and stringent environmental regulations on waste management, there is a clear need to develop a sustainable strategy for recovering cotton from textile waste through an eco-responsible approach.

Recycling can be achieved by mechanically extracting fibres from waste yarns and fabrics through shredding, a process that forcefully tears the materials back into their original fibre components. However, this method often results in fibres of very short lengths and small fibre clumps, which are unsuitable for spinning into yarns on their own [18]. To overcome this limitation, recycled fibres are blended with virgin fibres, which serve as carriers during the spinning process. However, this approach enables the production of coarser and disoriented yarns [10]. To overcome this issue, ring spinning is the most commonly used spinning system due to its versatility in producing a wide range of yarn types, from low-twist soft and absorbent yarns to highly twisted, coarse or fine yarns [19]. Ring-spun yarns,

which lack wrapper fibres, provide a smoother texture for the wearer [20].

Previous research on textile waste recycling has primarily focused on single-source waste streams. This study is innovative, as it comprehensively compares fabrics made from both pre- and post-consumer textile waste, alongside virgin cotton, particularly for terry fabric. This dual-waste approach offers a more holistic perspective on textile waste reuse. A detailed comparison of recycled and virgin yarns was conducted to assess their fibre properties, yarn characteristics and fabric performance, with the aim of demonstrating the potential of recycled fibres for terry fabric production. This study highlights the environmental benefits and economic viability of producing terry fabric from recycled yarn, without compromising fabric quality. The study's findings are readily applicable to existing textile manufacturing processes, making them practical and valuable for industry adoption. By addressing both sustainability and economic aspects, this research provides valuable contributions to the field of sustainable textile production. This paper explores the importance of textile waste recycling and its potential benefits. It delves into the economic and environmental advantages of recycling, while also discussing the challenges and opportunities associated with the recycling method. By understanding the significance of textile waste recycling, we can work towards a more sustainable and circular economy.

2 Materials and methods

The chemicals used in the bleaching process were hydrogen peroxide (50%, Merk, Germany), sodium hydroxide (99%, Sigma Aldrich, USA) and acetic acid (99%, Fisher scientific, UK). The experimentation was carried out by collecting two different types of waste. The waste includes pre-consumer and post-consumer waste. The waste was first converted into fibre, and then spun into yarn. The recycled yarn was then used for the weaving of the final

product i.e., terry towels. Pakistani virgin cotton was used as raw material for virgin yarn. The recycling process utilized both pre-and post-consumer waste and involves the steps shown in Figure 1.

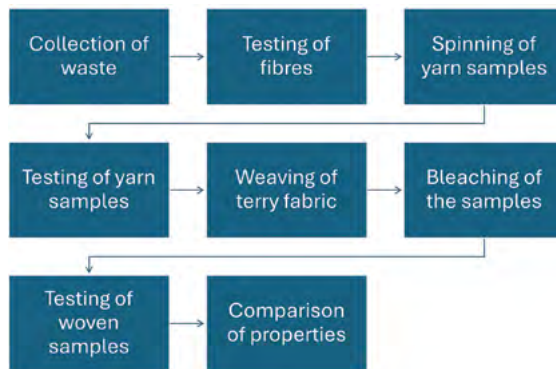


Figure 1: Flowchart illustrating the production of ring-spun yarns from blends of virgin cotton and recycled cotton fibres sourced from pre- and post-consumer textile waste

2.1 Collection of waste

For the preparation of pre-consumer waste (PCW), blow room dropping, card licker and card fly were employed. Approximately 10–11% of the waste from both the blowroom and carding processes was extracted. Post-consumer textile cotton waste was collected from used cotton garments and household textiles and then sorted to remove non-cotton items and heavily contaminated or damaged fabrics. Only 100% cotton textiles were selected, cleaned and processed to remove non-fibrous components before being shredded into fibres for yarn production.

The collection and processing of both pre-consumer and post-consumer textile waste were conducted systematically to ensure efficient reuse. Pre-consumer waste was gathered during the spinning and weaving stages. In the spinning process, blow room, carding and draw frame wastes were collected using suction systems, thereby facilitating their direct utilization. Similarly, warping, sizing and loom selvedge wastes from the weaving process were recovered. Post-consumer waste primarily consisted of garment cutting remnants collected from garment

manufacturing facilities. These remnants underwent a manual sorting process to eliminate non-textile and non-cotton components, such as zippers, buttons and synthetic materials.

After sorting, the textile waste was reduced to smaller pieces using a MARGASA MC 1500 machine. The cut pieces were then conditioned by applying 2% water (based on the fabric's weight) and left for at least 12 hours to minimize the risk of fire during shredding. The shredding machine was equipped with carding cylinders fitted with sets of strong, sharp wires arranged in opposing directions. These wires effectively tore the yarns and cut fabric pieces, gradually transforming them into individual fibres through robust carding actions. The sharp wires on the cylinders facilitated this process by applying heavy and abrasive forces. The extracted fibres were subsequently compacted into bales and transported to the mixing room for further processing.

2.2 Process for producing yarn from pre-consumer textile waste

Due to the inadequate quality of pre-consumer fibre, it could not be used alone. Therefore, virgin cotton fibre was added to ensure the overall quality of the yarn. The ratio used for producing pre-consumer yarn consisted of 20% pre-consumer/post-consumer waste fibre and 80% virgin cotton fibre. This consistent mixing ratio was maintained to facilitate a clear and fair comparison between the two types of recycled fibres. During the spinning process, the following specifications were standardized to ensure comparability: the yarn count for all fibres (pre-consumer, post-consumer and virgin) was maintained at the same level, all yarns were ring-spun carded yarns and the mixing percentages for both pre-and post-consumer fibres were identical. The yarn was produced using a ring spinning machine, which is known for its consistent quality and efficiency. The yarn count was set to 49.2 tex (12 Ne), and the twist number was set to 20 TPI, thereby ensuring the required strength and evenness of the yarn. Spinning conditions were maintained under standard industry parameters, with

the temperature controlled at approximately 20–22 °C and relative humidity maintained at 65–70%. These conditions were optimized to ensure stable processing and achieve the desired yarn properties for subsequent applications.

2.3 Spinning of yarn

The spinning of pre-consumer, post-consumer and virgin yarns was performed according to the ring spinning method. Yield percentages for pre-consumer, post-consumer and virgin cotton yarns were 81%, 83.5% and 83%, respectively. The blowroom process revealed significant differences between the three yarn types. Pre-consumer yarn experienced increased wastage, decreased growth and decreased staple length. In contrast, post-consumer yarn showed decreased wastage, increased growth and increased staple length. Virgin yarn maintained standard waste, exhibited improved growth and had good staple length. During the carding, drawing/simplex, ring frame and auto cone processes, pre-consumer yarn generally exhibited lower quality, higher wastage and poorer appearance compared to post-consumer and virgin yarns. Post-consumer yarn often had better quality and similar production parameters to virgin yarn, with some exceptions. Overall, virgin yarn consistently demonstrated higher quality, better appearance and similar production performance to post-consumer yarn.

2.4 Terry fabric weaving

To compare the performance of pre-consumer, post-consumer and virgin yarns in terry fabric production, three terry samples were woven using each type of yarn using a rapier weaving machine, which is commonly employed for its flexibility and high precision in fabric construction, especially for complex weave patterns such as terry fabrics. In this setup, Rapier weft insertion was used, a technique that ensures the smooth and efficient insertion of the weft yarn, which is crucial for creating the loops characteristic of terry cloth. The machine was configured with a Twin Beam system, one beam

for the ground yarn and the other for the pile yarn, thus facilitating the optimal control of tension and proper loop formation. The 4-Pick Terry Pile Design was employed, which is typical for terry fabrics, as it facilitates the creation of the pile loops needed for high absorbency. The specific terry weave pattern is shown in Figure 2, which illustrates the loop structure and weave configuration used in the fabric. This configuration was chosen to balance fabric strength and softness, providing the necessary properties for towel production. The pre-consumer, post-consumer and virgin samples were constructed under identical parameters to ensure a consistent basis for comparison. All samples were designed with a length of 140 cm, width of 77 cm and a mass per unit area of 500 g/m². The hem dimensions (4.5 cm) and type (04-pick terry pile weave design) were standardized, along with the picks per cm (15), pile height (3.8 mm), pile ratio (4 cm per 5 loops) and the total pile yarn length per centimetre (12.2 cm). By maintaining these uniform dimensions and construction attributes, the study ensured that variations in fabric properties were solely attributed to the yarn type, enabling a direct and meaningful comparison of pre-consumer, post-consumer and virgin samples.

X			
		X	
X			
X			
Ground	Pile	Ground	Pile

Figure 2: Weave pattern of fabricated terry samples

2.5 Terry finishing process

During processing, only bleaching was performed on the samples. The process involved the use of hydrogen peroxide (50%) as the bleaching agent, along with caustic soda to maintain an alkaline pH and formic acid for pH neutralization after bleaching. The bleaching conditions were standardized for all

three samples of 100% cotton to ensure uniformity. The bleaching bath recipe comprised 50 g/L hydrogen peroxide (50%), 2 g/L caustic soda and 1 g/L wetting agent to enhance chemical penetration. The fabric was treated at a temperature of 95 °C for 60 minutes, maintaining a bath pH of around 10.5–11. After bleaching, the fabric was thoroughly rinsed to restore pH to neutral. The bleaching chemicals had a direct effect on the ground of the terry, which was consistent across all three samples of 100% cotton. For this reason, the ratio of chemicals was kept the same for each sample. This process did not significantly affect the pile of the towel. An analysis was performed to evaluate the impact of bleaching on the pile length of terry fabrics, by comparing measurements taken before and after the bleaching process. The study included three sample types: pre-consumer, post-consumer and virgin cotton terry fabrics. Statistical evaluation was conducted using a paired t-test implemented in Python software to assess the significance of the observed changes. The analysis resulted in a p-value of 0.0742, indicating that the changes in pile length were statistically non-significant ($p > 0.05$). These findings suggest that the bleaching process did not have a substantial effect on the pile structure of the terry fabrics.

2.6 Determining the properties of fibres, yarns and fabrics

The collected fibres were characterized using the Advanced Fibre Information System (AFIS) and High-Volume Instrument (HVI) reports. AFIS (e.g., USTER AFIS PRO 2) provided detailed insights into fibre length, fineness, nep content and short fibre content under standard conditions (20 °C \pm 2 °C and 65% \pm 2% relative humidity), while the HVI (e.g.,

USTER HVI 1000) evaluated micronaire, strength, elongation, maturity index and trash content under controlled conditions. The prepared yarns were characterized using the USTER Tester 6, which measured yarn evenness, imperfections and hairiness according to the ISO 2060:1994 standard, with samples conditioned under standard laboratory conditions. Additionally, yarn tensile strength was assessed using a single yarn strength tester (e.g., USTER Tensojet) following ASTM D2256, which provide data regarding breaking force and elongation at break. The terry fabric samples underwent dimensional stability testing to washing, conducted according to AATCC Test Method 135-2018, where samples were subjected to repeated washing cycles at 40 °C, with dimensional changes measured after five cycles. Finally, the water absorbency of the terry fabrics was evaluated using the AATCC 79-2018 test method, where a drop test quantified the time taken for complete absorption, indicating the fabric's performance as a terry towel.

3 Results and discussions

3.1 Characterization of fibres

Fibre testing and evaluation were conducted on all three fibres using standard methods, with the results discussed below. Initially, the individual properties of each fibre are presented, followed by a comparative analysis to determine which fibre exhibited the best overall properties. The comparison of the properties of all three fibres revealed that virgin fibre exhibited the best overall characteristics, followed by post-consumer fibre, which had lower properties, and pre-consumer fibre, which had the lowest properties among the three.

Table 1: Comparison of AFIS report parameters of all fibres

Fibre sample	NFE ^{a)} (neps/g)	ASN ^{b)} (μ m)	SCN ^{c)} (neps/g)	MLF ^{d)} (cm)	LCV ^{e)} (%)	SFC ^{f)} (%)	Linear density (dtex)
Pre-con	743	733	91	1.65	59.1	39.0	1.65
Virgin	268	741	38	2.33	30.9	7.1	1.67
Post-con	399	645	15	1.98	45.6	23.6	1.67

^{a)} number of fibre entanglements; ^{b)} average size of neps; ^{c)} seed coat neps; ^{d)} means length of fibre; ^{e)} coefficient of variation of fibre length; ^{f)} short fibre contents

These findings are supported by the Advanced Fibre Information System (AFIS) report (Table 1), which provided detailed insights into various fibre properties such as fibre length distribution, fineness, nep content, trash content, maturity ratio, short fibre content and fibre strength. The AFIS data confirmed that virgin fibre outperformed the other two fibres, particularly in terms of the number of neps per gram (268 number of neps/g), the average size of neps in microns (741 μm), mean length (2.33 cm), coefficient of variation of fibre length LCV (30.9), short fibre content SFC (7.1%) and fineness (1.67×10^{-6} g/cm), while post-consumer fibre showed a moderate quality and pre-consumer fibre displayed the least favourable results across these parameters. This difference in properties arises because pre-consumer fibres, derived from spinning waste, generally exhibit inferior characteristics compared to both virgin and post-consumer fibres. Their source material often includes shorter and weaker fibres, resulting in reduced strength, poor length uniformity and lower durability. In contrast, post-consumer fibres, obtained from highly finished textile garments, benefit from higher-quality input materials. Although they are slightly lower in quality than virgin fibres, post-consumer fibres demonstrate improved performance in terms of fibre strength, length and overall integrity due to the superior quality of their source materials and the processing methods involved.

The comparison of the High Volume Instrument (HVI) reports (Table 2) for all the fibres indicates that pre-consumer fibre exhibited the lowest quality

properties compared to post-consumer and virgin fibres, with virgin fibre demonstrating the best overall qualities. The HVI report provides a comprehensive analysis of key parameters such as fibre length, uniformity index, strength, micronaire, colour grade, trash content, reflectance (R_d) and yellowness (+b). These metrics reveal that virgin fibre outperforms the others in terms of length consistency, tensile strength, fineness and colour quality, while pre-consumer fibre falls short in these areas, highlighting its lower overall quality.

In the spinning process, the highest quality raw material is utilized for production, while the leftover material, known as spinning waste, is recycled into pre-consumer fibre. Since pre-consumer fibre is derived from this leftover waste, which often contains dust and other impurities, it exhibits lower properties compared to post-consumer and virgin fibres [21]. Post-consumer fibres, on the other hand, possess superior qualities because they are recycled from used garments, which were originally high-quality products [22]. Additionally, used garments generally contain fewer impurities, contributing to the better properties of post-consumer fibres in comparison to pre-consumer fibres [23]. Given the inherent differences in the properties of pre-and post-consumer fibres, both are blended with a specific percentage of virgin fibre to enhance their spinnability. To ensure consistent the comparability of results, the same mixing ratio was maintained for both pre-and post-consumer fibres.

Table 2: Comparison of HVI report parameters of all fibres

Fibre sample	MIC ^{a)}	MI ^{b)}	SCI ^{c)}	L ^{d)} (cm)	UI ^{e)}	SFI ^{f)}	σ ^{g)} (g/tex)	ϵ ^{h)} (%)	M ⁱ⁾ (%)	R_d ^{j)}	+b ^{k)}
Pre-con	4.27	0.85	6	2.23	65.6	35.8	23.4	5.6	5.7	53.9	9.7
Virgin	4.27	0.87	105	2.57	80.3	10.6	27.6	4.6	6.1	69.3	9.9
Post-con	4.14	0.86	63	2.38	71.7	19.0	28.0	4.3	6.1	71.2	9.3

^{a)} micronaire, ^{b)} maturity index, ^{c)} spinning consistency index, ^{d)} staple length, ^{e)} uniformity index, ^{f)} short fibre index,

^{g)} strength, ^{h)} elongation, ⁱ⁾ moisture, ^{j)} reflectance, ^{k)} yellowness

3.2 Characterization of yarns

The comparison of the USTER reports properties shown in Figure 3a for the three yarns indicates that virgin yarn exhibited the best overall properties, with superior evenness, lower imperfections and better strength. For instance, the unevenness percentage (U%) for virgin yarn is 10.2, yarn coefficient of mass variation (CVm%) is 13 and the Hairiness Index (H Index) is 8.82, reflecting its high quality. Post-consumer yarn, while slightly lower in quality than virgin yarn, still maintains better properties than pre-consumer yarn, with a U% of 10.5, CVm% of 13.4 and an H Index of 9.55. In contrast, pre-consumer yarn demonstrates the lowest quality, with a U% of 11.6, CVm% of 14.7 and an H Index of 7.8. This difference in properties arises because pre-consumer fibre, derived from spinning waste, generally exhibits inferior characteristics compared to both virgin and post-consumer yarn. Its source material often consists of shorter and weaker fibres, which negatively affect the yarn's strength, evenness and durability. On the other hand, post-consumer yarn, obtained from highly finished textile garments, benefits from higher-quality input materials. Although it is slightly lower in quality than virgin yarn, post-consumer yarn demonstrates improved performance in terms of yarn evenness, tensile

strength and overall durability due to the superior material quality of its source.

The comparative analysis for breaking strength shown in Figure 3b reveals that virgin yarn exhibited the highest strength among the three types, with a breaking strength of 158 N, breaking tenacity of 0.443 N/tex and a breaking factor of 10400 Ntex. This superior strength can be attributed to the high-quality raw materials used, which contributed to its enhanced performance [24]. Post-consumer yarn, while showing lower strength compared to virgin yarn, demonstrated better properties than pre-consumer yarn, with a breaking strength of 754.4 N, breaking tenacity of 0.387 N/tex and a breaking factor of 9190 Ntex. This is due to the fact that post-consumer yarn is derived from previously high-quality garments, which retain more desirable characteristics despite being recycled. In contrast, pre-consumer yarn exhibited the lowest strength, with a breaking strength of 565 N, breaking tenacity of 0.291 N/tex and a breaking factor of 6832.4 Ntex. The reduced strength of pre-consumer yarn can be attributed to the lower quality of the waste material used, which often includes various impurities and shorter fibre lengths, which affect the overall yarn strength [25].

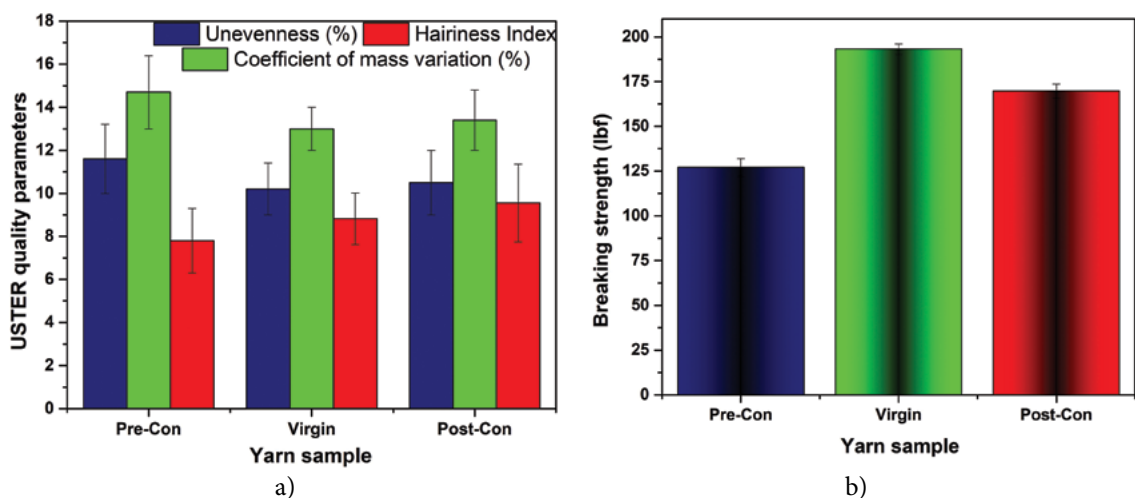


Figure 3: Yarn test results: a) USTER quality parameters; and b) breaking strength

3.3 Dimensional stability of terry fabric

The dimensional stability of three terry fabrics (pre-consumer, post-consumer and virgin samples) was analysed according to Table 3. All three fabrics exhibited similar shrinkage percentages in both

length (approximately 5.38%) and width (between -1.67% and -1.80%). Based on the data, no significant difference in dimensional stability between the three fabric types was recorded.

Table 3. Comparison of dimensional stability of the prepared terry samples

Dimensional stability of the terry fabric	Pre-consumer sample			Post-consumer sample			Virgin sample		
	Before wash	After wash	Shrinkage (%)	Before wash	After wash	Shrinkage (%)	Before wash	After wash	Shrinkage (%)
Length ($\pm 6\%$)	139.6	132.1	-5.38	139.4	131.9	-5.38	139.4	131.9	-5.38
Width ($\pm 4\%$)	72.2	70.9	-1.80	72.0	70.8	-1.67	72.0	70.8	-1.67

3.4 Absorbency test

The water absorbency of terry fabric from virgin, pre-consumer and post-consumer waste yarns was evaluated using the weight gain method. Fabric samples of standard dimensions (10 cm \times 10 cm) were first dried in an oven at 105 °C for two hours to remove any residual moisture. The dry weight of each sample (W_{dry}) was recorded using a precise balance. The samples were then fully submerged in distilled water at room temperature (25 °C) for one minute to ensure saturation. After immersion, excess surface water was gently removed by pressing the sample between blotting papers, without squeezing the internal water, and wet weight (W_{wet}) was recorded. The water absorbency (%) was calculated using equation 1:

$$\text{Water absorbency} = \frac{(W_{wet} - W_{dry})}{(W_{wet})} \times 100 (\%) \quad (1)$$

A comparative analysis of absorbency was conducted on three terry fabrics (pre-consumer, post-consumer and virgin) and is presented in Figure 4. The results indicated that the virgin fabric exhibited the highest absorbency (70%), followed by the post-consumer fabric (68%). The pre-consumer fabric displayed the lowest absorbency (62%). Notably, the post-consumer fabric demonstrated comparable absorbency to the virgin fabric. These findings suggest that recycled yarn derived from

post-consumer waste can serve as a viable alternative to virgin yarn for the pile component of terry fabric. The absorbency of fabrics is influenced by multiple factors, including yarn structure, fibre properties, fabric density and the surface treatment of the material. The results observed in this study can be attributed primarily to differences in yarn structure and the properties of fibres derived from virgin, post-consumer and pre-consumer sources. The yarn structure plays a significant role in absorbency. Virgin yarn, characterized by its lower unevenness percentage (U%), coefficient of mass variation (CVm%) and moderate hairiness index (H Index), results in a more uniform and compact structure. This uniformity enables the fabric to retain moisture effectively without gaps that hinder water wicking. In contrast, post-consumer yarn, though slightly less uniform than virgin yarn, still exhibits sufficient structural integrity to support good absorbency. Pre-consumer yarn, with its higher unevenness and CVm% values, creates more irregular spaces within the fabric, leading to reduced capillary action and hence lower absorbency.

In addition to yarn properties, fabric density and porosity also significantly influence absorbency. Higher-density fabrics tend to trap more water, while excessive porosity in fabrics made from pre-consumer yarn may cause faster drainage, thereby limiting water retention. The virgin fabric's superior absorbency can

also be attributed to its smoother surface finish, which minimizes resistance to water penetration, compared to the rougher surfaces found in fabrics made from recycled yarns.

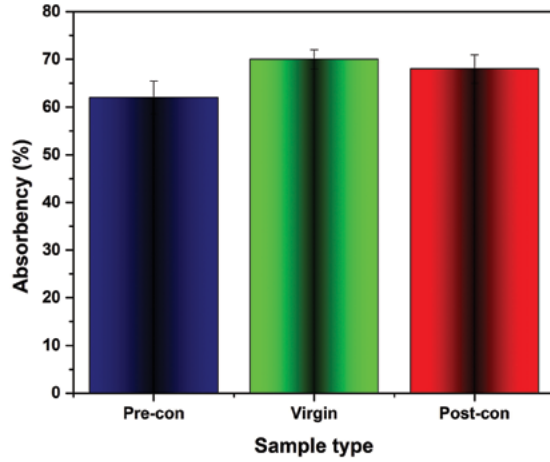


Figure 4: Comparison of absorbency results for the prepared terry samples

3.5 Tensile strength

Tensile strength was measured using a Universal Testing Machine (UTM), following the ASTM D5035 standard, where fabric samples were subjected to a constant rate of extension and the maximum force before breakage was recorded. The terry fabrics made from the virgin yarn exhibited the highest tensile strength of 0.954 MPa due to the superior quality and uniformity of the fibres. Post-consumer yarn showed slightly lower tensile strength of 0.890 MPa, as it is derived from recycled garments, but still retains a relatively high-quality fibre. Pre-consumer yarn, made from spinning waste, demonstrated the lowest tensile strength of 0.784 MP due to the presence of shorter, weaker fibres and higher yarn irregularities. These differences reflect the impact of fibre quality and yarn structure on fabric strength.

3.6 Cost analysis of yarn samples

The cost analysis of the three yarn types (shown in Table 4) reveals that the highest profit margin is obtained

through the recycling of pre-consumer waste. Despite pre-consumer yarn exhibiting lower properties than post-consumer and virgin yarns, it proves well-suited for upcycling, thereby addressing both economic viability and sustainability objectives. Products typically manufactured from virgin and post-consumer yarns can be effectively substituted with those made from pre-consumer yarn, which offers comparable properties while optimizing profit margins. This strategy not only enhances profitability but also aligns with environmental and user-friendly principles. It can thus be concluded that recycling both pre-and post-consumer waste enables the production of environmentally sustainable and cost-effective yarns, and thus results in higher profitability than virgin yarns while advancing sustainability and recycling goals.

The following equations were used in calculating the cost analysis:

i. Net cost per kilogram (EUR):

$$\text{Net cost/kg} = \text{Price/kg} + \text{Transport expenses/kg} + \text{Spinning cost/kg} + \text{Cotton cost/kg} + \text{Conversion cost/kg} + \text{Packing cost/kg} \quad (2)$$

ii. Net profit per kilogram (EUR):

$$\text{Net profit/kg} = \text{Price/kg} - \text{Net cost/kg} \quad (3)$$

iii. Profit per frame (EUR):

$$\text{Profit/Frame} = \text{Net profit/kg} \times \text{Production per frame (kg)} \quad (4)$$

iv. Profit per bag (EUR):

$$\text{Profit/Bag} = \text{Net profit/kg} \times \text{Bag weight (kg)} \quad (5)$$

3.7 Cost analysis of terry fabric

The cost analysis of terry fabric conversion (Table 5) reveals that utilizing pre-consumer yarn as the pile yarn results in the highest profit margin compared to the use of virgin or post-consumer yarn. This finding is corroborated by the test results for the terry samples, which demonstrate that the properties of fabric produced from pre-consumer yarn are nearly equivalent to those of fabrics made from virgin and post-consumer yarns. Consequently, pre-consumer

Table 4: Cost analysis of prepared yarn samples (pre-consumer, post-consumer and virgin)

Costing value	Virgin yarn	Pre-cons yarn	Post-cons yarn
Price (EUR/kg)	1.156	1.03	1.10
Transport expenses (EUR/kg)	0.014	0.01	0.01
Sp cost (EUR)	0.084	0.08	0.08
Cotton cost (EUR/kg)	1.254	1.12	1.20
Conversion cost (EUR/kg)	0.155	0.16	0.16
Packing cost (EUR/kg)	0.014	0.01	0.01
Net cost (EUR/kg)	1.422	1.30	1.37
Sale price (EUR/kg)	1.735	1.67	1.70
Net profit (EUR/kg)	0.312	0.37	0.34
Production (kg/frame)	836.68	798.05	817.37
Profit (EUR/frame)	261.18	295.32	273.98
Profit (EUR/bag) (1 bag = 45.37 kg)	14.16	16.79	15.21

Table 5: Costing of prepared terry fabric samples (conversion of yarn to fabric)

Costing value	Virgin yarn	Pre-con	Post-con
Yarn price/kg for ground (EUR)	0.498	0.498	0.498
Yarn price/kg for pile (EUR)	1.735	1.664	1.702
Yarn price for terry fabric (50%ground + %50% pile) (EUR)	1.116	1.081	1.099
Terry fabric conversion cost@Euro 0.297/kg (EUR)	0.297	0.297	0.310
Wastage % of terry (EUR)	0.013	0.014	0.014
Bleaching and dyeing cost@Euro 0.254/kg avg (EUR)	0.255	0.255	0.255
Wastage % of wet processing	7	7.75	7.1
Total wastage (%)	11.10	12.25	11.40
Total Conversion cost of processed terry/kg (EUR)	0.552	0.552	0.565
Finished terry fabric cost (EUR)	1.792	1.752	1.785
Sales price of terry fabric/kg (EUR)	2.249	2.249	2.249
Cost/kg of terry fabric	0.457	0.496	0.464
Profit as a ratio relative to the virgin (%)		8.6	1.5

yarn presents a viable substitute for virgin yarn in terry fabric production, thereby providing a cost-effective and sustainable alternative, without compromising fabric quality.

3.8 Comparison with other recycling methods

Various technologies are employed to break down textiles and convert them into reusable products,

each offering unique advantages and facing distinct challenges. These aspects are systematically summarized in Table 6, which provides a comparative overview of their strengths, limitations and suitability for specific applications.

Table 6: Pros and cons of different textile recycling technologies

Recycling method	Pros	Cons	Reference
Pyrolysis	A simple process that can be applied to a broad range of materials without requiring prior treatment of textile waste.	Requires a high-temperature chemical reaction that demands excessive electrical power.	[26]
Hydrothermal	This method produces low ash while operating at a lower temperature compared to pyrolysis.	Involves a long reaction time and results in reduced purification.	[27]
Biological	This method offers an eco-friendly solution with a high potential for removing dyes from clothing during textile recycling.	This method generates toxic intermediates at a high cost and with a longer retention time.	[28]
Mechanical	The physical method of textile recycling is eco-friendly, economical and facilitates easy quality control, without requiring chemicals or high temperatures.	Collecting and segregating waste is a challenging task.	This work

4 Conclusion

In conclusion, this study successfully developed a sustainable and cost-effective terry fabric using yarns spun from pre- and post-consumer textile waste. A comprehensive evaluation of fibres, yarns and fabrics was conducted, including HVI and AFIS reports for fibres, USTER tests and tensile strength measurements for yarns. The fibre analysis revealed that pre-consumer fibres exhibited lower quality than post-consumer and virgin fibres. However, blending 80% virgin fibre with recycled fibres resulted in yarns with comparable yields and production rates. Tensile strength measurements of the terry fabrics confirmed that both pre-consumer (0.784 MPa) and post-consumer (0.890 MPa) recycled yarns produced fabrics with mechanical properties comparable to those of virgin cotton (0.954 MPa), supporting their durability and suitability for end-use applications. Further testing, including absorbency and washing durability, showed no significant differences between terry fabrics made from pre-consumer, post-consumer and virgin yarns. The results indicated that the virgin fabric exhibited the highest absorbency (70%), followed by the post-consumer fabric (68%) and the pre-consumer fabric with the lowest absorbency (62%). The dimensional stability analysis of the three terry fabrics revealed consistent shrinkage percentages in length (approximately 5.38%), with no significant differences

observed among them. These results indicate that the evaluated properties – mechanical strength, absorbency and washing durability – are sufficient to validate the use of terry fabrics developed from pre- and post-consumer waste as performance-ready materials for end-use applications. Importantly, the production process required no significant adjustments to machine settings or chemical processes, regardless of the yarn type, thereby reinforcing the practicality of integrating recycled fibres into existing manufacturing systems. Moreover, terry fabrics developed from pre- and post-consumer waste not only exhibit comparable performance in terms of other properties but also offer significant economic advantages, with profit margins of 8.6% and 1.5%, respectively, relative to virgin cotton samples. These economic benefits underscore the potential of recycled fabrics as a cost-effective and sustainable alternative in the textile industry. These findings highlight the potential of using recycled fibres in terry towel production as a sustainable and cost-effective alternative to virgin cotton, ensuring quality and durability while contributing to circular economy practices in the textile industry.

Limitations and future prospects

This study faced a few limitations. First, the quality of pre- and post-consumer waste was inconsistent due to variability in source materials, which could affect reproducibility. Second, the mechanical shredding of fibres resulted in reduced fibre length

and strength, necessitating blending with virgin fibres for acceptable yarn quality. The bleaching process applied uniform chemical ratios across all samples, which may not fully address the variability in contamination levels or initial fabric compositions. Additionally, the scope of testing was limited to mechanical and absorbency properties, ignoring other aspects such as durability under extended usage.

Future research could explore advanced recycling technologies, such as enzymatic or chemical methods, to enhance the quality of recycled fibres and minimize reliance on virgin fibres. Industrial-scale trials are needed to validate the commercial feasibility of the processes developed in this study. Comprehensive life-cycle analyses, including environmental impact assessments, such as water and energy savings and carbon footprint reduction, could further substantiate the sustainability claims. Expanding the application of recycled yarns to other textile products, such as upholstery or technical fabrics, could demonstrate their versatility.

Conflicts of Interest: The authors hereby declare that there were no potential conflicts of interest concerning the research, authorship and/or publication of this article.

Funding: The authors received no financial support for the research, authorship and/or publication of this article.

References

1. RODRÍGUEZ-ESPÍNDOLA, O., CUEVAS-ROMO, A., CHOWDHURY, S., DÍAZ-ACEVEDO, N., ALBORES, P., DESPOUDI, S., MALESIOS, C., DEY, P. The role of circular economy principles and sustainable-oriented innovation to enhance social, economic and environmental performance: evidence from Mexican SMEs. *International Journal of Production Economics*, 2022, **248**, 1–18, doi: 10.1016/j.ijpe.2022.108495.
2. VADICHERLA, T., SARAVANAN, D. Textiles and apparel development using recycled and reclaimed fibers. In *Roadmap to Sustainable Textiles and Clothing: Eco-friendly Raw Materials, Technologies, and Processing Methods*. Edited by Subramanian Senthilkannan Muthu. Singapore: Springer, 2014, 139–160, doi: 10.1007/978-981-287-065-0_5.
3. ABDEL-SHAIFY, H.I., MANSOUR, M.S.M. Solid waste issue: sources, composition, disposal, recycling, and valorization. *Egyptian Journal of Petroleum*, 2018, **27**(4), 1275–1290, doi: 10.1016/j.ejpe.2018.07.003.
4. RIBEIRO, M.C.S., FIÚZA, A., FERREIRA, A., DINIS, M.D.L., MEIRA CASTRO, A.C., MEIXEDO, J.P., ALVIM, M.R. Recycling approach towards sustainability advance of composite materials' industry. *Recycling*, 2016, **1**(1), 178–193, doi: 10.3390/recycling1010178.
5. YANG, Y., BOOM, R., IRION, B., VAN HEERDEN, D.-J., KUIPER, P., DE WIT, H. Recycling of composite materials. *Chemical Engineering and Processing: Process Intensification*, 2012, **51**, 53–68, doi: 10.1016/j.cep.2011.09.007.
6. SÖDERHOLM, P., TILTON, J.E. Material efficiency: an economic perspective. *Resources, Conservation and Recycling*, 2012, **61**, 75–82, doi: 10.1016/j.resconrec.2012.01.003.
7. JUANGA-LABAYEN, J.P., LABAYEN, I. V, YUAN, Q. A review on textile recycling practices and challenges. *Textiles*, 2022, **2**(1), 174–188, doi: 10.3390/textiles2010010.
8. SHIRVANIMOGHADDAM, K., MOTAMED, B., RAMAKRISHNA, S., NAEBE, M. Death by waste: fashion and textile circular economy case. *Science of The Total Environment*, 2020, **718**, 1–10, doi: 10.1016/j.scitotenv.2020.137317.
9. NIINIMÄKI, K., PETERS, G., DAHLBO, H., PERRY, P., RISSANEN, T., GWILT, A. The environmental price of fast fashion. *Nature Reviews Earth & Environment*, 2020, **1**, 189–200, doi: 10.1038/s43017-020-0039-9.

10. ARAFAT, Y., UDDIN, A.J. Recycled fibers from pre- and post-consumer textile waste as blend constituents in manufacturing 100% cotton yarns in ring spinning: a sustainable and eco-friendly approach. *Heliyon*, 2022, **8**, 1–19, doi: 10.1016/j.heliyon.2022.e11275.
11. AZAD, A.K., HAQ, U.N., KHAIRUL AKTER, M.M., UDDIN, M.A. Recycling practices of pre-consumer waste generated from textile industry. In *Sustainable Manufacturing Practices in the Textiles and Fashion Sector*. Edited by Subramanian Senthilkannan Muthu. Springer, 2024, 301–324, doi: 10.1007/978-3-031-51362-6_12.
12. LEAL FILHO, W., ELLAMS, D., HAN, S., TYLER, D., BOITEN, V.J., PAÇO, A., MOORA, H., BALOGUN, A.-L. A review of the socio-economic advantages of textile recycling. *Journal of Cleaner Production*, 2019, **218**, 10–20, doi: 10.1016/j.jclepro.2019.01.210.
13. PIRIBAUER, B., BARTL, A. Textile recycling processes, state of the art and current developments: a mini review. *Waste Management & Research*, 2019, **37**(2), 112–119, doi: 10.1177/0734242X18819277.
14. UPASANI, P.S., JAIN, A.K., SAVE, N., AGARWAL, U.S., KELKAR, A.K. Chemical recycling of PET flakes into yarn. *Journal of Applied Polymer Science*, 2012, **123**(1), 520–525, doi: 10.1002/app.34503.
15. KHANZADA, H., KHAN, M.Q., KAYANI, S. Cotton based clothing. In *Cotton Science and Processing Technology: Gene, Ginning, Garment and Green Recycling*. Edited by Hua Wang and Hafeezullah Memon. Springer, 2020, 377–391, doi: 10.1007/978-981-15-9169-3_15.
16. HAN, T., LIU, G., ZHANG, L. The global cotton trade network reveals a shift in the cotton import center to the global south from 1986 to 2020. *Journal of Rural Studies*, 2024, **108**, 1–13, doi: 10.1016/j.jrurstud.2024.103262.
17. RIDLEY, W., DEVADOSS, S. Competition and trade policy in the world cotton market: implications for US cotton exports. *American Journal of Agricultural Economics*, 2023, **105**(5), 1365–1387, doi: 10.1111/ajae.12370.
18. BALOYI, R.B., GBADEYAN, O.J., SITHOLE, B., CHUNILALL, V. Recent advances in recycling technologies for waste textile fabrics: a review. *Textile Research Journal*, 2024, **94**(3-4), 508–529, doi: 10.1177/00405175231210239.
19. ABDKADER, A., HOSSAIN, M. A critical review on recent developments and solutions in the high-speed ring spinning process. *Textile Research Journal*, 2023, **93**(23–24), 5485–5504, doi: 10.1177/00405175231194793.
20. SRINIVASAN, J. Engineering finer and softer textile yarns. In *Technical Textile Yarns*. Edited by R. Alagirusamy and A. Das. Woodhead Publishing, 2010, 185–214, doi: 10.1533/9781845699475.1.185.
21. UTEBAY, B., CELIK, P., CAY, A. Valorization of fabric wastes through production of recycled cotton yarns by compact ring and open-end rotor spinning. *Journal of Cleaner Production*, 2023, **409**, 1–9, doi: 10.1016/j.jclepro.2023.137135.
22. PATTI, A., CICALA, G., ACIERNO, D. Eco-sustainability of the textile production: waste recovery and current recycling in the composites world. *Polymers*, 2021, **13**(1), 1–25, doi: 10.3390/polym13010134.
23. STANESCU, M.D. State of the art of post-consumer textile waste upcycling to reach the zero waste milestone. *Environmental Science and Pollution Research*, 2021, **28**, 14253–14270, doi: 10.1007/s11356-021-12416-9.
24. LU, L., FAN, W., MENG, X., XUE, L., GE, S., WANG, C., FOONG, S.Y., TAN, C.S.Y., SONNE, C., AGHBASHLO, M., TABATABAEI, M., LAM, S.S. Current recycling strategies and high-value utilization of waste cotton. *Science of the Total Environment*, 2023, **856**, 1–14, doi: 10.1016/j.scitotenv.2022.158798.

25. FAYSAL, G.M., AZAD, T.N.S., REPON, M.R., HOSSAIN, M.T., JALIL, M.A. Sustainable yarn production using leftover fabric from apparel industries. *Heliyon*, 2022, **8**(11), 1–6, doi: 10.1016/j.heliyon.2022.e11377.
26. YOUSEF, S., EIMONTAS, J., STRIUGAS, N., TATARIANTS, M., ABDELNABY, M.A., TUCKUTE, S., KLIUCININKAS, L. A sustainable bioenergy conversion strategy for textile waste with self-catalysts using mini-pyrolysis plant. *Energy Conversion and Management*, 2019, **196**, 688–704, doi: 10.1016/j.enconman.2019.06.050.
27. MATAYEVA, A., BILLER, P. Hydrothermal liquefaction of post-consumer mixed textile waste for recovery of bio-oil and terephthalic acid. *Resources, Conservation and Recycling*, 2022, **185**, 1–9, doi: 10.1016/j.resconrec.2022.106502.
28. HUSSAIN, A., KAMBOJ, N., PODGURSKI, V., ANTONOV, M., GOLIANDIN, D. Circular economy approach to recycling technologies of post-consumer textile waste in estonia: a review. *Proceedings of the Estonian Academy Science*, 2021, **70**(1), 80–90, doi: 10.3176/proc.2021.1.07.

Sultan Ullah,¹ Arvydas Palevicius,¹ Giedrius Janusas,¹ Zeeshan Ul Hasan²

¹ Department of Mechanical Engineering, Faculty of Mechanical Engineering and Design, Kaunas University of Technology, Studentų 56, LT-51424, Kaunas, Lithuania

² Department of Materials Engineering, School of Engineering & Technology, National Textile University, Sheikhpura Road, Faisalabad-37610, Pakistan

Impact Properties of Composite Materials: The Significance of Glass Microspheres

Odpornost kompozitnih materialov proti udarcem: pomen steklenih mikrokroglic

Original scientific article/Izvirni znanstveni članek

Received/Prispelo 9–2024 • Accepted/Sprejeto 1–2025

Corresponding author/Korespondenčni avtor:

Sultan Ullah

E-mail: sultan.ullah@ktu.edu

ORCID iD: 0000-0003-1233-1926

Abstract

Due to their exceptional qualities, polymer matrix composite materials are finding more and more use in high-tech applications. The purpose of this work was to improve these composites' resilience to impact by adding glass microspheres to thermosetting phenolic resins. Glass fabric was used as the reinforcing material. The main objective of the study was to determine how different glass microsphere percentages affected the composites' mechanical characteristics. A fibre volume fraction of 0.6 was attained by utilising compression moulding to create the composites, which were made from four glass fabric plies. The mechanical properties were considerably improved by the addition of glass microspheres; the best results were noted at concentrations of 6–8%. More specifically, there was a noticeable improvement in tensile strength and a 6% rise in tensile modulus. Based on the results, the addition of glass microspheres to composite materials improves both their mechanical and energy-absorbing capabilities, thus making them more appropriate for use in impact applications.

Keywords: 2D woven fabric, polymer matrix composites, glass microspheres, thermosetting resins, impact strength, automotive applications

Izvleček

Polimerne kompozite zaradi njihovih izjemnih lastnosti čedalje več uporabljajo za visokotehnološke aplikacije. Namen te raziskave je bil izboljšati odpornost polimernih kompozitov proti udarcem z dodajanjem steklenih mikrokroglic termoreaktivnim fenolnim smolam. Za ojačitev je bila uporabljena steklena tkanina. Glavni cilj raziskave je bil ugotoviti, kako različni odstotki dodanih steklenih mikrokroglic v polimerno matrico vplivajo na mehanske lastnosti kompozitov. Ti so bili izdelani s stiskanjem štirih plasti steklenih tkanin, katerih utežni delež v kompozitih je znašal 0,6. Mehanske lastnosti kompozitov so se znatno izboljšale z dodajanjem steklenih mikrokroglic. Najboljše rezultate so dosegli pri 6–8 ut. odstotku dodanih mikrokroglic, kjer se je opazno izboljšala



Content from this work may be used under the terms of the Creative Commons Attribution CC BY 4.0 licence (<https://creativecommons.org/licenses/by/4.0/>). Authors retain ownership of the copyright for their content, but allow anyone to download, reuse, reprint, modify, distribute and/or copy the content as long as the original authors and source are cited. No permission is required from the authors or the publisher. This journal does not charge APCs or submission charges.

natezna trdnost, za šest odstotkov pa se je povečal natezni modul. Dodatek steklenih mikrokroglic je izboljšal mehanske lastnosti kompozitnih materialov in sposobnost absorpcije energije, zato so tovrstni kompoziti primerni za izdelke, odporne proti udarcem.

Ključne besede: 2-D tkanina, polimerni kompoziti, steklene mikrosfere, termoreaktivne smole, udarna trdnost, uporaba v avtomobilski industriji

1 Introduction

Materials made of two or more different components together on a macroscopic level are known as composite materials [1]. To provide mechanical strength and load-bearing capacities, reinforcement materials in composites, such as fibres, textiles or particles, are essential. The matrix's role in the composite network is to bind these reinforcement materials together and distribute loads among them. The similar mechanical properties of composites have made them attractive alternatives for metals in recent years. From sports equipment to high-tech sectors such as aerospace, these materials are used in a wide range of industries [2]. Glass and glass microspheres were combined to manufacture composite using compression moulding, and it was determined that there was a relationship between the microspheres' properties and tensile strength, elastic modulus, bending strength, pendulum impact resistance and drop weight impact tests. It was observed that as the microsphere concentration increased the mechanical characteristics and impact resistance improved. The lightweight nature and high mechanical properties of glass fibre-reinforced composites with a polymer matrix make them suitable choices for investigation as possible alternatives to conventional metals. The procedures for manually placing specimens are covered in this article. Tensile strength, impact resistance and drop weight impact characteristics were among the aspects that have been described by different ASTM standards. The investigation's matrix material, phenolic resin, was reinforced with a variety of microsphere particles. The mechanical and impact capabilities of composite materials were greatly enhanced by the addition of

microspheres, indicating the potential use of these materials to enhance the durability and performance of automobile components.

Recent work has challenged the widely held view that filled modules behave consistently across all matrices by examining the relationships between various polymer matrices. This study demonstrated that the specific matrix used can significantly affect the glass microspheres' effectiveness. After a detailed investigation of the variables affecting composite performance, it was shown that the addition of glass microspheres can improve material properties even at low concentrations. These results emphasise the adaptability and promising mechanical capabilities of microsphere-based composite materials, which could lead to innovations in a range of applications. Thermosetting and thermoplastic matrices are the two primary categories of matrix materials used in composite production. Thermosetting matrices are made using condensation polymerization and are liquid at room temperature. Vinyl ester, polyester, phenolic resins and green epoxies are a few examples. In general, these materials are fragile. In contrast, addition polymerization is used to create thermoplastic matrices, which are solid at room temperature. They lack crosslinks and feature branching or linear structures. One of thermoplastics' main qualities is their flexibility, which contributes to their impact resistance. They are stable at room temperature and can be solidified upon cooling after being cooled, or they can be softer when heated, allowing for recycling and moulding. As opposed to empty composites, the inclusion of micro- or nanoparticles improves the impact strength of composite materials. For riot shields, battle helmets, tactical vests and sporting equipment,

such as tennis rackets and hockey sticks, high-impact strength is required [3].

1.1 Recent advances in composite materials: fillers and reinforcements

Compared to fillers such as silica, potato flour and chonta palm wood, high-density polyethylene (HDPE) exhibits better energy absorption qualities when added with high-impact fillers with gamma-alumina and silica. All the mechanical properties are improved when the polymer matrix is hybridised with these fillers, surpassing the capabilities of simple polymer materials only [4, 5]. The integration of amino-functional, multi-walled carbon nanotubes (MWCNTs) enhances projectile resistance incarceration in epoxy/glass materials. However, higher concentrations of MWCNTs increase epoxy viscosity, making it difficult to wet glass fabrics properly, leading to reduced mechanical properties [6]. Incorporating glass micro powder into epoxy resin was found to increase the stiffness and bending strength of basalt-reinforced composites, although it displayed no discernible impact on their tensile force. This enhancement demonstrates the potential of microglass powder to improve the mechanical properties [7]. The effect of fillers on composites reinforced with epoxy and glass fibre was examined by researchers, who observed that fly ash increased impact strength by up to 300% at low concentrations but decreased compressive strength. However, small additions increased crack length and surface area. Nano- Al_2O_3 at 2 PHR (parts per hundred resin) showed an optimal balance in mechanical, thermal, and viscoelastic properties. The flexural modulus increased significantly with 0.5 PHR Al_2O_3 but higher amounts reduced the modulus [8, 9].

Researchers found that plain weave fabrics as reinforcement performed well against both high-speed and low-speed impacts, while basket weave fabrics provided better resistance at higher speeds. On the contrary, satin weave showed weaker impact resistance [10]. The study highlighted that the structure of woven fabrics plays a critical role in energy absorp-

tion. Additionally, treated fabrics showed increased yarn pull-out force due to restricted yarn movement and impact energy, though this does not fully indicate energy absorption. Increasing the fabric set improved the impact strength by ensuring primary yarn contact with the impactor and energy distribution through secondary yarns. In general, treated fabrics demonstrated better energy absorption compared to untreated fabrics [11]. The impact of the density, thickness and stacking sequence of aramid-kenaf fabric layers on composite properties was studied by many researchers. They found that increasing areal density and thickness improved energy absorption. Kevlar and kenaf fabrics were used for ballistic impact testing, showing that higher proportions of kenaf reduced ballistic properties. The treatment of kenaf fabrics with 6% sodium hydroxide improved tensile properties compared to untreated kenaf. The outer layers of Kevlar improved mechanical and flexural properties, while the inner layers improved the tensile strength [12] absorption of the compound, which does not directly correlate with its thickness. Instead, it is influenced by the interaction time, which depends on the projectile velocity and the thickness of the composite. Higher thickness can lead to composite failure due to delamination and tensile failure, whereas lower thickness may result in energy absorption through fibre breaking. The desired depth and speed of the projectile both affect the deformation [13, 14]. Researchers examined how the number of layers influenced composites with various fibres made of Kevlar, carbon and glass under ballistic impact. Five hybrid composites and a pure carbon composite were produced with different sequences of fibre layers. The results showed that placing glass fibre as the first layer provided superior energy absorption compared to carbon and glass, or glass and carbon fibres in the centre of the composite [15].

Various techniques were employed in previous research to improve the strength characteristics of polymeric composite materials, including the optimisation of the ratio of natural to synthetic reinforcements, fibre treatments and the addition of

different additives to the matrix. However, the potential of glass microspheres in composite materials has not been fully explored. This study investigated the optimal concentration of glass microspheres in phenolic resin to achieve improved structural features. The results indicate that integrating glass microspheres improves the composites' mechanical characteristics and energy absorption, making them more appropriate for impact applications. Moreover, mixed composite materials have been identified as viable options for potential uses [16].

2 Materials and composite assembly

2.1 Materials

Plain weaved glass fabric with 514.55 g/m² and glass microspheres (Thomas No. C990Z93) with a molecular weight of 60.08 g/mol were used as reinforcement during this research. Reinforcement was obtained from the local market, while filler particles were imported from ALDRICH Chemistry, USA. The glass fabrics used in this study had a yarn count of 598.56 tex, with 22.86 yarns/cm in warp and weft directions. Glass microspheres, sized 9–13 µm, were incorporated into phenolic resin as an impact modifier for the composite material. The thermoset polymer named phenolic resin is sold under the Phenolic Resole NR 9430 brand name. Its pH range is 6.5 to 7.5, while its viscosity is 400–700 cps at 25 °C. The equipment and tools utilised in this research included a weight balance, measuring scale, beakers, fabric cutter/scissors, curing oven, agitator (OST 25), compression moulding apparatus, universal tensile testing machine (UTM), pendulum impact tester and drop weight impact tester.

2.2 Composite fabrication

The phenolic resin was used to create reinforced polymer laminates measuring 304 mm × 304 mm × 2 mm, which were reinforced with glass fibre and filled with glass microspheres. As indicated in Figure 1a, glass microspheres were introduced to phenolic resin and stirred for 20 minutes at 391 rpm with a mechanical stirrer. The presence of glass microspheres caused the phenolic resin's viscosity to rise. The solution's viscosity was decreased during stirring by using dimethyl formamide solvent. The resin was then applied to the woven glass fabrics using the hand layup method as presented in Figure 1b. Initially, a wet lay-up technique was utilised to make the composite, which was then subjected to pressure on a compression moulding machine as shown in Figure 1c. In the hand-laying process, a phenolic resin mixed with glass microspheres was applied to each layer sequentially, resulting in the formation of a four-layer composite. The hand-laminated sample was placed on a compression moulding machine for the curing of the phenolic resin. The curing process lasted for 5 hours and 10 minutes at a temperature of 140 °C and under a pressure of 3 tonnes. During the curing process, the machine's temperature was first adjusted to 100 °C for four hours. It was then raised to 120 °C for thirty minutes and to 140 °C for the final 40 minutes. The purpose of exerting pressure was to solidify the materials and remove any air or voids between them. Following the completion of the curing process, the sample was taken out of the compression moulding machine and cut into different sizes in accordance with ASTM standards for evaluation. The experimental design with various percentages of glass microspheres is detailed in Table 1.

Table 1: Experimental design utilising various glass microsphere concentrations

Sample code	2D woven reinforcement	Matrix	Glass microspheres (%)
P	Glass fibre	Phenolic resin	0
PG2	Glass fibre	Phenolic resin	2
PG4	Glass fibre	Phenolic resin	4
PG6	Glass fibre	Phenolic resin	6
PG8	Glass fibre	Phenolic resin	8
PG10	Glass fibre	Phenolic resin	10

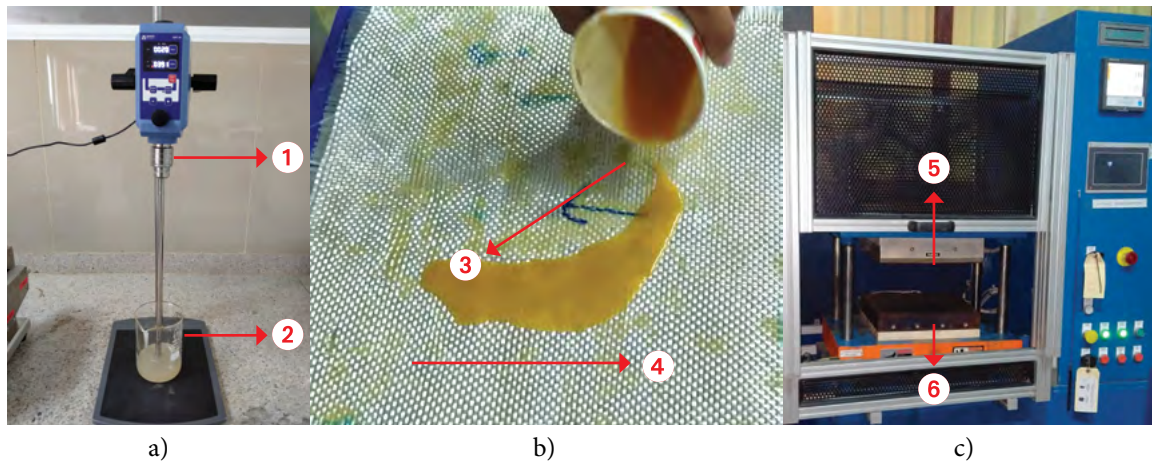


Figure 1: Incorporation of micro fillers in resin (a); application of resin to glass fabrics (b); and compression moulding (c)

Legend: 1 – electric stirrer, 2 – micro fillers in resin, 3 – glass fabric, 4 – resin application on fabric, 5 – upper mould, 6 – lower mould

2.3 Testing

The mechanical performance of the manufactured composite samples was evaluated using several tests: tensile, three-point bending, pendulum impact (Charpy impact) and drop weight impact. One kind of destructive structural assessment intended to assess a material's mechanical attributes, especially its strength and stiffness, is the tensile test. A universal testing machine (UTM) and the standard test method (ASTM D3039) were used to measure the tensile properties of polymer matrix composite materials. This method outlines the procedure for determining the in-plane tensile properties of polymer matrix composites reinforced by high-modulus fibres. The testing involved preparing specimens with precise dimensions and loading them in tension at a controlled rate until failure to evaluate parameters such as tensile strength, modulus of elasticity, strain and elongation at break. The fabricated samples, measuring 203.2 mm by 25.4 mm, were put through testing, and the mean of three samples was recorded for every test. The three-point bending test for fibre-reinforced composites is a mechanical test utilised to analyse the flexural force, stiffness and behaviour of laminate under bending load.

The standard test method for flexural properties of polymer matrix composite materials (ASTM

D7264) specifies the procedures to determine the flexural properties, such as flexural strength, flexural modulus and flexural strain, of polymer matrix composites under defined conditions. The test is conducted by placing the specimen on two supports and applying a load at a controlled rate until failure, using either a three-point or a four-point bending setup. Parameters such as span length, crosshead speed and specimen dimensions are meticulously followed as prescribed by the standard. The dimensions of the samples must be 120 mm × 13 mm.

The Charpy impact test, referred to as the pendulum impact strength test, determines a material's resilience and capacity to absorb impact. In this test, a movable arm with an attached weight is raised to a specific height and then released. This arm swings like a pendulum and strikes a V-notched sample. The energy absorbed by the sample is determined by measuring the height of the arm before and after impact, which reflects the energy required to break the sample. Charpy impact testing of the composite material was conducted according to ISO-179 standards. A strip of every laminate was prepared, with a dimension of 80 mm × 10 mm. The impact force of the composite material was the determined applying the following formula:

$$\text{Impact strength} = a_c = \frac{W_b \cdot 1000}{bh} \quad (1)$$

where W_b represents the energy at break expressed in J, a_c represents the impact strength stated in kJ/m^2 , b represents sample width and h represents the sample thickness.

The ASTM D7136 standard test method for measuring the damage resistance of a fibre-reinforced polymer matrix composite to a drop-weight impact event is a method for assessing the impact strength and damage tolerance of composites. In this test, a particular mass is lowered from a predetermined elevation to a composite to simulate real-world impact conditions. Materials energy absorption and resulting damage are then assessed [17]. The test is carried out using a composite plate of $101.6 \text{ mm} \times 152.4 \text{ mm}$. Damage is induced perpendicularly to the plane of the flat plate using a semicircular striker tip. The resistance to damage is assessed by evaluating the cracks formed in the flat plate.

2.3 Experimental setup

A universal tensile tester (UTM) was used for mechanical testing according to ASTM D3039, facilitating the evaluation of both tensile strength and elongation. The three-point bending configuration, also compliant with ASTM D7264, allowed the flexural tests to be performed on the same machine. Impact resistance was assessed using a Charpy impact testing machine, following ISO-179, while energy absorption during free fall was measured with a drop weight impact tester, in line with ASTM D7136. Surface examination, fibre distribution and microstructural analysis, including failure analysis, were carried out using an optical microscope, in accordance with ASTM 7570. Three specimens were evaluated based on every mechanical description and the average results were used for analysis. For comparison of the mechanical properties of glass microspheres in phenolic resin with plain woven composites, the combinations were coded as PG2, PG4, PG6, PG8 and PG10, while the neat composite

laminate with zero glass microsphere particles in phenolic resin was named P.

3 Results and discussion

3.1 Tensile properties of the prepared composites

Glass woven fabric composites were examined during tensile testing to determine the impact of various glass microsphere contents. Figure 2 illustrates variations in tensile strength by varying glass microsphere ratios. The tensile strength was higher for PG6 and PG8 than for P, PG2, PG4 and PG10. The maximum tensile force values for PG6 and PG8 were 307.83 MPa and 282.14 MPa, respectively. Tensile stress was considerably reduced and PG10 exhibited better extension than pure phenolic resin. While tensile strength decreased, PG2 and PG4 composites provided more extension than P, accordingly. The incorporation of glass microspheres into composites was only observed to improve their tensile properties at concentrations of 6% and 8%.

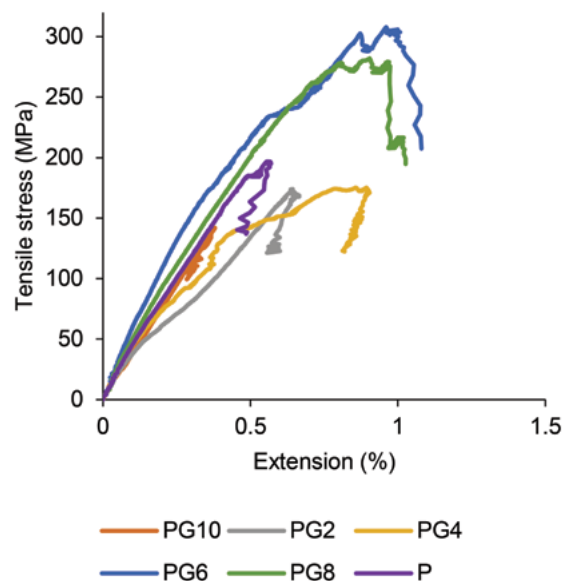


Figure 2: Tensile stress versus an extension of glass microsphere composites

As glass microspheres are infused with resin and subsequently applied to composite materials,

sufficient extension was shown. By adding 6% glass microspheres in phenolic resin, the modulus increased to 47.17 GPa as a result of fracture propagation. The modulus of phenolic resin was 41.96 GPa. A greater surface area stress-concentrated zone was produced by glass microspheres. The modulus of the composite increased in the samples PG2, PG4 and PG6 due to the stress distribution facilitated by the glass microspheres. Table 2 summarises the modulus of glass microspheres-based composites.

Table 2: Glass microsphere composites' modulus and tensile strength

Sample code	Tensile modulus (GPa)	Tensile strength (MPa)
P	41.96	214.3618
PG2	43.19	174.0243
PG4	45.59	175.197
PG6	47.17	307.838
PG8	39.79	282.1484
PG10	36.30	196.7399

3.1.1 Optical microscopic representation of the PG6 tensile fracture specimen

Figure 3 is an optical microscopic image of the PG6 sample to analyse the surface topography of the deformed composite.

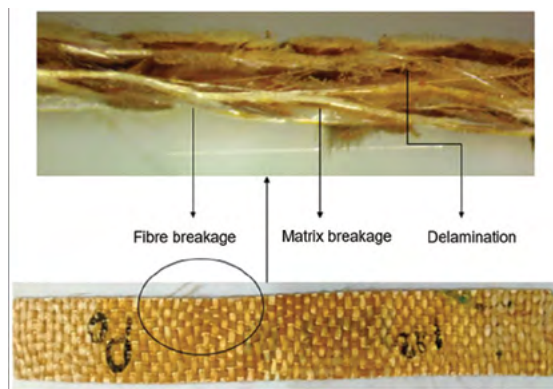


Figure 3: Optical microscopic image of the PG6 composite material before and after fracture

The figure reveals various forms of damage, including fibre breakage, matrix failure and delamination.

3.2 Flexural properties of composites

The glass flexural capacity used as a reinforcement fibre in fabric form was assessed by incorporating glass microspheres into phenolic resin. Testing was carried out to ascertain how the chemical processing affected the bending properties of the material. Distinctions among untreated laminates and those containing glass microspheres are shown in Figure 4. The fabricated composites demonstrated adequate flexural strength, even in the absence of glass microspheres in the composite material. This resulted from the woven fibres' anisotropic nature. The results of the bending tests indicate that the addition of glass microspheres to phenolic resin reduced deformation. The force-deformation curves demonstrated brittle behaviour, which is consistent with the inherent brittleness of the glass. Initially, all composite curves displayed a linear trend with increasing load, eventually transitioning to a non-linear trend. In particular, the PG8 sample exhibited the least deformation at 238 MPa, attributed to the incorporation of 8% glass microspheres into the phenolic resin.

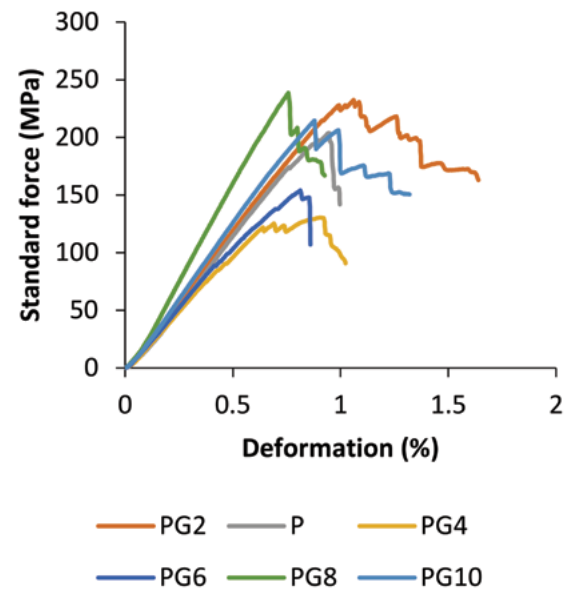


Figure 4: Flexural stress versus deformation curves of glass microspheres-based phenolic resin composite

The flexural strength of the composites containing pure phenolic resin glass fibre (P) was significantly higher than most other samples, except for PG8, which exhibited a strength of 238.66 MPa. This can be attributed to the fibre's ability to support the absorption and propagation of employed loads. Bending strength was utilised to compare the strength of various glass microsphere-based composites. Only PG8 of these composites showed a substantial improvement in strength over the initial sample (P). Conversely, increasing the percentage of glass microspheres to 2%, 4%, 6% and 10% caused flexural property to reduce. According to experimental results, the incorporation of a suitable quantity of glass microsphere filler increased the flexural capabilities of the PG8 composite. However, the glass fibre could no longer support the exerted force. The PG6 and PG8 samples had the highest tensile and bending abilities, suggesting that the glass microsphere content enhanced strength. The scientific conclusion is that because of the substantial interaction between the polymer and the fibre, the outer layer of the glass fibre was more rigid and robust. The procedure with optimal glass microsphere concentrations of 6% and 8% met the specifications for endurance and surface ability. The percentage of glass microspheres increased the flexural stress and modulus at these optimum values. Table 3 presents the results of the flexural strength and flexural modulus of glass microspheres-based composites.

Table 3: Results of the flexural testing of glass microspheres-based composites

Sample code	Flexural strength (MPa)	Flexural modulus (GPa)
P	232.52	24.46
PG2	203.82	24.89
PG4	130.46	25.42
PG6	231.2336	28.14
PG8	238.66	34.37
PG10	214.65	26.43

3.2.1 Optical microscopic image of the PG6 flexural fracture specimen

Figure 5 illustrates the bending behaviour and subsequent fracture in composite materials containing 6% glass microspheres in phenolic resin. It also shows the fractures in similar composites prepared with fibres. This fracture did not appreciably impair the PG6 composite's ability to withstand flexural stress.

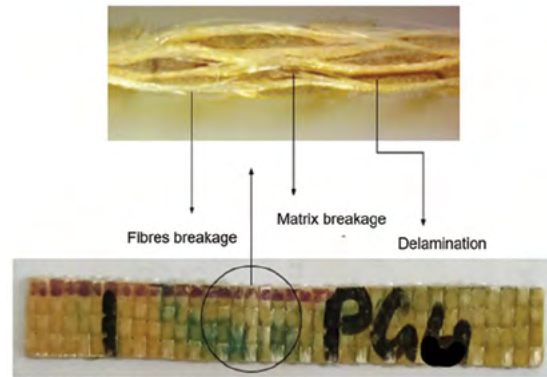


Figure 5: Optical microscopic representation of the PG6 composite material before and after the flexural test

3.3 Composite impact characteristics

Charpy impact measurement revealed that the pure phenolic resin composite exhibited the highest impact strength, absorbing 37.37 kJ/m², indicating superior energy absorption compared to composites containing glass microspheres. Composites with glass microspheres (PG2, PG4, PG6, PG8 and PG10) demonstrated lower impact strength, with values ranging from 14.11 kJ/m² to 25.11 kJ/m² as shown in Table 4. This reduction in impact strength can be attributed to the brittleness of the glass microspheres, which reduces materials' properties for energy capturing during impact. While the addition of glass microspheres enhances the stiffness and modulus of the composites, it compromises their toughness, making them less suitable for applications requiring high-impact resistance. This trade-off highlights the need to balance stiffness and toughness when designing composite materials for specific applications. Figure 6 shows the work-standard travel curves for different composite

samples (P, PG2, PG4, PG6, PG8 and PG10) during the Charpy impact testing. The pure phenolic resin composite (P) showed the highest initial peak force (~ 126 N) and the highest displacement, indicating its superior impact strength. In contrast, composites with glass microspheres (PG2, PG4, PG6, PG8 and PG10) exhibited lower peak forces and reduced impact strength, which is explained by the glass microspheres' delicate tendency. Among these, PG6 and PG8 showed relatively higher impact resistance, with PG6 showing a notable peak force around 25 N, suggesting that a glass microsphere content may provide a balanced improvement in toughness without significantly compromising strength. Overall, while glass microspheres reduced impact strength compared to pure phenolic resin, they enhanced the composite's ability to absorb energy before failure, with PG6 and PG8 being the most promising formulations for applications requiring a trade-off between impact resistance and material strength.

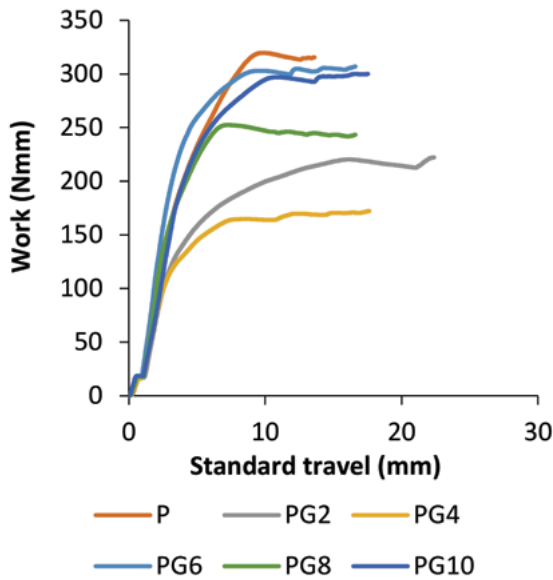


Figure 6: Glass microsphere composites' work vs standard travel curves

3.3.1 Optical microscopic representation of PG6 impact energy absorption

Figure 7 is an optical microscopic image of the PG6 composite material showing the impact area before and after Charpy impact tests

Table 4: Charpy impact values of glass microsphere-based composites

Sample code	Pendulum impact energy, a_c (kJ/m ²)
P	37.37
PG2	15.86
PG4	14.11
PG6	25.11
PG8	24.86
PG10	24.44

and after testing. The PG6 composite recorded the second highest energy absorption value of 25.11 KJ/, surpassed only by the pure phenolic resin-based composite material. The impact energy was significantly compromised. The impact energy of glass microsphere-based composite materials, such as the PG6 composite, was compromised due to the inherent brittleness of glass microspheres. When subjected to impact, the glass microspheres tended to crack and fracture easily, and absorbed less energy than more ductile materials. This brittleness reduced the ability to dissipate impact energy, leading to lower overall impact strength. Additionally, the inclusion of glass microspheres can create stress concentration points within the composite, further facilitating crack initiation and propagation under impact loading.

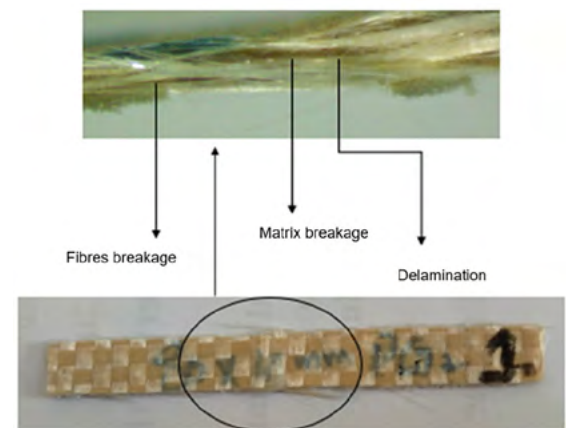


Figure 7: Optical microscopic image of the PG6 composite material before and after Charpy impact tests

Thus, while the PG6 composite demonstrated better energy absorption than other glass microsphere composites, it still fell short of the impact energy absorption capabilities of pure phenolic resin composites.

3.4 Impact test of the drop weight

The results of the drop weight impact evaluation for fibre-reinforced composites reveal significant information regarding the material's ability to store energy. The sample code "P", representing the pure phenolic resin-based composite, absorbed 21.40 J of energy. With the addition of 2% glass microspheres (PG2), energy absorption increased to 26.91 J, indicating that glass microspheres enhanced the impact resistance. Further increases in glass microsphere content continued this trend, with PG4 absorbing 27.72 J and PG6 absorbing the highest amount of 29.14 J, demonstrating the optimal concentration for the enhancement of impact resistance. Beyond this point, however, energy absorption decreased slightly, as seen with PG8 absorbing 25.23 J and PG10 absorbing 21.78 J as shown in Table 5. This

decline suggests that while adding glass microspheres improves impact resistance up to a certain concentration, excessive amounts may lead to brittleness and reduced energy absorption. Overall, the results indicate that an optimal concentration of glass microspheres significantly enhances the composite's resilience to impact, with the PG6 composite exhibiting the best performance.

Figure 8 illustrates the force versus test time for composite samples with varying percentages of glass microspheres (PG2, PG4, PG6, PG8 and PG10) and a pure phenolic resin-based composite (P) during drop weight impact testing. Initially, all samples showed a sharp increase in force upon impact, with the pure resin composite (P) exhibiting a lower peak force than those with glass microspheres. The maximum forces for PG2 and PG4 were higher than those for the pure resin sample, indicating improved impact resistance. PG6 and PG8 maintained high peak forces, demonstrating significant enhancement of up to 8% glass microspheres. However, PG10 showed a decrease in peak force, suggesting diminishing benefits at higher concentrations. Force

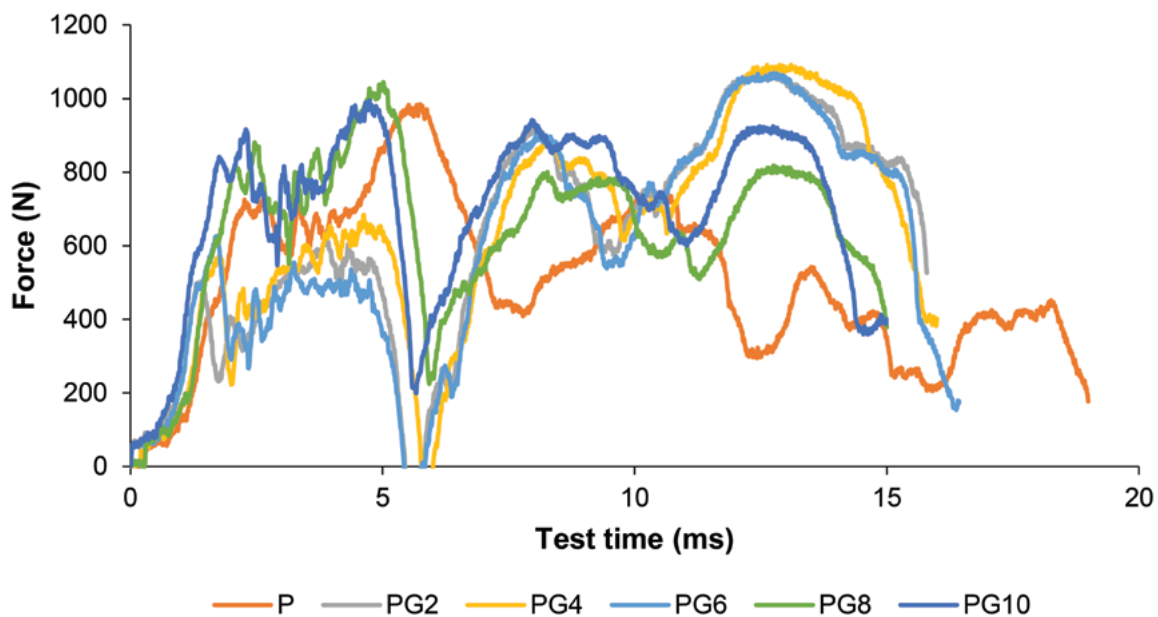


Figure 8: Comparison of the impact force of the impact weight test versus test time curves of various composite samples

fluctuations represent the material's response to impact energy, with a higher glass microsphere content leading to more consistent force levels, indicating better energy absorption. The pure resin sample failed more quickly, while PG6 and PG8 sustained higher forces longer, showing improved toughness and resistance to impact-induced failure. The study therefore confirms that incorporating 6–8% glass microspheres into the phenolic resin matrix optimises the composite's impact properties.

Table 5: Energy absorption of pure phenolic resin composites compared to those reinforced with glass microspheres

Sample code	Energy absorbed (J)
P	21.40
PG2	26.91
PG4	27.72
PG6	29.14
PG8	25.23
PG10	21.78

3.4.1 Optical microscopic representation of PG6 drop weight impact energy absorption

The optical microscopic representation of the PG6 composite material, shown in Figure 9, highlights the effects of the drop weight impact test. The upper part of the image indicates three distinct failure modes: fibre breakage, matrix breakage and delamination. Fibre breakage is observed where the reinforcement fibres have snapped due to the impact. The matrix breakage shows where the phenolic resin matrix has cracked or shattered. Delamination represents the separation of layers within the composite material. The lower part of the image provides a broader view of the composite surface of the sample before testing, with the circled area indicating the specific location where the matrix breakage occurred. This detailed analysis helps to understand how the composite material absorbs and dissipates impact energy, with PG6 showing a substantial energy absorption value of 29.14 J, second only to the pure phenolic resin composite. The presence of glass microspheres in

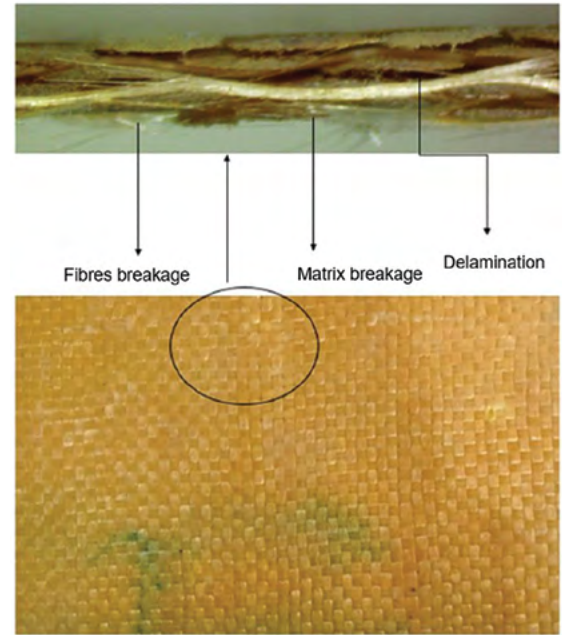


Figure 9: Optical microscopic image of the PG6 composite material before and after impact testing with drop weight

PG6 appears to improve its impact resistance by improving the interaction between the matrix and the fibres, thus delaying catastrophic failure mechanisms such as delamination and fibre breakage.

3.4.2 Force versus displacement

Figure 10 illustrates the force-displacement resistance of various composite samples, each containing different percentages of glass microspheres. The initial sharp increase in force for all samples indicates their resistance to impact. In particular, the PG6 and PG8 composites, containing 6% and 8% glass microspheres, respectively, exhibited higher peak forces and sustained the force over a greater displacement range, indicating superior impact resistance. In contrast, the pure phenolic resin composite (P) showed a lower maximum force and a rapid decrease in force, highlighting its lower impact resistance. The data suggest that incorporating glass microspheres of up to 8% enhances impact properties, while higher percentages, such as 10%, may negatively affect performance.

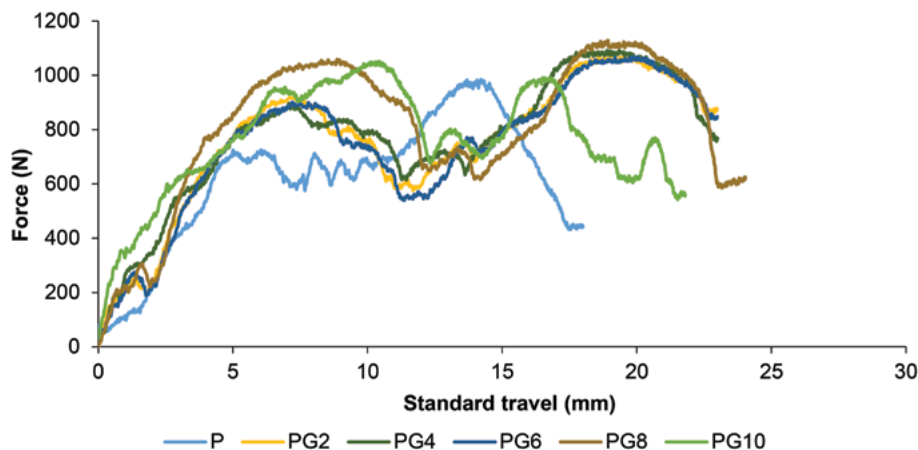


Figure 10: Force versus standard travel curves of various composite samples

4 Conclusion

Based on the extensive mechanical testing conducted in this study, the incorporation of glass microspheres into phenolic resin composites significantly enhanced their mechanical properties. Tensile testing revealed that glass microspheres increased the tensile modulus and achieved maximum tensile strength at concentrations of 6–8%. However, there was no improvement in Charpy impact strength, and the composites exhibited reduced pendulum impact energy compared to pure phenolic resin. Energy absorption increased with the addition of glass microspheres, reaching a peak at a concentration of 8%. The flexural modulus also peaked at a concentration of 8%, with a slight decrease observed beyond this concentration. Impact testing by drop weight also demonstrated that the optimal concentration for improved impact resistance enhancement was found in 6–8% concentrations of glass microspheres, with the PG6 compound absorbing the highest amount of energy at 29.14 J. Force versus time curves showed that composites with 6–8% concentrations of glass microspheres sustained higher peak forces and exhibited improved toughness compared to both pure resin and higher concentration composites. Therefore, this study confirms that 6–8% concentrations of glass microspheres optimise the phenolic resin composites' structural and impact attributes, which

qualify them for potential applications such as automotive components, aerospace structures, marine equipment and construction materials that require high stiffness, strength and impact resistance.

Funding statement: No funding was available for this research.

Authorship contribution: Sultan Ullah – conceptualization, methodology, data collection, writing original draft, visualization, and validation; Zeeshan Ul Hasan – fabrication and testing; Arvydas Palevicius – conceptualization and resources; Giedrius Janusas – supervision.

Conflict of interest disclosure: The authors have no relevant financial or non-financial interests to disclose.

References

1. ABDULGANIYU, I.A., ADESOLA, O.E., OGUOCHA, I.N., ODESHI, A.G. Dynamic impact properties of carbon-fiber-reinforced phenolic composites containing microfillers. *Polymers*, 2023, **15**(14), 1–25, doi: 10.3390/polym15143038.
2. MUSTHAQ, M.A., DHAKAL, H.N., ZHANG, Z., BAROUNI, A., ZAHARI, R. The effect of various environmental conditions on the impact damage behaviour of natural-fibre-reinforced composites (NFRCS) – a critical review. *Polymers*, 2023, **15**(5), 1–40, doi: 10.3390/polym15051229.

3. MOHAMMADI, H., AHMAD, Z., MAZLAN, S.A., FAIZAL JOHARI, M.A., SIEBERT, G., PETRU, M., RAHIMIAN KOLOOR, S.S. Lightweight glass fiber-reinforced polymer composite for automotive bumper applications: a review. *Polymers*, 2022, **15**(1), 1–30, doi: 10.3390/polym15010193.
4. HARO, E.E., ODESHI, A.G., SZPUNAR, J.A. The effects of micro-and nano-fillers' additions on the dynamic impact response of hybrid composite armors made of HDPE reinforced with Kevlar short fibers. *Polymer-Plastics Technology and Engineering*, 2017, **57**(7), 609–624, doi: 10.1080/03602559.2017.1332207.
5. HARO, E.E., ODESHI, A.G., SZPUNAR, J.A. The energy absorption behavior of hybrid composite laminates containing nano-fillers under ballistic impact. *International Journal of Impact Engineering*, 2016, **96**, 11–22, doi: 10.1016/j.ijimpeng.2016.05.012.
6. RAH, M., HOSUR, M., ZAINUDDIN, S., VAIDYA, U., TAUHID, A., KUMAR, A., TROVILLION, J., JEELANI, S. Effects of amino-functionalized MWCNTs on ballistic impact performance of E-glass/epoxy composites using a spherical projectile. *International Journal of Impact Engineering*, 2013, **57**, 108–118, doi: 10.1016/j.ijimpeng.2013.01.011.
7. KHALILI, S.M.R., DAGHIGH, V., ESLAMI FAR-SANI, R. Mechanical behavior of basalt fiber-reinforced and basalt fiber metal laminate composites under tensile and bending loads. *Journal of Reinforced Plastics and Composites*, 2011, **30**(8), 647–659, doi: 10.1177/0731684411398535.
8. GUPTA, N., SINGH BRAR, B., WOLDESENBET, E. Effect of filler addition on the compressive and impact properties of glass fibre reinforced epoxy. *Bulletin of Materials Science*, 2001, **24**, 219–223, doi: 10.1007/BF02710105.
9. OMRANI, A., ROSTAMI, A.A. Understanding the effect of nano- Al_2O_3 addition upon the properties of epoxy-based hybrid composites. *Materials Science and Engineering: A*, 2009, **517**(1–2), 185–190, doi: 10.1016/j.msea.2009.03.076.
10. CHU, C.K., CHEN, Y.L. Ballistic-proof effects of various woven constructions. *Fibres & Textiles in Eastern Europe*, 2010, **18**(6(83)), 63–67.
11. ARORA, S., MAJUMDAR, A., BUTOLA, B.S. Structure induced effectiveness of shear thickening fluid for modulating impact resistance of UHMWPE fabrics. *Composite Structures*, 2019, **210**, 41–48, doi: 10.1016/j.compstruct.2018.11.028.
12. YAHAYA, R., SAPUAN, S.M., JAWAID, M., LEMAN, Z., ZAINUDIN, E.S. Measurement of ballistic impact properties of woven kenaf-aramid hybrid composites. *Measurement*, 2016, **77**, 335–343, doi: 10.1016/j.measurement.2015.09.016.
13. ATMAKURI, A., PALEVICIUS, A., VILKAUSKAS, A., JANUSAS, G. Review of hybrid fiber based composites with nano particles – material properties and applications. *Polymers*, 2020, **12**(9), 1–30, doi: 10.3390/POLYM12092088.
14. REDDY, P.R.S., REDDY, T.S., MADHU, V., GOGIA, A.K., RAO, K.V. Behavior of E-glass composite laminates under ballistic impact. *Materials & Design*, 2015, **84**, 79–86, doi: 10.1016/j.matdes.2015.06.094.
15. RANDJBARAN, E., ZAHARI, R., ABDUL JALIL, N.A., ABANG ABDUL MAJID, D.L. Hybrid composite laminates reinforced with Kevlar/carbon/glass woven fabrics for ballistic impact testing. *The Scientific World Journal*, 2014, **2014**, 1–7, doi: 10.1155/2014/413753.
16. RAMADAN, N., TAHA, M., LA ROSA, A.D., ELSABBAGH, A. Towards selection charts for epoxy resin, unsaturated polyester resin and their fibre-fabric composites with flame retardants. *Materials*, 2021, **14**(5), 1–45, doi: 10.3390/ma14051181.
17. BELINGARDI, G., VADORI, R. Low velocity impact tests of laminate glass-fiber-epoxy matrix composite material plates. *International Journal of Impact Engineering*, 2002, **27**(2), 213–229, doi: 10.1016/S0734-743X(01)00040-9.

Sofien Benltoufa,¹ Hind Algamdy²

¹ Laboratory for the Study of Thermal and Energy Systems (LESTE, LR99ES31), National Engineering School of Monastir, University of Monastir, Tunisia, 05000, Monastir, Tunisia

² Fashion Design and Fabric Department, Turabah University College, Taif University, Taif, Saudi Arabia

Breathability and Dynamic Evaporative Cooling Heat Flow of a Ripstop Defence Fabric

Dihalnost in hladilni dinamični izparilni toplotni tok zaščitne tkanine ripstop

Original scientific article/Izvirni znanstveni članek

Received/Prispelo 9–2024 • Accepted/Sprejeto 1–2025

Corresponding author/Korespondenčni avtor:

Ass. Prof. Dr-Eng. Sofien Benltoufa

E-mail: benltoufa@gmail.com

ORCID iD: 0000-0001-6520-0802

Abstract

This study investigated the breathability and dynamics of evaporative cooling heat flow through a defence fabric. Two ripstop fabrics were developed by changing the floats in the delimiting plain grid. The influence of fibre kinds was studied using weft threads made of 100% cotton, 65% polyester/35% cotton and 100% polyester. First, the breathability of used materials was evaluated using relative water vapour permeability (RWVP), resistance (Ret) and air permeability. Second, a more in-depth examination was conducted using evaporative cooling heat flow kinetics, and certain distinguishing variables that describe the various evaporative cooling heat flow phases were found. Those parameters consider the evaporative heat flow at 0 seconds, defining the skin's first contact and the time spent to reach equilibrium. The results demonstrated that adding polyester to a fabric makes it more breathable, cooler, faster drying, and provides a more refreshing sensation on initial contact with the skin. Adding floats to the delimiting plain grid reduces the fabric's porosity and breathability.

Keywords: ripstop, breathability, evaporative cooling heat flow, refreshing sensation

Izvilleček

V raziskavi sta bila proučevana dihalnost in dinamični izparilni toplotni tok zaščitne tkanine. Z vključitvijo različnih dolžin flotirajočih niti v ojačitveno mrežo osnovne tkanine v vezavi platno sta bili razviti dve tkanini ripstop. Vpliv različne vrste vlaken je bil proučevan z uporabo različnih niti v votku, ki so bile iz 100 % bombaža, 65 % poliestra/35 % bombaža in 100 % poliestra. Najprej je bila ocenjena dihalnost tkanin na podlagi relativne prepustnosti vodne pare, izparilnega toplotnega upora (Riz) in zračne prepustnosti. Sledila je podrobnejša analiza kinetike hladilnega izparilnega toplotnega toka, pri čemer so bile uvedene spremenljivke za opis ugotovljenih različnih faz izparilnega toplotnega toka. Parametri, ki se nanašajo na izparilni toplotni tok v času nič sekund, opredelijo prvi stik s kožo in čas, potreben za doseganje ravnotežja. Rezultati so pokazali, da dodajanje poliestra



Content from this work may be used under the terms of the Creative Commons Attribution CC BY 4.0 licence (<https://creativecommons.org/licenses/by/4.0/>). Authors retain ownership of the copyright for their content, but allow anyone to download, reuse, reprint, modify, distribute and/or copy the content as long as the original authors and source are cited. No permission is required from the authors or the publisher. This journal does not charge APCs or submission charges.

tkanini omogoči večjo zračnost in hladnejši otip, ki se hitreje suši in zagotavlja hladen občutek ob prvem stiku s kožo. Dodajanje flotirajočih niti v ojačitveno mrežno strukturo zmanjša poroznost in zračnost tkanine. Ključne besede: tkanina ripstop, zračnost, izparilni toplotni tok, hladni občutek

1 Introduction

Ripstop is a lightweight and exceptionally durable fabric from polyester, polyamide or natural fibres. It is specifically intended to withstand tearing and wear due to its grid structure, which includes reinforcing threads sewn regularly to form a checkered pattern [1, 2].

Ripstop fabric is often used in military uniforms, which require materials that are both durable and comfortable. The mix of strength, lightweight lightness and breathability make ripstop fabric an excellent choice for these outfits [3]. Its tear-resistant characteristics increase longevity, guaranteeing that uniforms can sustain severe use in extreme environments [4].

Ripstop fabric is also used in daily clothing articles, including casual pants, shorts and jackets. Its durability and comfort make it appropriate for everyday use, and its distinct texture lends a distinctive touch to clothing items.

Ripstop fabric has evolved significantly in terms of materials employed over time. Originally made of polyamide, manufacturers soon began experimenting with various fabrics such as polyester and cotton.

Polyester fibre is an ideal choice for textiles and clothes due to its high durability, wrinkle resistance and colour retention. The global polyester fibre market is anticipated to reach \$153.5 billion by 2030, with a 7.5% growth rate throughout the forecast period. The market volume was 70,195.3 kt in 2022, representing a 6.7% increase from 2019 to 2022 [5]. Cotton is a natural fibre. Its cross-section exhibits a shape akin to beans, allowing air to flow easily through it. Thus, air circulation improves evaporation and the resulting cooling freshens the air in contact with the skin. Cotton absorbs moisture fast and dries slowly, so you may remain dry for a certain (limited) time while performing tasks outdoors. The

worldwide cotton yarn market was worth \$82.81 billion in 2023 and is expected to expand from \$86.11 billion in 2024 to \$117.79 billion by 2032, with a CAGR of 4.0% during the forecast period [6].

Breathability, as one of the important comfort properties, is expressed in terms of air and water vapour permeability. Thermal evaporative resistance (RET) is used to test textiles' breathability and water vapour transmission [7, 8]. The ability of cloth to allow moisture vapour to pass through it is known as water vapour resistance [9]. The lower this resistance is, the more breathable the fabric is. The ISO 11092 standard [10] defines the associated test procedure.

Water vapour diffusion via textile fabrics, also known as the breathability of materials, is intended to provide water vapour evacuation while preventing water liquid from penetrating [11, 12]. Cooling textiles are made with moisture-wicking characteristics that effectively transport moisture away from the skin [13]. Cooling is primarily the function of water vapour permeability level, and wicking fabrics must be in thermal contact with the skin to cause cooling effects. These materials are designed to provide comfort by efficiently regulating moisture [14], particularly in situations when the body releases sweat during physical activity or in hot environmental conditions [15].

Cooling from fabrics improves moisture transport from the skin to the fabric's outer surface [16], as sweat is released onto the skin surface when the body perspires. The moisture evaporates into the surrounding air, absorbing heat energy from the body. This is known as evaporative cooling, which is an important technique for regulating body temperature and improving comfort [17, 18].

The cooling heat flow mechanism has applications in various industries, including sportswear, outdoor clothes, bedding and protective equipment for hot

conditions. The cooling heat flow of textile materials relies on a variety of mechanisms to govern heat transfer and disseminate cooling [15]. Thus, water vapour transfer is a significant factor in textile design [19]. The necessity to examine moisture transfer through textile textiles originates from the human body's continual loss of water, mostly through evaporation from the skin [20, 21]. Water vapour evacuation through clothes is crucial to preserving body temperature balance and comfort. Textile fabric should facilitate fast sweat removal [22] by diffusion and evaporation into the surrounding air [23].

Extensive research work has been performed on water vapour transfer mechanisms across textile fibres [24–26], simple fabrics [27–31], layered fabrics [32, 33], textile systems [34, 35] and clothing assemblies [36–38]. Nevertheless, most investigations were carried out in static conditions where equilibrium conditions were considered, with little work done under dynamic states. Dynamic tests should be considered, as water vapour transfer is strongly related to water vapour diffusion in fibres and condensation in pores, and is time-dependent [39, 40].

Several test methods for measuring the moisture transfer abilities of textile materials have been developed, with different methodologies and testing conditions used. Although every test method applied near real-world conditions, no single test method could fully reconstruct the complicated process [41].

Moisture absorption varies between natural and synthetic fibres. As the solid-water characteristic energy of a polymer increases, the hydrophilic surface attracts water molecules more strongly than the hydrophobic surface [42]. Moisture sorption mechanisms, particularly in hydrophilic fibre materials, are very complicated due to the constant change in fibre structure caused by swelling. This results in a shift in geometric confirmation in the fabric's pores [43, 44]. As a result, it is essential to study the kinetics of water vapour transport. According to the evaluation described in this section, there is little research dealing with dynamic evaporative cooling heat flow through textile textiles.

In this study, two ripstop samples were designed and woven as defence materials utilising 100% cotton, 65% polyester/35% cotton and 100% polyester weft threads. First, the breathability of the utilised samples was studied in terms of water vapour resistance, relative water vapour permeability and air permeability. Second, dynamic evaporative cooling heat flow during evaporation was visualised using the Permetest device. Some characteristic parameters describing the different evaporative cooling heat flow phases were identified. While (Q_0) represents the evaporative cooling heat flow at first contact with the skin, (Q_{\min}) represents the minimal evaporative cooling heat flow, (Q_{\max}) represents the maximum evaporative cooling heat flow, (Q_{eq}) represents the evaporative cooling heat flow at equilibrium, ($t_{Q_0} - > Q_{\min}$) represents the time spent to reach the minimum evaporative cooling heat flow, and (t_{eq}) represents the heat flow equilibrium time. These factors may be useful for comparing and evaluating the competitiveness of comfortable textile textiles.

2 Materials and methods

2.1 Rip-stop fabric pattern design

Two types of rip-stop fabric pattern design are illustrated in Figure 1. Fabric design was based on the delimiting grid variation between the plain-woven structure. Samples were woven using a rigid rapier Dornier HTV/HTVS/PTV weaving machine. The shedding system was controlled by the Bonas ZJ2 jacquard mechanism.

The used fabrics were woven using the same warp yarn with a composition of 100% polyester and a yarn number of 25 Nm. Weft yarns of 25 Nm with different materials (100% cotton, 65%/polyester, 35% cotton and 100% polyester) were used. The chosen warp and weft count were (24 ± 2) threads/cm. The woven fabric thickness was evaluated using the ISO 5084:1996 standard [45]. Mass per unit area, warp and weft densities were measured according to the ISO 7211-6:2020 standard [46]. A yarn's linear

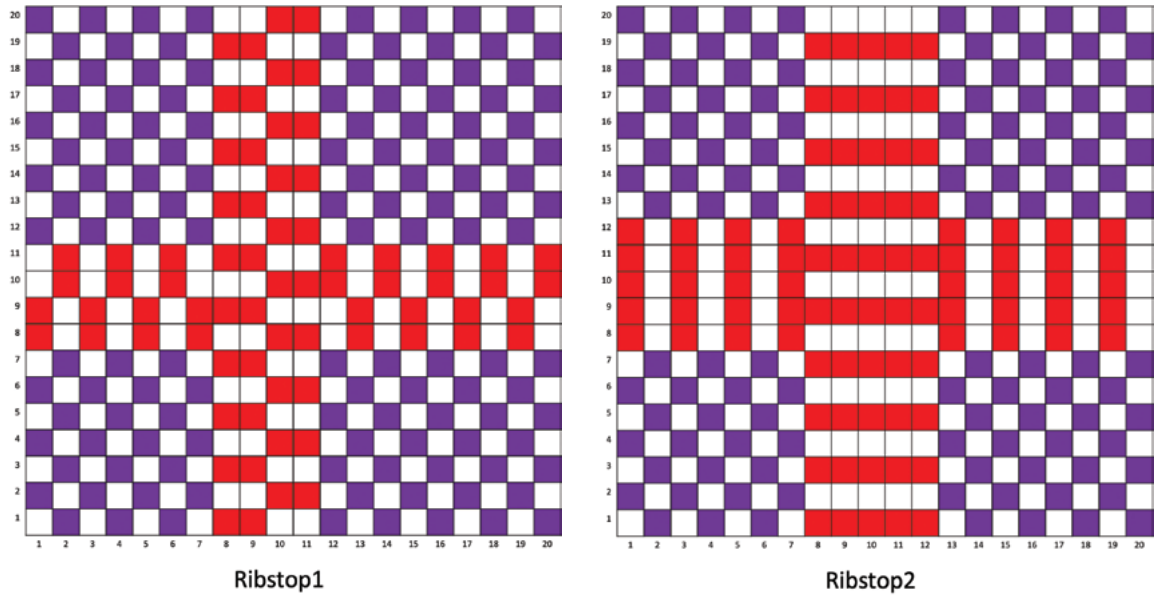


Figure 1: Ripstop fabrics design: ■ plain woven design; ■ floats on the delimiting grid

densities were determined using the ISO 2060:1994 standard [47]. The warp and weft densities were calculated based on the ISO 7211-2:2024 standard [48].

2.2 Total porosity

The total fabric porosity (ϵ_{total}) was determined using the following equation [49]:

$$\epsilon_{total} = 1 - \frac{\rho_{fabric}}{\rho_{fibre}} \quad (1)$$

where ρ_{fabric} represents the fabric density (g/m^3) and was determined as follows:

$$\rho_{fabric} = \frac{M}{t} \quad (2)$$

where M represents the fabric mass per unit area (g/m^2) and t represents the fabric thickness (m).

Here, the fibre density average was determined according to the percentage of blend ratio of each fibre in the produced yarns, as mentioned by Kakvan et al. [50]:

$$\rho_{fibre} = \sum_{i=1}^n p_i \times \rho_i \quad (3)$$

where p_i represents the percentage of each fibre_i ratio and ρ_i represents its density.

The woven fabric structural parameters are presented in Table 1.

Table 1: Structural parameters of fabrics used

Sample code	Weft yarn composition	Thickness (mm)	Mass per unit area (g/m^2)	Total porosity (%)
Ribstop1-CT	100% cotton	0.56 ± 0.06	215 ± 6	68 ± 4
Ribstop1-PC	65% polyester/35% cotton	0.55 ± 0.02	212 ± 4	73 ± 3
Ribstop1-PO	100% polyester	0.54 ± 0.01	211 ± 3	78 ± 2
Ribstop2-CT	100% cotton	0.59 ± 0.05	217 ± 7	69 ± 2
Ribstop2-PC	65% polyester/35% cotton	0.56 ± 0.01	214 ± 5	71 ± 4
Ribstop2-PO	100% polyester	0.55 ± 0.01	213 ± 2	76 ± 3

2.3 Air permeability

The air permeability measurements were conducted on an FX 3300 Labotester III Textest air permeability tester with a 100 Pa pressure difference according to the ISO 9237:1995 standard [51].

2.4 Relative water vapour permeability and resistance

A Permetest Sensora device, simulating the human skin (Figure 2), was used to measure the relative

water vapour resistance and relative permeability according to the ISO 11092 standard [10]. A heated porous semipermeable foil was used to simulate the sweating skin. The heat required for the water to evaporate from the membrane, with and without a fabric covering, was recorded in the steady state. The fabric sample was set on a measuring head over the semi-permeable membrane under a parallel air flow velocity of 1 m/s, simulating walking speed.

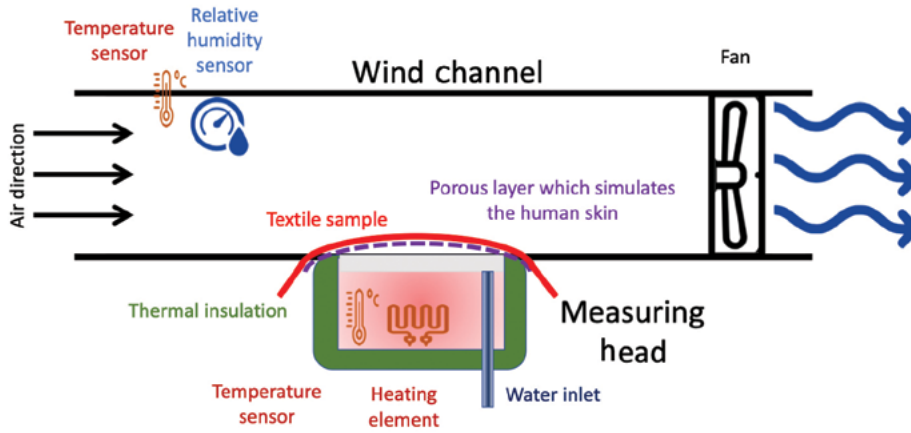


Figure 2: Permetest skin model working principle [52]

The water vapour resistance (R_{et}) of a textile sample according to the ISO 11092 standard [10] was expressed as follows:

$$Ret(m^2Pa/W) = (P_{sat} - P_v) \left(\frac{1}{q_s} - \frac{1}{q_0} \right) \quad (4)$$

where R_{et} represents water vapour resistance (m^2Pa/W), P_{sat} represents saturated water vapour partial pressure at test temperature (Pa) and is equivalent to the skin vapour pressure, P_v represents air partial water vapour pressure (Pa), q_s represents measuring head heating power with sample (W/m^2) and q_0 represents measuring head heating power without sample (W/m^2).

The relative water vapour permeability (R_{wvp}) was determined using the following relation [53]:

$$R_{wvp} = 100 \times \frac{q_s}{q_0} \quad (5)$$

All tests were carried out under standard conditions in an atmosphere of $20 \text{ }^\circ\text{C} \pm 2 \text{ }^\circ\text{C}$ and $65\% \pm 4\%$ relative humidity according to ISO 139:2005 standard [54]. Isothermal conditions inside the instrument during the R_{et} measurements were maintained with a precision of $\pm 0.1 \text{ }^\circ\text{C}$. All fabric samples were conditioned in the same atmosphere 24 hours before testing.

3 Results and discussion

In this part, the breathability properties were initially investigated in terms of water vapour resistance (R_{et}), relative water vapour permeability (RWVP) and air permeability. Second, cooling evaporative heat flow kinetics during evaporation were visualised to identify the various stages of the evaporative cooling heat flow.

3.1 Breathability parameters

Breathability parameters are expressed in terms of water vapour resistance (R_{et}), relative water vapour permeability (RWVP) and air permeability, as presented in Table 2.

It is evident that the relative water vapour permeability and the air permeability look similar and are proportional to total porosity values. On the contrary, water vapour resistance is inversely proportional to total porosity.

Table 2: Breathability parameters of fabrics used

Sample	R_{et} ^{a)}			RWVP ^{b)}			Air permeability		
	\bar{x} ^{c)} (m ² Pa/W)	SD ^{d)} (m ² Pa/W)	CV ^{e)} (%)	\bar{x} ^{c)} (%)	SD ^{d)} (m ² Pa/W)	CV ^{e)} (%)	\bar{x} ^{c)} (l/m ² /s)	SD ^{d)} (m ² Pa/W)	CV ^{e)} (%)
Ribstop1-CT	2.51 ± 0.17	0.19 ± 0.09	4.24 ± 0.8	80.2 ± 1.4	3.6 ± 1.3	8.5 ± 0.4	151.8 ± 4.9	7.2 ± 0.7	4.8 ± 0.8
Ribstop1-PC	2.34 ± 0.15	0.17 ± 0.06	3.29 ± 0.5	82.5 ± 1.2	2.4 ± 0.8	6.3 ± 0.3	158.3 ± 2.0	3.9 ± 0.4	3.8 ± 0.6
Ribstop1-PO	2.23 ± 0.14	0.15 ± 0.05	2.34 ± 0.4	86.1 ± 1.3	1.7 ± 0.3	4.1 ± 0.7	165.2 ± 1.6	4.1 ± 0.3	4.6 ± 0.3
Ribstop2-CT	2.98 ± 0.22	0.21 ± 0.08	4.47 ± 0.5	71.6 ± 2.3	3.2 ± 1.1	6.1 ± 0.6	137.5 ± 3.1	6.6 ± 0.6	3.4 ± 0.4
Ribstop2-PC	2.61 ± 0.18	0.19 ± 0.06	3.25 ± 0.3	76.7 ± 2.1	2.1 ± 0.5	4.4 ± 0.4	147.2 ± 1.8	3.8 ± 0.3	3.6 ± 0.5
Ribstop2-PO	2.43 ± 0.116	0.16 ± 0.04	2.23 ± 0.3	82.4 ± 1.5	1.6 ± 0.2	3.9 ± 0.5	157.4 ± 1.2	3.6 ± 0.2	2.4 ± 0.4

^{a)} water vapour resistance; ^{b)} relative water vapour permeability; ^{c)} average; ^{d)} standard deviation; ^{e)} coefficient of variation

According to Table 2, the Ribstop1-PO sample was the most breathable fabric, registering a water vapour resistance of about (2.23 ± 0.14) m²Pa/W. Its relative water vapour permeability was 86.1% ± 1.3%, while its air permeability was about (165.2 ± 1.6) l/m²/s.

The least breathable fabric was Ribstop2-CT fabric, with a water vapour resistance of about (2.98 ± 0.22) m²Pa/W. Its relative water vapour permeability was around 71.6% ± 2.3%, while its air permeability was around (137.5 ± 3.1) l/m²/s.

As evident from Table 2, polyester fabrics are more breathable than cotton fabrics. The presented values only consider a steady state. Thus, the dynamics of the evaporative cooling heat flow should be considered for a more in-depth investigation of water vapour transfer through a textile fabric.

3.2 Dynamic evaporative cooling heat flow

Evaporative cooling heat flow kinetics during evaporation are presented in this subsection. It is important to study in detail how water vapour is transferred through textile fabrics. The cooling heat flow kinetics

under 1 m/s of air velocity are presented in Figure 3.

Figure 3 suggests that displaying the cooling heat flow dynamics resulted in three phases. Initially, the maximum cooling heat flow was measured as the difference between the sample temperatures at 20 °C ± 2 °C and 65% ± 2% relative humidity and the temperature at the top of the measuring heat, which was around 18 °C ± 2 °C owing to evaporation from the semi-permeable foil. During the second stage, known as the transition phase, cooling heat flow reduces to a minimum value before increasing to an equilibrium value, signalling the beginning of the third stage, i.e. the steady state phase. The initial heat flow drop in most of the heat flow lines is caused by exothermal moisture absorption in the measured fabric.

At zero seconds, the Ribstop1-PO sample had a heating flow of 135.1 W ± 8.2 W, whereas the Ribstop2-PO sample had a heating flow of 121.6 W ± 6.9 W. During evaporation on a Permetest device, samples conditioned at room temperature (20 °C ± 2 °C) had higher temperatures than those in the wind channel (18 °C ± 2 °C), as recorded by an infrared

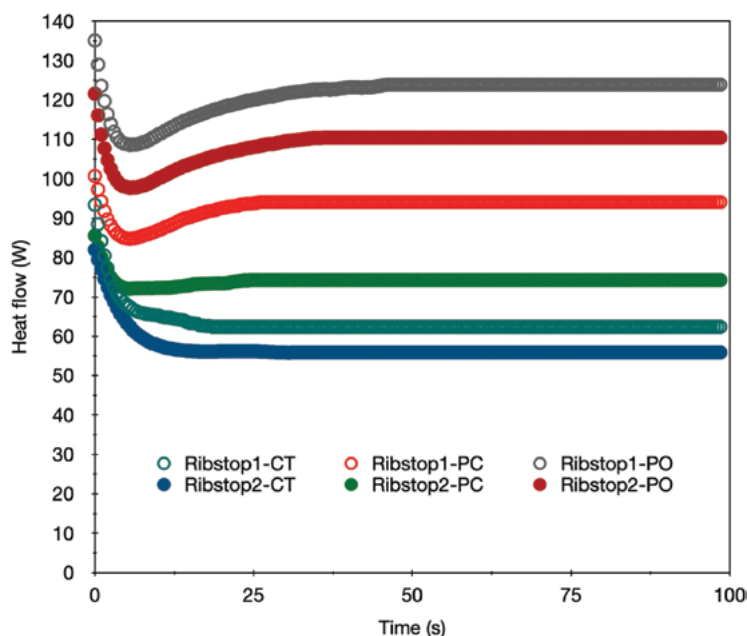


Figure 3: Evaporative cooling heat flow of studied fabrics under an air velocity of 1 m/s

thermometer, due to cooling from the wetted porous grid under the tested fabric.

In the subsequent stage, to equalise the temperature between the fabric and the measuring top head, the heat flow dropped to $108.6 \text{ W} \pm 6.4 \text{ W}$ in Ribstop1-PO compared to $97.7 \text{ W} \pm 4.8 \text{ W}$ in Ribstop2-PO. In the third step, cooling heat flow was increased until it reached equilibrium. The increase in flow was induced by evaporation through the fabric from the semi-permeable membrane, which cools the fabric's top surface. Equilibrium cooling heat flow is defined as the continual penetration of water vapour through a textile fabric. Figure 3 also shows that the Ribstop1-PO fabric felt cooler than the Ribstop2-PO fabric. This is due to crosshatch lines placed between the plain pattern design, which were observed to have longer drying periods and an increased water vapour concentration.

Concerning the two woven fabrics from 100% of weft threads (Ribstop1-CT and Ribstop2-CT), it is evident that they are less cool than fabrics containing polyester fibres.

Cotton fibre, as a natural cellulosic fibre, has high absorbency due to its many hydrophilic -OH groups. The hydroxyl group is a univalent OH group. OH groups are polar and thus attract water molecules, which are also polar. As a result, the OH groups are responsible for the fibre's ability to absorb moisture [55, 56].

Thus, when textile fabrics made of hydrophilic fibres absorb humidity, the causing swelling of fibres and thus a decrease in the fabric's porosity [57], the phenomena of water vapour diffusion occur.

Regarding polyester-containing textiles, polyester fibre is a hydrophobic fibre that repels water vapour molecules and resists moisture absorption. This fluctuation is generated by a film of water vapour condensing on a sample's pores and blocking evaporation. This process is known as water vapour condensation.

Table 3 shows some of the distinctive factors that define the various evaporative cooling heat flow phases based on Figure 3.

Table 3: Evaporative cooling heat flow characteristics

Sample	$Q_0^a)$ (W)	$Q_{min}^b)$ (W)	$Q_{max}^c)$ (W)	$Q_{eq}^d)$ (W)	$t_{Q_0 \rightarrow Q_{min}}^e)$ (s)	$t_{eq}^f)$ (s)
Ribstop1-CT	93.4 ± 1.1	62.4 ± 0.5	93.4 ± 1.0	62.4 ± 0.4	18.5 ± 1.5	18.5 ± 0.5
Ribstop1-PC	100.7 ± 1.3	84.8 ± 0.7	100.7 ± 1.1	94.1 ± 0.6	5.5 ± 0.5	26 ± 1.0
Ribstop1-PO	135.1 ± 1.4	108.6 ± 1.1	135.1 ± 1.2	123.9 ± 1.0	5.5 ± 0.5	46 ± 1.5
Ribstop2-CT	82 ± 0.6	55.8 ± 0.4	82 ± 0.6	55.9 ± 0.3	29 ± 1.5	29 ± 0.5
Ribstop2-PC	85.595 ± 0.5	72.08 ± 0.6	85.595 ± 0.5	74.3 ± 0.7	5.5 ± 0.5	24.5 ± 0.5
Ribstop2-PO	121.59 ± 0.8	97.74 ± 0.7	121.59 ± 0.9	110.43 ± 1.0	5.5 ± 0.5	36 ± 1.5

^{a)} heat power at 0 s; ^{b)} minimum registered heat power; ^{c)} maximum registered heat power; ^{d)} equilibrium heat power; ^{e)} elapsed time in seconds from the heat power from Q_0 to the Q_{min} values; ^{f)} heat flow equilibrium time

Based on the results presented in Table 3, the Ribstop1-PO is the coolest fabric, offering a better fresh feeling for the wearer. Cotton fabrics are less cool than those containing polyester. Moreover, all fabrics containing polyester reach equilibrium at about 5.5 ± 0.5 s compared to those composed of cotton, which reach equilibrium at about 18.5 ± 1.5 s in the case of Ribstop1-CT compared to 29 ± 1.5 s in the case of Ribstop2-CT. Thus, adding polyester to a fabric makes it cooler and fast drying.

4 Conclusion

This study focused on the breathability and the dynamics of evaporative cooling heat flow in a defence fabric. Two ripstop textiles were designed and woven with various weft thread materials: 100% cotton (hydrophilic), 65% polyester/35% cotton and 100% polyester (hydrophobic). A Permetest device was used to determine water vapour resistance (RET) and relative water vapour permeability (RWVP). The same device was used to visualise the dynamics of heat movement during evaporative cooling.

It was discovered that employing various fibre materials (hydrophilic or hydrophobic) had a considerable impact on breathability. Adding floats to the barrier to the delimiting plain woven grid reduces a fabric's breathability.

This is due to overlapping warp and weft floats, resulting in thickness and mass per unit area. This

reduces overall porosity and modifies geometrical and pore arrangement.

Three phases were identified when studying the dynamics of evaporative cooling heat flow. Initially, the maximum cooling heat flow was measured as the difference between the sample temperatures at $20 \text{ }^\circ\text{C} \pm 2 \text{ }^\circ\text{C}$ and $65\% \pm 2\%$ relative humidity and the temperature at the top of the measuring heat, which was approximately $18 \text{ }^\circ\text{C} \pm 2 \text{ }^\circ\text{C}$ due to evaporation cooling from the semi-permeable membrane. During the second stage, known as the transition phase, cooling heat flow dropped to a minimum value before increasing to an equilibrium value, indicating a steady state phase.

The influence of environmental conditions (temperature and relative humidity) on cooling heat flow dynamics will be a key topic of focus for future frameworks.

Declaration of conflicts of interests: The authors declare there are no conflicts of interest.

Funding: The authors received no financial support for the research, authorship and/or publication of this article.

Acknowledgment: The author would like to acknowledge the Deanship of Graduate Studies and Scientific Research, Taif University for funding this work.

References

1. BEHERA, G.R., MUKHOPADHYAY, A., SIKKA, M. Development of scheme to evaluate the performance of parachute canopy fabrics under tensile impact. *Journal of Industrial Textiles*, 2022, **51**(suppl. 2), 2283S–3305S, doi: 10.1177/15280837221080103.
2. BEHERA, G.R., SIKKA, M., MUKHOPADHYAY, A. Effect of fabric construction, seam angle, and impact force on the performance of the parachute canopy. *The Journal of the Textile Institute*, 2023, **114**(8), 1257–1267, doi: 10.1080/00405000.2022.2131360.
3. AMRI SAFIAI, M.S., ARIS, A., ABD RAHMAN, N.H. Dielectric constant measurement technique on army ripstop nylon material. In *2022 IEEE International RF and Microwave Conference (RFM)*, Kuala Lumpur, Malaysia, 2022, 1–4, doi: 10.1109/RFM56185.2022.10064823.
4. ERYURUK, S.H., KALAOĞLU, F. The effect of weave construction on tear strength of woven fabrics. *Autex Research Journal*, 2015, **15**(3), 207–214, doi: 10.1515/aut-2015-0004.
5. Polyester fiber market size, share & trends analysis report by form (solid, and hollow), by grade, by product type (polyester staple fiber (PSF), and polyester filament yarn (PFY)), by application, by regional outlook and forecast, 2023 - 2030 [online]. Research and Markets [accessed 31 May 2024]. Available on World Wide Web: < <https://www.researchandmarkets.com/reports/5928446/polyester-fiber-market-size-share-and-trends>>.
6. KABISH, A.K., DEGEFU, D.T., GEBREGIORGIS, Z.D. Cotton value chain and economics. In *Cotton Sector Development in Ethiopia: Challenges and Opportunities*. Edited by K. Murugesh Babu, Abera Kechi Kabish, Getnet Belay Tesema and Bizuayehu Kerisew Semahagn. Singapore : Springer, 2024, 441–463, doi: 10.1007/978-981-99-9149-5_18.
7. RUCKMAN, J.E. Water resistance and water vapour transfer. In *Textiles in Sport*. Edited by R. Shishoo. Woodhead Publishing, 2005, 287–305, doi: 10.1533/9781845690885.4.287.
8. REN, Y.J., RUCKMAN, J.E. Water vapour transfer in wet waterproof breathable fabrics. *Journal of Industrial Textiles*, 2003, **32**(3), 165–175, doi: 10.1177/1528083703032003002.
9. RUCKMAN, J.E. The application of a layered system to the marketing of outdoor clothing. *Journal of Fashion Marketing and Management*, 2005, **9**(1), 122–129, doi: 10.1108/13612020510586442.
10. ISO 11092:2014. Textiles – Physiological effects – Measurement of thermal and water-vapour resistance under steady-state conditions (sweating guarded-hotplate test). Geneva : International Organization for Standardization, 2017, 1–15.
11. MANDAL, S., ANNAHEIM, S., CAMENZIND, M., ROSSI, R.M. Evaluation of thermo-physiological comfort of clothing using manikins. In *Manikins for Textile Evaluation*. Edited by Rajkishore Nayak and Rajiv Padhye. Elsevier, 2017, 115–140, doi: 10.1016/B978-0-08-100909-3.00005-4.
12. GHOLAMREZA, F., SU, Y., LI, R., NADARAJA, A.V., GATHERCOLE, R., LI, R., GOLOVIN, K., ROSSI, R.M., ANNAHEIM, S., MILANI, A.S. Modeling and prediction of thermophysiological comfort properties of a single layer fabric system using single sector sweating torso. *Materials*, 2022, **15**(16), 1–16, doi: 10.3390/MA15165786.
13. ULLAH, H.M.K., LEJEUNE, J., CAYLA, A., MONCEAUX, M., CAMPAGNE, C., DEVAUX, É. A review of noteworthy/major innovations in wearable clothing for thermal and moisture management from material to fabric structure. *Textile Research Journal*, 2022, **92**(17–18), 3351–3386, doi: 10.1177/00405175211027799.

14. BENLTOUFA, S., BOUGHATTAS, A., FAYALA, F., ALGAMDY, H., ALFALEH, A., LUBOS, H., ALJUAID, A. Water vapour resistance modelling of basic weaving structure. *The Journal of The Textile Institute*, 2024, **115**(12), 2456–2468, doi: 10.1080/00405000.2023.2293503.
15. ALFALEH, A., BENLTOUFA, S., FAYALA, F. Evaporation coefficient determination during the capillary rise. *Textile Research Journal*, 2023, **93**(17–18), 4191–4196, doi: 10.1177/00405175231168425.
16. NASRIN, S., MANDAL, S., ISLAM, M.M., PETROVA, A., AGNEW, R.J., BOORADY, L.M. Factors affecting the sweat-drying performance of active sportswear - a review. *Textiles*, 2023, **3**(3), 319–338, doi: 10.3390/TEXTILES3030022.
17. HES, L., LOGHIN, C. Heat, moisture and air transfer properties of selected woven fabrics in wet state. *Journal of Fiber Bioengineering and Informatics*, 2009, **2**(3), 141–149, doi: 10.3993/jfbi12200901.
18. BOGUSŁAWSKA-BACZEK, M., HES, L. Effective water vapour permeability of wet wool fabric and blended fabrics. *Fibres and Textiles in Eastern Europe*, 2013, **21**(1(97)), 67–71.
19. ZHANG, C., WANG, X., LV, Y., MA, J., HUANG, J. A new method for evaluating heat and water vapor transfer properties of porous polymeric materials. *Polymer Testing*, 2010, **29**(5), 553–557, doi: 10.1016/j.polymertesting.2010.02.004.
20. BECKER, S., POTCHTER, O., YAAKOV, Y. Calculated and observed human thermal sensation in an extremely hot and dry climate. *Energy and Buildings*, 2003, **35**(8), 747–756, doi: 10.1016/S0378-7788(02)00228-1.
21. KEATINGE, W.R. Principles and practice of human physiology. By O. G. Edholm and J. S. Weiner. Pp. 672. (Academic Press, 1981). *Quarterly Journal of Experimental Physiology*, 1981, **6**(4), 543–543, doi: 10.1113/expphysiol.1981.sp002598.
22. DONG, Y., KONG, J., MU, C., ZHAO, C., THOMAS, N.L., LU, X. Materials design towards sport textiles with low-friction and moisture-wicking dual functions. *Materials and Design*, 2015, **88**, 82–87, doi: 10.1016/j.matdes.2015.08.107.
23. ALFALEH, A., BENLTOUFA, S., FAYALA, F. Evaporation coefficient determination during the capillary rise. *Textile Research Journal*, 2023, **93**(17–18), 4191–4196, doi: 10.1177/00405175231168425.
24. ITO, H., MURAOA, Y. Water transport along textile fibers as measured by an electrical capacitance technique. *Textile Research Journal*, 1993, **63**(7), 414–420, doi: 10.1177/004051759306300706.
25. HONG, K., HOLLIES, N.R.S., SPIVAK, S.M. Dynamic moisture vapor transfer through textiles. Part I: clothing hygrometry and the influence of fiber type. *Textile Research Journal*, 1988, **58**(12), 697–706, doi: 10.1177/004051758805801203.
26. FOURT, L., CRAIG, R.A., RUTHERFORD, M.B. Cotton fibers as means of transmitting water vapor. *Textile Research Journal*, 1957, **27**(5), 362–368, doi: 10.1177/004051755702700504.
27. FORSMAN, N., JOHANSSON, L.S., KOIVULA, H., TUURE, M., KÄÄRIÄINEN, P., ÖSTERBERG, M. Open coating with natural wax particles enables scalable, non-toxic hydrophobation of cellulose-based textiles. *Carbohydrate Polymers*, 2020, **227**, 1–9, doi: 10.1016/j.carbpol.2019.115363.
28. MA, X., MAILLET, B., BROCHARD, L., PITOIS, O., SIDI-BOULENOUAR, R., COUSSOT, P. Vapor-sorption coupled diffusion in cellulose fiber pile revealed by magnetic resonance imaging. *Physical Review Applied*, 2022, **17**, 1–13, doi: 10.1103/PhysRevApplied.17.024048.
29. MACHATTIE, L.E., GOODINGS, A.C., TURL, L.H. The diffusion of water vapor through laminae with particular reference to textile fabrics. *Textile Research Journal*, 1957, **27**(5), 418–418, doi: 10.1177/004051755702700513.

30. ADAMU, B.F., GAO, J. Comfort related woven fabric transmission properties made of cotton and nylon. *Fashion and Textiles*, 2022, **9**, 1–10, doi: 10.1186/s40691-021-00285-2.
31. LEE, S., OBENDORF, S.K. Statistical modeling of water vapor transport through woven fabrics. *Textile Research Journal*, 2012, **82**(3), 211–219, doi: 10.1177/0040517511433145.
32. GIBSON, P.W. Factors influencing steady-state heat and water vapor transfer measurements for clothing materials. *Textile Research Journal*, 1993, **63**(12), 749–764, doi: 10.1177/004051759306301208.
33. FOHR, J.P., COUTON, D., TREGUIER, G. Dynamic heat and water transfer through layered fabrics. *Textile Research Journal*, 2002, **72**(1), 1–12, doi: 10.1177/004051750207200101.
34. WOODCOCK, A.H. Moisture transfer in textile systems. Part II. *Textile Research Journal*, 1962, **32**(9), 719–723, doi: 10.1177/004051756203200903.
35. WOODCOCK, A.H. Moisture transfer in textile systems. Part I. *Textile Research Journal*, 1962, **32**(8), 628–633, doi: 10.1177/004051756203200802.
36. CHEN, Y.S., FAN, J., ZHANG, W. Clothing thermal insulation during sweating. *Textile Research Journal*, 2003, **73**(2), 152–157, doi: 10.1177/004051750307300210.
37. LI, Y., ZHU, Q., YEUNG, K.W. Influence of thickness and porosity on coupled heat and liquid moisture transfer in porous textiles. *Textile Research Journal*, 2002, **72**(5), 435–46, doi: 10.1177/004051750207200511.
38. ADLER, M.M., WALSH, W.K. Mechanisms of transient moisture transport between fabrics. *Textile Research Journal*, 1984, **54**(5), 334–343, doi: 10.1177/004051758405400510.
39. LIN, Y., CHENG, N., MENG, N., WANG, C., WANG, X., YU, J., DING, B. A patterned knitted fabric with reversible gating stability for dynamic moisture management of human body. *Advanced Functional Materials*, 2023, **33**(44), 1–9, doi: 10.1002/adfm.202304109.
40. ABEDIN, F., DENHARTOG, E. The exothermic effects of textile fibers during changes in environmental humidity: a comparison between ISO:16533 and dynamic hot plate test method. *Fibers*, 2023, **11**(5), 1–15, doi: 10.3390/fib11050047.
41. DING, X. Fabric permeability testing. In *Fabric Testing*. Edited by Jinlian Hu. Woodhead Publishing, 2008, 189–227, doi: 10.1533/9781845695064.189.
42. NIU, D., TANG, G.H. The effect of surface wettability on water vapor condensation in nanoscale. *Scientific Reports*, 2016, **6**, 1–6, doi: 10.1038/srep19192.
43. BENLTOUFA, S., FAYALA, F., CHEIKHROUHO, M., NASRALLAH, B. Porosity determination of jersey structure. *Autex Research Journal*, 2007, **7**(1), 63–69, doi: 10.1515/aut-2007-070107.
44. BOUGHATTAS, A., BENLTOUFA, S., HES, L., AZEEM, M., FAYALA, F. Thermo-physiological properties of woven structures in wet state. *Industria Textila*, 2018, **69**(4), 298–303, doi: 10.35530/it.069.04.1452.
45. ISO 5084:1996. Textiles – Determination of thickness of textiles and textile products. Geneva : International Organization for Standardization, 1996, 1–5.
46. ISO 7211-6:2020. Textiles – Methods for analysis of woven fabrics construction. Part 6: Determination of the mass of warp and weft per unit area of fabric. Geneva : International Organization for Standardization, 2020, 1–4.
47. ISO 2060:1994. Textiles – Yarn from packages – Determination of linear density (mass per unit length) by the skein method. Geneva : International Organization for Standardization, 1994, 1–13.
48. ISO 7211-2:2024. Textiles – Methods for analysis of woven fabrics construction – Part 2: Determination of number of threads per unit length. Geneva : International Organization for Standardization, 2024, 1–5.

49. KAKVAN, A., SHAIKHZADEH NAJAR, S., PSIKUTA, A. Study on effect of blend ratio on thermal comfort properties of cotton/nylon-blended fabrics with high-performance Kermel fibre. *The Journal of the Textile Institute*, 2015, **106**(6), 674–682, doi: 10.1080/00405000.2014.934045.
50. VARSHNEY, R.K., KOTHARI, V.K., DHAMIJA, S. A study on thermophysiological comfort properties of fabrics in relation to constituent fibre fineness and cross-sectional shapes. *The Journal of the Textile Institute*, 2010, **101**(6), 495–505, doi: 10.1080/00405000802542184.
51. ISO 9237:1995. Textiles — Determination of the permeability of fabrics to air. Geneva : International Organization for Standardization, 1995, 1–5.
52. BENLTOUFA, S., ALGAMDY, H., GHITH, A., -FAYALA, F., HES, L. The water vapour resistance dynamic measurement of natural and synthetic fibre. *International Journal of Clothing Science and Technology*, 2024, **36**(6), 1094–1105, doi: 10.1108/IJCST-01-2024-0012.
53. HES, L., DE ARAUJO, M. Simulation of the effect of air gaps between the skin and a wet fabric on resulting cooling flow. *Textile Research Journal*, 2010, **80**(14), 1488–1497, doi: 10.1177/0040517510361797.
54. ISO 139:2005. Textiles – Standard atmospheres for conditioning and testing. Geneva : International Organization for Standardization, 2005, 1–6.
55. SAHU, P., GUPTA, M.K. Water absorption behavior of cellulosic fibres polymer composites: A review on its effects and remedies. *Journal of Industrial Textiles*, 2022, **51**(suppl. 5), 7480S–7512S, doi: 10.1177/1528083720974424.
56. ALOMAYRI, T., ASSAEDI, H., SHAIKH, FUA., LOW, I.M. Effect of water absorption on the mechanical properties of cotton fabric-reinforced geopolymer composites. *Journal of Asian Ceramic Societies*, 2014, **2**(3), 223–230, doi: 10.1016/J.JASCER.2014.05.005.
57. BENLTOUFA, S., FAYALA, F., NASRALLAH, S BEN. Determination of yarn and fiber diameters after swelling using a capillary rise method. *The Journal of the Textile Institute*, 2012, **103**(5), 517–522, doi: 10.1080/00405000.2011.589573.

Brigita Tomšič, Maja Blagojevič, Nuša Klančar, Erik Makoter, Klara Močenik, Nika Pirš, Sebastijan Šmid,
Marija Veskova, Marija Gorjanc, Mateja Kert, Barbara Simončič
University of Ljubljana, Faculty of Natural Sciences and Engineering, Aškerčeva 12, 1000 Ljubljana, Slovenia

Multifunctional Properties of Cotton Fabric Tailored via Green Synthesis of TiO₂/Curcumin Composite

Večfunkcionalne lastnosti bombažne tkanine, pripravljene z zeleno sintezo kompozita TiO₂/kurkumin

Original scientific article/Izvirni znanstveni članek

Received/Prispelo 11–2024 • Accepted/Sprejeto 1–2025

Corresponding author/Korespondenčna avtorica:

Prof. dr. Barbara Simončič

Tel: +38513712557

E-mail: barbara.simoncic@ntf.uni-lj.si

ORCID iD: 00000-0002-6071-8829

Abstract

In this study, a novel green process was developed to produce a multifunctional cotton (CO) fabric incorporating TiO₂/curcumin composites that simultaneously provides UV protection and photocatalytic performance. For this purpose, TiO₂ was synthesised using the sol–gel process; loaded with the natural colourant curcumin as a visible light absorber at two temperatures, i.e., 70 and 350 °C; and applied to the CO fabric via the pad–dry–cure process. For comparison, TiO₂ was synthesised without curcumin under the same conditions. The synthesis conditions at 70 °C ensured the formation of predominantly amorphous TiO₂, while curcumin promoted TiO₂ crystallisation despite the low synthesis temperature. A 350 °C synthesis temperature was high enough to form the polymorphic TiO₂ anatase phase. Although the increase in synthesis temperature and the presence of curcumin in the composites caused a bathochromic shift in light absorption, the photocatalytic activity of all samples was mainly driven by UV light. Chemically modifying the CO fabric significantly reduced the light transmittance of the samples, with the highest absorption of UV light obtained for the sample containing the TiO₂/curcumin composite synthesised at 70 °C. This sample provided excellent UV protection with a UPF value of 51.6. All chemically modified CO samples showed photocatalytic activity, degrading coffee stains and decolourising methylene blue and Rhodamine B dye solutions. The highest photocatalytic efficiency and reusability were obtained again for the CO sample with the TiO₂/curcumin composite synthesised at 70 °C, demonstrating the synergistic effect between TiO₂ and curcumin in the composite prepared under these synthesis conditions.

Keywords: multifunctional cotton, titanium dioxide, *Curcuma longa*, green synthesis

Izvleček

Razvit je bil nov zelen postopek za izdelavo večfunkcionalne bombažne (CO) tkanine z vgrajenimi kompoziti TiO₂/kurkumin, ki hkrati zagotavlja UV-zaščito in fotokatalitsko delovanje. V ta namen je bil sintetiziran TiO₂ s postopkom sol–gel v prisotnosti naravnega barvila kurkumina kot stabilizatorja in absorberja vidne



Content from this work may be used under the terms of the Creative Commons Attribution CC BY 4.0 licence (<https://creativecommons.org/licenses/by/4.0/>). Authors retain ownership of the copyright for their content, but allow anyone to download, reuse, reprint, modify, distribute and/or copy the content as long as the original authors and source are cited. No permission is required from the authors or the publisher. This journal does not charge APCs or submission charges.

svetlobe pri dveh temperaturah, in sicer 70 in 350 °C, ter nanosen na CO-tkanino z impregnirnim postopkom. Za primerjavo je bil TiO_2 sintetiziran pri enakih pogojih brez prisotnosti kurkumina. Pogoji sinteze pri 70 °C so omogočili nastanek pretežno amorfne TiO_2 , je pa prisotnost kurkumina podprla kristalizacijo TiO_2 kljub nizki temperaturi sinteze. Temperatura sinteze 350 °C je bila dovolj visoka za tvorbo TiO_2 v polimorfni fazi anatasa. Čeprav sta zvišanje temperature sinteze in prisotnost kurkumina v kompozitih povzročila batokromni premik absorbirane svetlobe, je bila fotokatalitska aktivnost vseh vzorcev pogojena predvsem z UV-svetlobo. Kemijska modifikacija CO-tkanine je bistveno zmanjšala prepustnost svetlobe vseh vzorcev, pri čemer je bila najvišja absorpcija UV-svetlobe dosežena pri vzorcu, ki je vseboval kompozit TiO_2 /kurkumin, sintetiziran pri 70 °C. Ta vzorec je zagotovil odlično UV-zaščito z UZF vrednostjo 51,6. Vsi kemijsko modificirani CO-vzorci so bili fotokatalitsko aktivni, kar je privedlo do razgradnje madežev kave in razbarvanja raztopin barvil metilensko modro in Rhodamine B. Največji fotokatalitska učinkovitost in sposobnost ponovne uporabe sta bili tudi v tem primeru doseženi pri CO-vzorcju s kompozitom TiO_2 /kurkumin, sintetiziranim pri 70 °C, kar kaže na sinergijski učinek med TiO_2 in kurkuminom v kompozitu, pripravljenim pri teh sinteznih pogojih.

Ključne besede: večfunkcionalni bombaž, titanov dioksid, *Curcuma longa*, zelena sinteza

1 Introduction

Titanium dioxide (TiO_2) is a wide-band-gap semiconductor that represents one of the most versatile nanomaterials (NMs) in various environmental, energy and biochemical fields owing to its unique properties, including photocatalytic activity; ultraviolet (UV) light absorption; chemical, photochemical and thermal stability; biocompatibility; and non-toxicity [1–3]. In the field of textiles, TiO_2 is an established textile finishing agent, where the application of TiO_2 NMs can impart multifunctional properties such as photocatalytic self-cleaning, UV protection, antimicrobial activity, deodorising properties, hydrophobicity, thermal stability, flame retardancy and electrical conductivity [4]. Furthermore, textiles functionalised with TiO_2 can be advantageously used for smart energy-harvesting textiles and to degrade various pollutants in air or water through a photocatalytic reaction. Regarding the latter, it has been reported that textile substrates can serve as an excellent scaffolding for TiO_2 NMs to enhance their photocatalytic activity [4].

The photocatalytic process in TiO_2 is initiated by irradiation with UV light, enabling the absorption of photons that excite electrons from the valence band (VB) into the conduction band (CB), leaving holes

in the valence band. This forms electron–hole pairs that can migrate to the TiO_2 surface and participate in redox reactions in the presence of oxygen and water, forming highly reactive oxygen species (ROS). The latter can react in subsequent reactions with various pollutants, including dye molecules in the water, and cause their degradation [5–7].

The photocatalytic activity of TiO_2 is directly influenced by various factors, including the morphology of NMs and their crystallinity and modifications of the TiO_2 surface and interface [8–11]. It has been reported that nanostructured TiO_2 exhibits better photocatalytic performance compared with bulk materials and that the most effective photocatalytic activity can be obtained for TiO_2 NMs with polymorphic anatase crystal structures owing to their high surface-to-volume ratio and nanoscale crystallite size. Different surface and interfacial engineering strategies for TiO_2 are crucial for improving photocatalytic performance and enhancing visible light photocatalytic activity. These mainly include multiphase heterojunctions, ion doping, metal doping/loading, coupling with other semiconductors and surface sensitisation [10]. As TiO_2 surface sensitisers, synthetic dyes are

usually adsorbed onto the TiO_2 surface to improve its absorption properties for visible light. Such photocatalytic systems are commonly used in dye-sensitised solar cells, with ruthenium-based dyes being the most extensively studied as sensitisers because of their high performance in improving system efficiency. The mechanism of photocatalytic activity for dye-sensitised TiO_2 is based on the dye's absorption of visible light, promoting electron excitation from the highest occupied molecular orbital of the dye (HOMO) to the lowest unoccupied molecular orbital (LUMO), followed by electron transfer from the LUMO with a higher energy level to the CB of the TiO_2 with a lower energy level. This transfer is crucial, as it allows the oxygen reduction reaction to generate superoxide radicals, one of the most important ROS, to take place on the surface of the TiO_2 under visible light [12].

However, synthesising heavy-metal-based dyes is not in line with the principles of green chemistry because of the toxicity and environmental impact of ruthenium [13]. Therefore, replacing ruthenium-based dyes in dye-sensitised TiO_2 composites with non-toxic alternatives is a major research challenge. Following sustainable approaches, natural dyes and pigments derived from natural sources have already been used not only as stabilisers in TiO_2 NM synthesis but also as visible light activators in the construction of dye-sensitised TiO_2 [14–20].

Among the natural colourants, turmeric powder extract, obtained from the *Curcuma longa* plant, has a long tradition in daily life, where it is used as a spice in cooking and as a natural remedy in health and skin care [21–25]. Turmeric powder is also often used as a natural colourant because of its orange-coloured active ingredient, curcumin (diferuloyl methane) [26, 27]. Curcumin contains phenolic hydroxyl and carbonyl groups in its chemical structure that can form attractive hydrogen bonds with TiO_2 [28], contributing to the stability and durability of the composite.

This research aims to develop a new process for the green synthesis of dye-sensitised TiO_2 in the

presence of the natural dye curcumin as a visible light absorber and stabiliser and to construct a cotton/ TiO_2 /curcumin composite with effective multifunctional photocatalytic performance. Cotton fabric was selected as the textile substrate because it is one of the most versatile textile substrates, with a wide range of applications. As a natural fibre with many advantages – such as hydrophilicity, breathability, flexibility, durability and biodegradability – cotton is a very suitable textile substrate for incorporating TiO_2 NMs to produce multifunctional composites for apparel and technical purposes. In addition, cotton can form close bonds with dye-sensitised TiO_2 because of its high functional hydroxyl group content, improving the stability of the composite. In this experiment, two methods were used to synthesise dye-sensitised TiO_2 , the first at a temperature of 350 °C, ensuring the formation of the anatase crystal structure of TiO_2 , and the second at the more sustainable low temperature of 70 °C, during which the formation of amorphous TiO_2 was expected. We hypothesised that curcumin in the composite would activate the TiO_2 and enhance photocatalytic activity, even when synthesised at lower temperatures. For comparison, TiO_2 was synthesised without curcumin. The effectiveness of the photocatalytic performance of cotton/ TiO_2 /curcumin composites compared with that of cotton/ TiO_2 composites was investigated by determining their UV protection properties and photocatalytic activity.

2 Experimental

2.1 Materials

Chemically bleached 100 % cotton (CO) fabric in plain weave with a mass per unit area of 120 g/m² was kindly provided by Tekstina d.o.o., Ajdovščina, Slovenia, for this study. Titanium(IV) isopropoxide (TTIP; $\geq 97.8\%$ concentration), isopropanol (iPrOH; $\geq 99\%$ concentration) and acetic acid (AA; 99% concentration), all products from Sigma Aldrich (USA), were used to prepare TiO_2 nanoparticles (NPs). Turmeric powder (Maestro, Podravka d.d.,

Croatia) was purchased from the local supermarket. Methylene Blue (MB; Sigma Aldrich, USA) and Rhodamine B (RhB; Sigma Aldrich, USA) were used as dyes for monitoring the photocatalytic activity of the samples.

2.2 Synthesis of curcumin-sensitised TiO₂

The curcumin-sensitised TiO₂ synthesis comprised a synthesis of TiO₂ NPs loaded with curcumin. To synthesise TiO₂ NPs, a 4% solution of hydrolysed TTIP in isopropanol and acetic acid was prepared (12 g TTIP in a mixture of 168 g of iPrOH and 20 g of AA). The solution was prepared in a beaker and placed on a magnetic stirrer. While the solution was stirring, 200 g of distilled water was added drop by drop. Afterwards, the sol was left stirring for the next 15 minutes at room temperature to complete the TiO₂ synthesis. The TiO₂ NPs were then filtered and dried at 70 °C. Turmeric extract was prepared in bi-distilled water at a concentration of 5 g/L. Turmeric powder was dispersed into the bi-distilled water at room temperature. The dispersion was boiled for five minutes and then left to cool down for 30 minutes. Afterwards, the dispersion was filtered and dried.

To load TiO₂ NPs with curcumin, a 4 % TiO₂ solution was prepared in 5 g/L of turmeric extract and stirred for 12 hours in the dark at room temperature. The sample was then centrifuged, decanted, rinsed in water three times, and centrifugated and decanted

to remove all the unadsorbed curcumin. One half of the sample was then dried at 70 °C for 3 hours and labelled (T+C)70. The other half of the sample amount was additionally calcinated at 350 °C, and that sample was labelled (T+C)350.

For comparison, TiO₂ NPs without curcumin were synthesised under the same conditions at both temperatures, i.e. at 70 °C for the (T)70 sample and at 350 °C for the (T)350 sample.

2.3 Chemical modification of cotton samples

To chemically modify the CO fabric samples, (T)70, (T+C)70, (T)350 and (T+C)350 sols were prepared at 4 % concentration in distilled water and sonicated for 2 hours to obtain homogeneous dispersions. Sols were applied to the CO samples using a pad-dry-cure process, which included fully immersing the CO samples in the sol for 1 minute (four 6 cm × 7 cm CO samples for each sol), squeezing the samples with a 95 ± 2% wet pick-up, drying them at 100 °C for 1 min, and curing them at 150 °C for 5 min. Afterwards, the functionalised CO samples were rinsed with distilled water three times for one minute to remove unbound TiO₂. The synthesis processes for the (T)70, (T+C)70, (T)350 and (T+C)350 powder samples and their application to the CO fabric samples are schematically presented in Figure 1. The sample codes are shown in Table 1 according to the functionalised chemical modification and fabrication of multifunctional cotton samples.

Table 1: Sample codes and description of the cotton chemical modification process

Sample code	Process description
CO(UN)	Untreated cotton sample
CO(T)70	Cotton sample chemically modified with TiO ₂ dried at 70 °C
CO(T+C)70	Cotton sample chemically modified with TiO ₂ /curcumin composite dried at 70 °C
CO(T)350	Cotton sample chemically modified with TiO ₂ calcinated at 350 °C
CO(T+C)350	Cotton sample chemically modified with TiO ₂ /curcumin composite calcinated at 350 °C

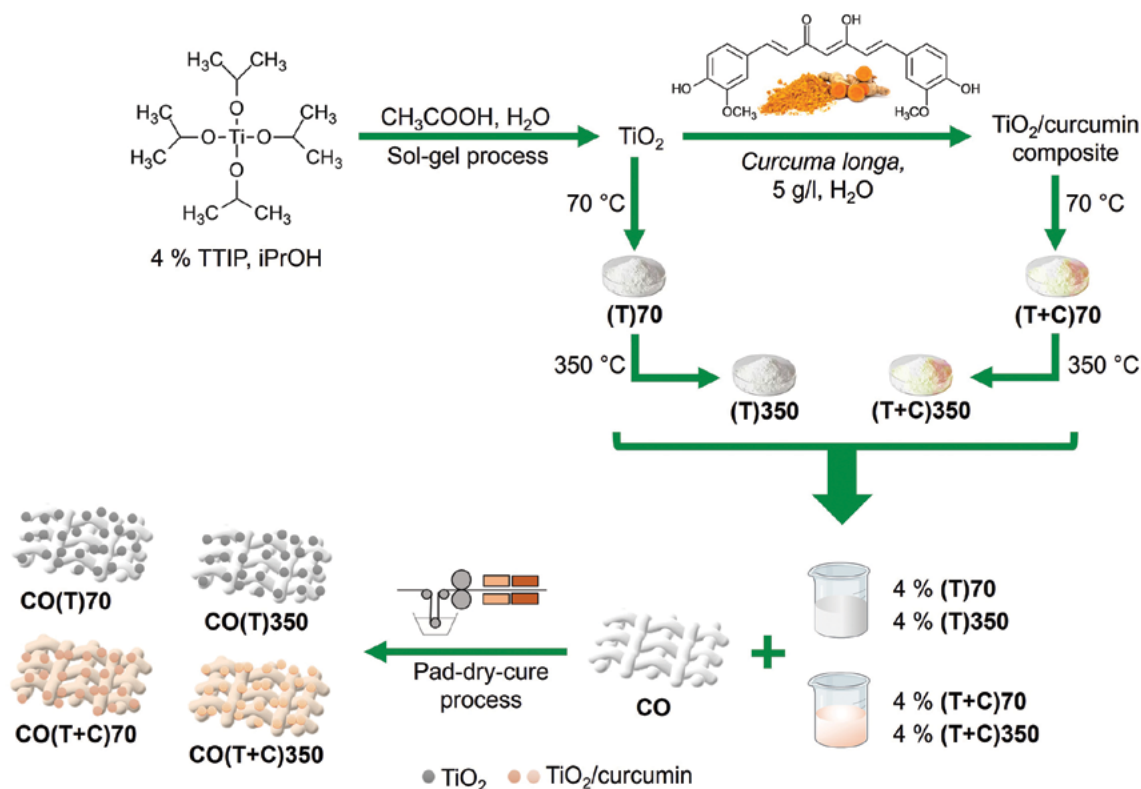


Figure 1: Schematic presentation of the synthesis process for TiO_2 and TiO_2 /curcumin composites and the chemical modification of CO samples

2.4 Analysis and Measurement

2.4.1 X-ray diffraction (XRD)

An XRD characterisation was performed for the synthesised (T)70, (T+C)70, (T)350 and (T+C)350 powders, the CO(UN), and the chemically modified CO(T)70, CO(T+C)70, CO(T)350 and CO(T+C)350 samples using a PANalytical X'Pert PRO X-ray diffractometer (XRD) ($\text{CuK}\alpha 1 = 1.5406 \text{ \AA}$) with a fully open X'Celerator detector ($2.1225^\circ 2\theta$). The XRD pattern was measured from 10 to $90^\circ 2\theta$ with a step size of $0.034^\circ 2\theta$ and a 100 s integration time. The crystallite size, D , of the powder samples was determined from XRD spectra using the Debye-Scherrer equation [29]:

$$D = \frac{0.9 \lambda}{\beta \cos \theta} \quad (1)$$

where λ is the wavelength of X-rays equal to 0.154 nm ;

β is the full width at half-maximum (FWHM); and θ is the diffraction angle.

2.4.2 Scanning electron microscopy (SEM) and energy-dispersive X-ray spectroscopy (EDX)

SEM images of the untreated and chemically modified CO samples were acquired using a JSM 6060 LV scanning electron microscope (JEOL, Tokyo, Japan) operated with a primary electron beam accelerated to 10 kV . All samples were coated with a thin layer of gold before examination to provide conductivity and improve the quality of the images.

EDX analysis was performed using a field emission scanning electron microscope, FEG-SEM Thermo Scientific Quattro S (ThermoFischer Scientific, USA). Sample analysis was performed using an Oxford Instruments Ultim Max 65 energy-dispersive detector (EDX) and AZtec software Ver 6.0 (Oxford Instruments, USA). Samples were coated with a thin

carbon layer before analysis to provide conductivity and thus improve the quality of the images.

2.4.3 Inductively coupled plasma-mass spectrometry (ICP-MS)

The Ti concentrations in the CO(T)70, CO(T+C)70, CO(T)350 and CO(T+C)350 samples were determined via ICP-MS using a Perkin Elmer SCIED Elan DRC spectrophotometer. A 0.5 g sample was prepared in a Milestone microwave system via acid decomposition with 65% HNO₃ and 30% H₂O₂. Ti concentrations in studied samples were reported as the mean values of two measurements for each sample. Based on the measured Ti values, the TiO₂ concentration was calculated.

2.4.4 Fourier transform infrared spectroscopy (FTIR)

The chemical compositions was analysed for the synthesised (T)70, (T+C)70, (T)350 and (T+C)350 powder samples, the untreated CO(UN), and the chemically modified CO(T)70, CO(T+C)70, CO(T)350 and CO(T+C)350 samples using an FTIR spectrometer, Spectrum 3 (Perkin Elmer, UK). Spectra between 4000 cm⁻¹ and 400 cm⁻¹ were recorded with a 4 cm⁻¹ resolution and an average of 120 spectra per sample.

2.4.5 UV-Vis spectroscopy

The transmission spectra of the CO(T)70, CO(T+C)70, CO(T)350 and CO(T+C)350 samples were recorded in a wavelength, λ , range of 250–700 nm using a Lambda 850+ UV/Vis spectrophotometer (Perkin Elmer, UK). Three measurements were made for each sample at different warp alignment angles, and the average value of transmittance, T , at each λ was calculated. The average transmission spectra were converted into absorption spectra using the following equation:

$$A = -\log T \quad (2)$$

where A is absorbance. From the absorption spectra, the optical band gap energies, E_g , of the (T)70,

(T+C)70, (T)350 and (T+C)350 coatings on the CO samples were determined using the Tauc relation [30, 31]:

$$(\alpha h \nu)^2 = K(h \nu - E_g) \quad (3)$$

where α is the energy-dependent absorption coefficient, equal to $2.303 \times A$; h is Planck constant; ν is the frequency of the radiation; and K is a constant. According to Planck's radiation law, the energy, E , of radiation is equal to:

$$E = h \nu = \frac{1240}{\lambda} \quad (4)$$

The values of E_g are obtained through extrapolation to $\alpha = 0$ [31].

2.4.6 UV protection

The UV protection of the CO(UN), CO(T)70, CO(T+C)70, CO(T)350 and CO(T+C)350 samples was determined according to Standard EN 13758-1: 2001. Transmission was calculated at three different wavelength ranges, i.e., UVA from 315 to 400 nm and UVB from 290 to 315 nm. The UV protection factor (UPF) was calculated with the following equation [32]:

$$\text{UPF} = \frac{\sum_{290}^{400} E(\lambda) \times \varepsilon(\lambda) \times \Delta\lambda}{\sum_{290}^{400} E(\lambda) \times \varepsilon(\lambda) \times T(\lambda) \times \Delta\lambda} \quad (5)$$

where $E(\lambda)$ represents the solar spectral irradiance; $\varepsilon(\lambda)$ represents the relative erythral effectiveness; $\Delta(\lambda)$ represents the wavelength interval; and $T(\lambda)$ is the spectral transmittance at the wavelength, λ .

The UPF rating and protection categories were determined using UPF values with the Australian/New Zealand Standard for Sun-Protective Clothing—Evaluation and Classification (AS/NZS 4399, 2020), where UPF values of 15 are suited to the “minimum protection” category; UPF values of 30 are suited to the “good protection” category; and UPF values of 50 are suited to the “excellent protection” category.

2.4.7 Photocatalytic activity

The photocatalytic activity of the CO(T)70, CO(T+C)70, CO(T)350 and CO(T+C)350 samples was determined based on photocatalytic self-cleaning and photocatalytic dye degradation in the solution. To study the photocatalytic self-cleaning performance, the samples were immersed in decanted Turkish coffee (5 g of ground coffee/100 mL water) for 30 s and then air dried and illuminated in a Xenon Alpha instrument (Atlas, USA) at 35 °C and 70% humidity for 4 and 24 hours. Before and after the illumination, the colour coordinates L^* , a^* and b^* in the CIELAB colour space were determined for the samples using a Datacolor Spectro 1050 spectrophotometer (Datacolor, USA). Measurements were performed with a 9 mm aperture under D_{65} illumination and an observation angle of 10°. Ten measurements were performed for each sample, and the colour difference, ΔE_{ab}^* , was calculated using the following equation [33]:

$$\Delta E_{ab}^* = \sqrt{(\Delta L^*)^2 + (\Delta a^*)^2 + (\Delta b^*)^2} \quad (6)$$

where ΔL^* , Δa^* and Δb^* are the differences between the lightness, green–red and blue–yellow colour coordinates, respectively, calculated between the illuminated and nonilluminated samples.

For photocatalytic dye degradation, 0.01 mM MB and 0.02 mM RhB dyes were prepared in distilled water. The CO samples (3.5 cm × 0.8 cm) were immersed in the dye solution (3 ml) that the cuvettes were previously filled with (2 parallels for each sample) and stabilised in the dark for 30 minutes. Two additional cuvettes with only the dye solution were used as a reference (blank). Afterwards, the cuvettes were illuminated for a set period in a Xenotest Alpha instrument equipped with a visible xenon arc lamp (radiation attitude, 0.8–2.5 kVA, and extended radiation range, 300–400 nm). After each illumination period, the absorption spectrum of the dye solution was recorded, from which the maximal value of A at a suitable wavelength was determined (for RhB at 552.9 nm, MB at 664.0 nm) and the corresponding dye concentration in solution was

determined using previously prepared calibration curves. The measurements were performed using a Lambda 850+ UV–Vis spectrophotometer (Perkin Elmer, United Kingdom). The photocatalytic degradation efficiency of the RhB and MB dyes was determined based on the dye concentration ratio, C_t/C_0 , where C_t is the dye concentration at a given time of illumination, and C_0 is the initial concentration of the dye solution after the adsorption–desorption equilibrium was established [34]. The lower the C_t/C_0 ratio, the higher the degree of dye degradation. From these results, the apparent rate constant, K_{app} , of the photocatalytic reaction was calculated as a measure of the dyes' photocatalytic degradation efficiency, where pseudo-first-order kinetics was used as follow [34]:

$$\ln \frac{C_t}{C_0} = -K_{app} t \quad (7)$$

where t is the illumination time. In the case of RhB dye solution degradation, the reusability of the CO samples was determined after 4 repetitive operation cycles.

3 Results and discussion

3.1 Morphological, chemical and optical properties

The morphological, chemical and optical properties of synthesised powder particles and chemically modified CO samples were analysed using XRD, SEM, EDX, ICP-MS, FTIR and UV–Vis spectroscopy. The XRD patterns of the TiO_2 powder samples (Figure 2a) show that the peaks of the (T)350 and (T+C)350 samples were much more intense than those of the (T)70 and (T+C)70 samples. Strong diffraction 2θ peaks in the (T)350 and (T+C)350 samples appearing at 25.3°, 37.8°, 47.9°, 54.0°, 55.3° and 62.6° are characteristic TiO_2 peaks in anatase polymorph phase and correspond to tetragonal crystal planes (1 0 1), (0 0 4), (2 0 0), (1 0 5), (2 1 1) and (2 0 4), respectively [35–37]. In the case of the (T)70 powder sample, the un-sharpness and larger width of the low-intensity peaks indicate that TiO_2 formed

a mostly amorphous phase during the synthesis at 70 °C. Curcumin in the preparation of the (T+C)70 powder sample significantly increased the intensity of the peaks in the diffractogram, suggesting that curcumin promotes TiO₂ crystallisation even at low synthesis temperatures and that polymorphically modified anatase was also partly formed in this sample. Cellulose in the chemically modified CO(T)70,

CO(T+C)70, CO(T)350 and CO(T+C)350 samples blurred the characteristic TiO₂ peaks because of the intensive 2 θ peaks at 15.0°, 16.8°, 22.7° and 34.5°, which correspond to the (1 1 0), (1 1 0), (2 0 0) and (4 0 0) crystallographic planes of the crystalline structure of cellulose, respectively (Figure 2b) [38]. Only the TiO₂ diffraction 2 θ peaks at 25.3° can be seen in the CO(T)350 and CO(T+C)350 samples.

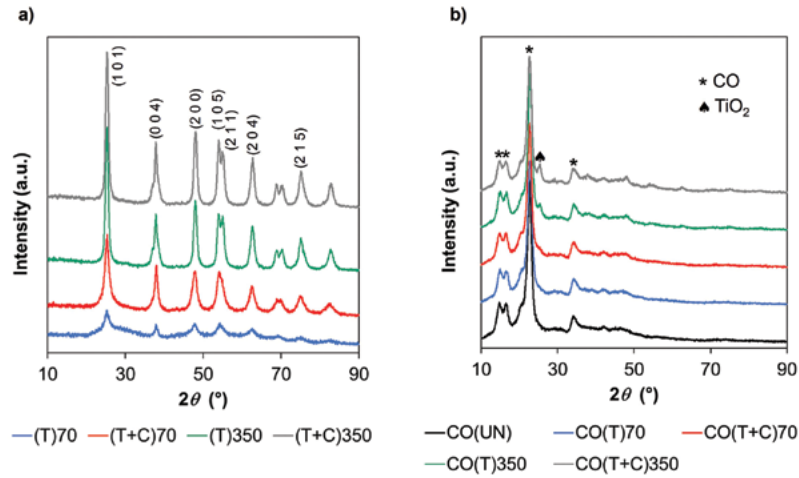


Figure 2: XRD patterns of (T)70, (T+C)70, (T)350 and (T+C)350 powder samples (a) and untreated CO(UN) and chemically modified CO(T)70, CO(T+C)70, CO(T)350 and CO(T+C)350 samples (b)

For the (T+C)70, (T)350 and (T+C)350 powder samples, where the anatase polymorph phase was determined from the XRD patterns, the average crystallite size was calculated using the Debye–Scherrer equation and was on the nanometre scale (Table 2).

This indicates that TiO₂ sol–gel synthesis enables the fabrication of NPs of very small sizes, around 10 nm. Similar results have been reported in the literature [39]. The curcumin in the (T+C)350 sample did not significantly influence the crystallite size.

Table 2: Crystallite size of the TiO₂ powder samples calculated using the Scherrer equation

Sample code	2 θ (°)	β (rad)	Crystallite size (nm)	Average crystallite size (nm)
(T+C)70	25.3	1.321	4.2	5.6
	47.9	1.468	7.0	
(T)350	25.3	0.876	12.4	11.6
	47.9	0.993	10.7	
(T+C)350	25.3	0.850	12.8	12.4
	47.9	0.954	11.9	

Applying (T)70, (T+C)70, (T)350 and (T+C)350 to the CO samples significantly increased the roughness of the fibre surfaces. Smaller and larger TiO₂ particle agglomerates could be seen at nano- and micro-dimensions (Figure 3a). Although sol–gel

synthesis enables the fabrication of very small TiO₂ NPs, they agglomerated after drying. Sonicating the dispersions for 2 hours before applying them to the CO samples did not sufficiently reduce the agglomerate size. The curcumin in the (T+C)70 and (T+C)350

samples increased the agglomeration tendency, as there were visible, micrometre-sized agglomerates in the CO(T+C)70 and CO(T+C)350 samples. The presence of TiO_2 in all chemically modified samples was confirmed by the EDX spectra (Figure 3b) and element mapping (Figure 3c). The ICP-MS results (Figure 3d) show that the highest amount of TiO_2

was present in the CO(T)350 sample, which was 16000 mg/kg. This value was more than three times higher than that in the CO(T)70 sample (5100 mg/kg), and significantly higher than in the CO(T+C)70 sample (10000 mg/kg) and the CO(T+C)350 sample (13000 mg/kg).

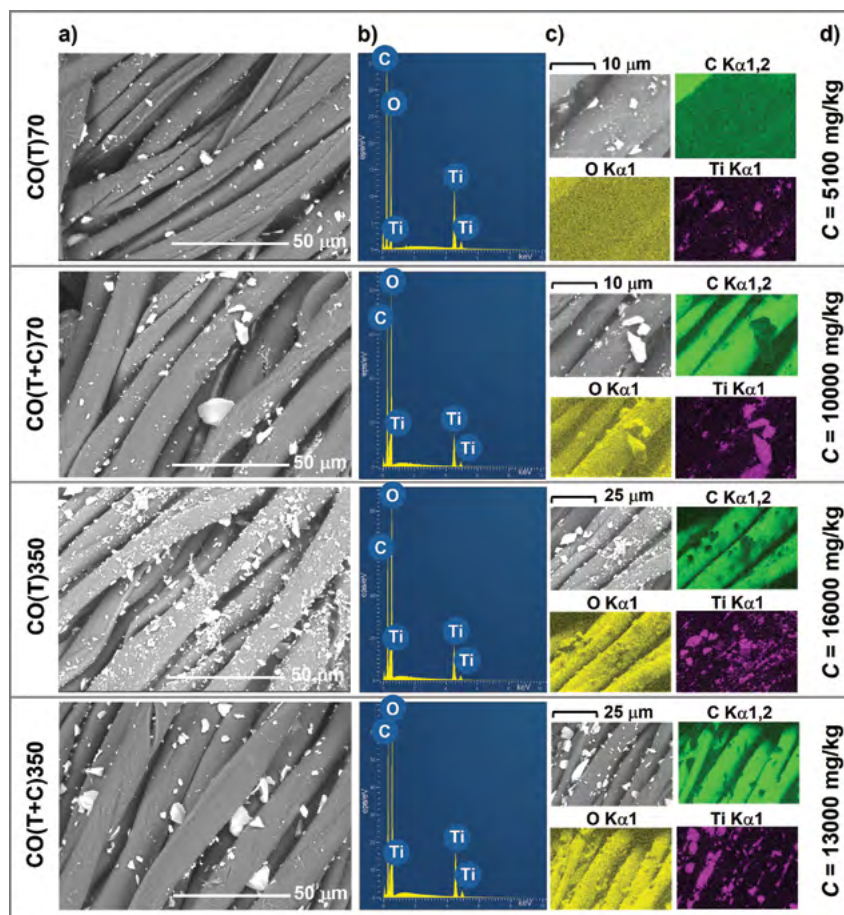


Figure 3: SEM images (a), EDX spectra (b), element mapping images (c) and the TiO_2 concentration determined by ICP-MS (d) of CO(T)70, CO(T+C)70, CO(T)350 and CO(T+C)350 samples

The FTIR spectra of the samples included characteristic absorption bands in the 1500–850 cm^{-1} region, belonging to the cellulose fingerprint [40, 41]. These strong vibrational cellulose bands also blurred the characteristic absorption bands of turmeric in the CO(T+C)70 and CO(T+C)350 samples, appearing in the 1740–1680 cm^{-1} region due to C=O absorption, at 1510 cm^{-1} due to aromatic skeletal stretching vibrations, and at 1030 cm^{-1} due to C–OH

stretching vibration [40, 42–44]. The same observation was noticed in our previous study [48]. The TiO_2 anatase absorption bands in the 400–800 cm^{-1} region characterise the stretching vibration modes of different Ti–O bonds (Ti–O–Ti, Ti–O–O, O–Ti–O) (Ti–O–Ti, Ti–O–O, O–Ti–O) [45–47], and could only be observed for the CO(T)350 sample with the highest TiO_2 NP load (see insert in Figure 4).

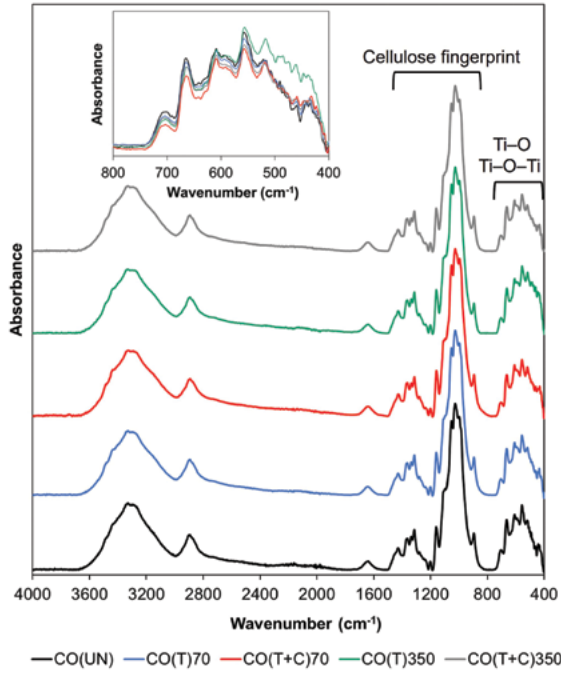


Figure 4: IR ATR spectra of untreated CO(UN) sample and chemically modified CO(T)70, CO(T+C)70, CO(T)350 and CO(T+C)350 samples

The presence of (T)70, (T+C)70, (T)350 and (T+C)350 in the CO samples significantly reduced the transmission of UV radiation through the CO fabric (Figure 5a) owing to increased UV radiation absorption (Figure 5b). The Tauc plots obtained from the absorption spectra (Figure 5c) show that TiO_2 calcination at 350 °C caused a bathochromic shift in the light absorption of TiO_2 , as expected, since the value of E_g decreased from 3.41 for CO(T)70 to 3.18 for CO(T)350 (Figure 5d). The presence of curcumin in the TiO_2 composites also slightly decreased the E_g values of the CO(T+C)70 and CO(T+C)350 samples compared with the CO(T)70 and CO(T)350 samples. However, E_g values of 3.30 and 3.16 eV for the CO(T+C)70 and CO(T+C)350 samples correspond to the absorbance values at 376 and 393 nm, respectively, lower than that of visible light. This indicates that despite the bathochromic shift in light absorption, the photocatalytic activity of the samples was mainly driven by UV light.

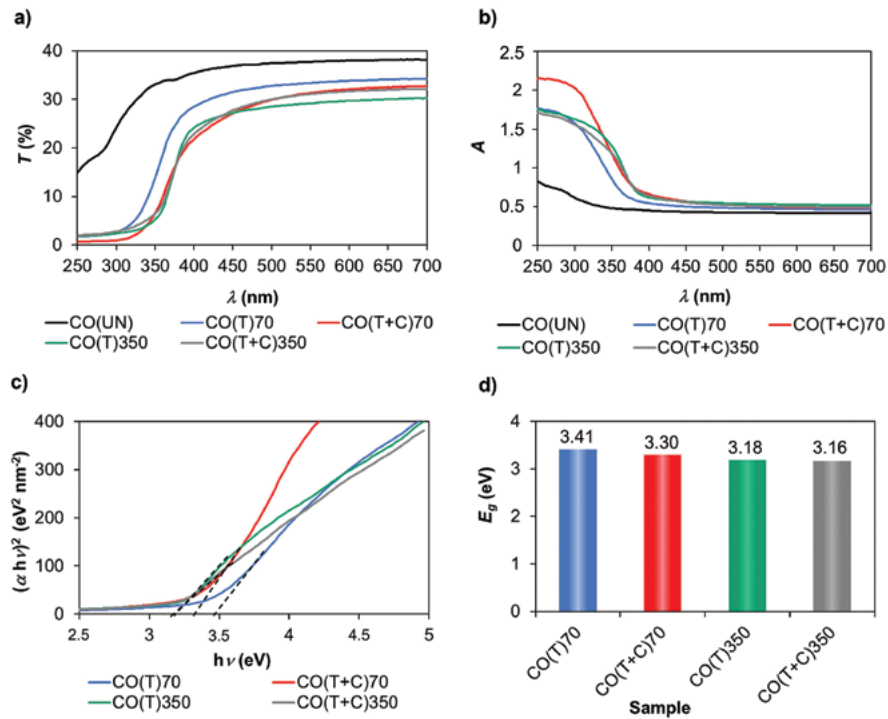


Figure 5: Transmission (a) and absorption (b) spectra of untreated CO(UN) and chemically modified CO(T)70, CO(T+C)70, CO(T)350 and CO(T+C)350 samples; Tauc plots (c) and band gap energy, E_g (d), of CO(T)70, CO(T+C)70, CO(T)350 and CO(T+C)350 samples

3.2 Functional properties

Since TiO_2 has established itself as an effective UV absorber, the UV protection properties of the chemically modified CO samples were determined using the transmission spectra in the 280–400 nm range (Figure 5a). Cotton alone does not offer sufficient protection against UV radiation, which is reflected in a very low UPF value (Table 3). All the chemically modified CO samples retained a higher UVA and UVB blocking effect, increasing the UPF values. Accordingly, the CO(T)70 and CO(T+C)350 samples

have minimal UV protection, CO(T)350 has good UV protection and CO(T+C)70 has excellent UV protection. The results also show that increased TiO_2 concentration from 5100 mg/kg for the CO(T)70 sample to 16000 mg/kg for the CO(T)350 sample increased the UPF value from 22.2 to 32.1. These results were expected, as according to our previous studies, both amorphous and crystalline TiO_2 exhibit UV protection properties that do not exceed UPF values of 35 irrespective of the application procedure or concentration [48, 49].

Table 3: UVA and UVB blocking, ultraviolet protection factor (UPF) and the protection categories for the untreated and chemically modified cotton samples

Sample code	UVA blocking (%)	UVB blocking (%)	UPF	Protection category ^{a)}
CO(UN)	67.1	75.4	3.7	I
CO(T)70	83.0	97.2	22.2	M
CO(T+C)70	89.6	99.0	51.6	E
CO(T)350	89.5	97.6	32.1	G
CO(T+C)350	89.1	97.2	27.3	M

^{a)} I – insufficient, M – minimum protection, G – good protection, E – excellent protection

The excellent UV protection factor of the CO(T+C)70 sample with a significantly lower TiO_2 amount than in the CO(T)350 sample was a surprise, as we had found that the curcumin dye alone at the concentration used in our experiment could not provide UV protection for the CO sample with a UPF of 8.75 [48]. The UV protection properties of CO(T+C)70 sample were also higher than those of the CO(T+C)350 sample, which contained TiO_2 in the (T+C) composite in an even higher concentration. However, the absorption spectra (Figure 5b) show that the absorption in the UVB range was significantly higher for the CO(T+C)70 sample than the other samples, blocking 99.0% of UVB radiation, giving a UPF of 51.6 (Table 3). These results indicate that the synergistic effect of TiO_2 and curcumin is undoubtedly achieved in the (T+C)70 composite, which is not the case for the (T+C)350 composite.

The photocatalytic self-cleaning performance of the chemically modified CO samples degraded the coffee stain, which faded and changed colour when

illuminated (Figure 6a, b). The results show that the CO(UN) sample had no self-cleaning properties, as the colour of the coffee stain did not fade during illumination but instead became slightly darker (Figure 6b). The colour difference between the non-illuminated CO(T+C)70 and CO(T+C)350 samples stained with coffee and the same stained samples illuminated for 4 and 24 hours was greater than that between the CO(T)70 and CO(T)350 samples, suggesting that the curcumin in the (T+C) composites enhanced the photocatalytic self-cleaning activity of the samples. When the colour coordinates of the chemically modified samples were examined after 24 h of illumination, it was found that the colour of the coffee stain became lighter, greener and bluer than the non-illuminated samples. A comparison of the CO(T+C)70 and CO(T+C)350 samples also shows that the photocatalytic self-cleaning performance of the CO(T+C)70 sample was much more effective than that of the CO(T+C)350 sample, with the greatest differences in the values of ΔE_{ab}^* and the colour

coordinates ΔL^* , Δa^* and Δb^* between the non-illuminated and the coffee stained samples illuminated for 24 hours.

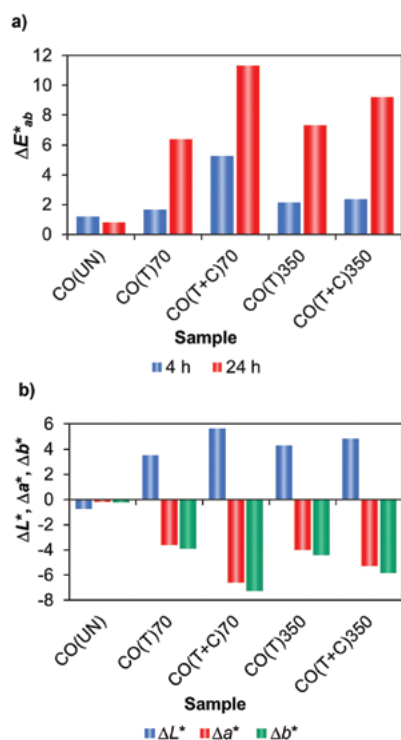


Figure 6: Colour difference, ΔE^*_{ab} , between the unilluminated samples stained by coffee and the stained samples illuminated for 4 and 24 hours (a); difference in colour coordinates, ΔL^* , Δa^* and Δb^* , between the unilluminated samples stained by coffee and the stained samples illuminated for 24 hours (b)

The results for the photocatalytic degradation of the MB and RhB dye solutions show that the photocatalytic degradation efficiency of the investigated dyes was influenced not only by the chemical modification of the CO samples but also by the chemical structure of the dyes (Figure 7 a–e). It should be emphasised that higher dye degradation is associated with a lower C_i/C_0 ratio at a given illumination time. In the case of the MB dye, all tested CO samples showed very similar dye decolourisation kinetics, regardless of their chemical modification (Figure 7a, b). It is also evident that the photostability of the MB dye is very low, as it degraded under illumination

even without photocatalytically active CO samples (blank curve in Figure 7a).

When the MB dye was replaced by the RhB dye with significantly higher photostability (blank curve in Figure 7c), the photocatalytic efficiency of the analysed CO samples differed considerably (Figure 7c, d). As expected, the CO(UN) sample showed no photocatalytic activity, but the chemically modified CO samples decolourised the RhB dye solution with the following increased photocatalytic efficiency: $\text{CO(T)70} < \text{CO(T)350} < \text{CO(T+C)350} < \text{CO(T+C)70}$. Accordingly, the curcumin in the TiO_2 composite undoubtedly increased the rate of photocatalytic dye degradation. However, the rate of dye decolourisation in the CO(T+C)70 sample was significantly higher than in the CO(T+C)350 sample, which can be seen in the digital images of the cuvettes filled with RhB solution after 180 minutes of illumination (Figure 7e). This also confirms the findings from the literature [50] that the RhB dye exhibits a strong sensitivity to photocatalytic decolourisation, even with visible light.

To determine the reusability of the photocatalytic performance, one of the most important properties from a technological point of view, the chemically modified CO samples were tested in four consecutive 180-minute cycles of RhB dye solution photodegradation. After each cycle, the degree of dye decolourisation was determined (Figure 7f). The results show that the combination of curcumin and TiO_2 again improved the reusability of the tested CO samples, with the highest photostability achieved for the CO(T+C)70 sample, resulting in 98% decolourisation for the RhB dye after the fourth cycle.

The low photocatalytic activity of the CO(T+C)350 sample compared with the CO(T+C)70 sample was somewhat surprising, as according to the literature, nanocrystalline TiO_2 has higher photocatalytic activity than amorphous TiO_2 [4]. This phenomenon was also confirmed by the higher photocatalytic activity of the CO(T)350 samples compared to the CO(T)70 sample. Therefore, the FTIR spectra of the powder samples were analysed to

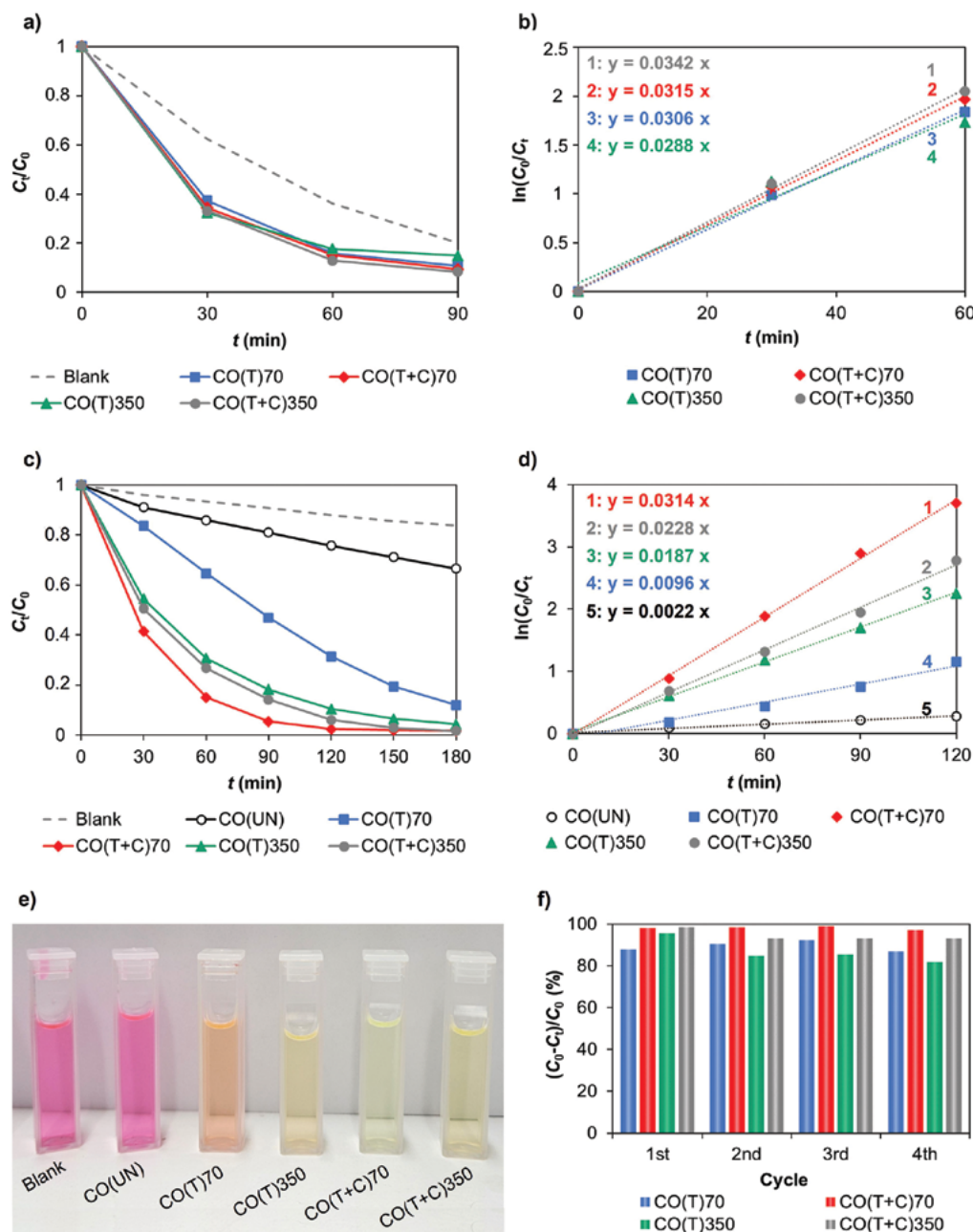


Figure 7: Photocatalytic degradation of MB dye solution without and in the presence of CO samples after different illumination times, t (a); photodegradation kinetics of MB dye solution in the presence of chemically modified CO samples (b); photocatalytic degradation of RhB dye solution without (blank) and in the presence of CO samples after a different illumination time, t (c); photodegradation kinetics of RhB dye solution in the presence of CO samples (d); digital images of cuvettes filled with RhB solution after 180 minutes of illumination without and in the presence of CO samples (e); consecutive 180 min cycles of RhB dye solution photodegradation in the presence of chemically modified CO samples (f)

clarify the chemical changes between the composites (Figure 8). The results show that the (T+C)70 powder sample exhibited characteristic curcumin bands at 1597 cm^{-1} and 1509 cm^{-1} owing to C=C stretching vibrations in the conjugated aromatic system of the curcumin and at 900 cm^{-1} owing to the out-of-plane bending vibrations of aromatic C–H bonds [42–44]. These bending vibrations were not clearly visible in the (T+C)350 powder sample. Furthermore, an additional band in the (T+C)350 powder sample at 1230 cm^{-1} —corresponding to aromatic C–H bending in smaller aromatic fragments such as vanillin or ferulic acid [51]—suggests that the curcumin was partially thermally degraded during the calcination of the composite at 350°C , which was also accompanied by a slight lightening of the composite colour. This could be why only an additive effect between curcumin and TiO_2 in the (T+C)350 composite was achieved, in contrast to the synergistic effect of the two components in the (T+C)70 composite.

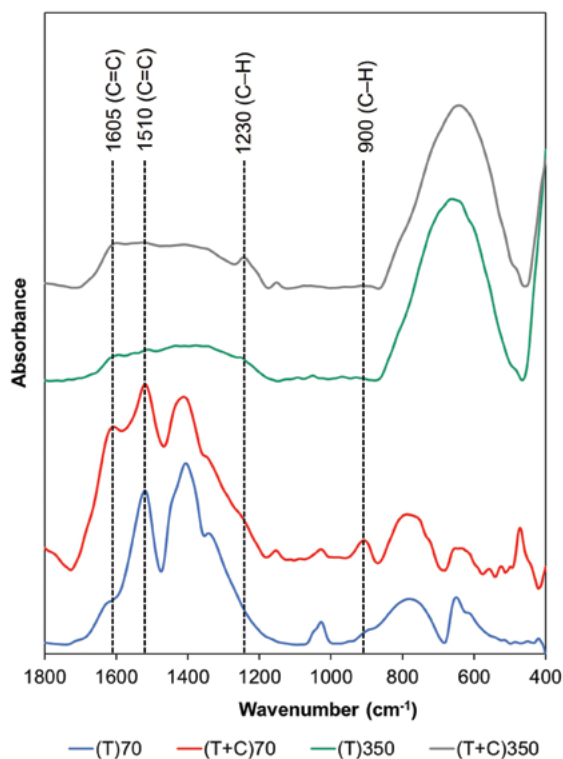


Figure 8: IR ATR spectra of the (T)70, (T+C)70, (T)350 and (T+C)350 powder samples.

4 Conclusion

To summarise, novel multifunctional hybrid CO/TiO_2 /curcumin composites with UV protection and photocatalytic self-cleaning performance were successfully prepared according to the principles of green chemistry. XRD analysis showed that the TiO_2 in the powdered (T)350 and (T+C)350 samples was present in the polymorphic anatase phase, while the TiO_2 in the powdered (T)70 sample was amorphous. Curcumin in the (T+C)70 sample significantly promoted the crystallisation of TiO_2 , partially converting the amorphous phase into the anatase phase. The crystallite size of the (T)350, (T+C)350 and (T+C)70 powdered samples was less than 13 nm. However, SEM analysis revealed that applying all the powdered samples to the CO fabric resulted in the formation of smaller and larger agglomerates. Increasing the synthesis temperature from 70 to 350°C and introducing curcumin into the (T+C) composites decreased the E_g values and consequently shifted the absorbance to longer wavelengths. Since the latter did not exceed 400 nm in any sample, it is reasonable to assume that all samples mainly absorb UV light.

The absorption in the UVA and UVB range showed minimal UV protection for the $\text{CO}(\text{T})70$ and $\text{CO}(\text{T+C})350$ samples with UPF values of 22.2 and 27.3, respectively; good UV protection for the $\text{CO}(\text{T})350$ sample with a UPF value of 32.1; and excellent UV protection for the $\text{CO}(\text{T+C})70$ sample with a UPF value of 51.6. Regarding the UPF values, TiO_2 and curcumin had a synergistic effect in the $\text{CO}(\text{T+C})70$ sample, as the UV-blocking effect was more efficient than the additive effect of the $\text{CO}(\text{T})70$ sample and the CO sample coloured only with curcumin at the same concentration.

The analysis of photocatalytic self-cleaning performance based on the degradation rate of coffee stains showed that all chemically modified CO samples caused colour fading, with the highest efficiency obtained for the $\text{CO}(\text{T+C})70$ sample. This showed the largest differences in ΔE^* values between the

non-illuminated and the 24-hour illuminated coffee-stained samples. Examining the photocatalytic degradation of the RhB dye solutions in the presence of the chemically modified CO samples revealed that the CO(T+C)70 sample was the most efficient, followed by the CO(T+C)350 and CO(T)350 samples, and that the lowest efficiency was obtained for the CO(T)70 sample. This confirms that the presence of curcumin in a composite with TiO₂ significantly increases photocatalytic activity, which also applies to the reusability of samples. The low photocatalytic activity of the CO(T+C)350 sample compared with the CO(T+C)70 sample was attributed to the partial thermal degradation of curcumin during the calcination of the (T+C)350 composite at 350 °C, which was confirmed by FTIR analysis.

Summarising the aspects of its composite production and functional properties, the CO(T+C)70 sample can be classified as a green textile-based composite produced via a low-temperature TiO₂ synthesis process in the presence of curcumin, exhibiting excellent multifunctional UV-blocking and recyclable photocatalytic performance. This composite has great application potential in areas such as protective and outdoor textiles, water purification systems, automotive and interior textiles, reusable food packaging.

Author contributions: Brigita Tomšič – conceptualization, methodology, investigation, validation, supervision, review and editing; Maja Blagojevič, Nuša Klančar, Erik Makoter, Klara Močenik, Nika Pirš, Sebastijan Šmid, Marija Veskova – investigation, visualization, writing, review and editing; Marija Gorjanc and Mateja Kert – conceptualization, methodology, review and editing; Barbara Simončič – conceptualization, methodology, validation, writing original draft, resources and supervision.

Conflict of interest disclosure: The authors have no relevant financial or non-financial interests to disclose.

Acknowledgments

This research was carried out within the framework of the courses on Advanced Finishing Processes and Chemical Functionalisation of Textiles in the Master Study Programme for Textile and Clothing Planning. The research was co-funded by the Slovenian Research and Innovation Agency (Programme P2-0213 Textiles and Ecology, Infrastructural Centre RIC UL-NTF). The authors would like to thank prof. dr. Matej Dolenc for the support in the XPS analysis and prof. dr. Aleš Nagode for the support in the EDS analysis.

References

1. HUMAYUN, M., RAZIQ, F., KHAN, A., LUO, W. Modification strategies of TiO₂ for potential applications in photocatalysis: a critical review. *Green Chemistry Letters and Reviews*, 2018, **11**(2), 86–102, doi: 10.1080/17518253.2018.1440324.
2. NAM, Y., LIM, J.H., KO, K.C., LEE, J.Y. Photocatalytic activity of TiO₂ nanoparticles: a theoretical aspect. *Journal of Materials Chemistry A*, 2019, **7**(23), 13833–13859, doi: 10.1039/C9TA03385H.
3. NOMAN, M.T., ASHRAF, M.A., ALI, A. Synthesis and applications of nano-TiO₂: a review. *Environmental Science and Pollution Research*, 2019, **26**, 3262–3291, doi: 10.1007/s11356-018-3884-z.
4. RASHID, M.M., SIMONČIČ, B., TOMŠIČ, B. Recent advances in TiO₂-functionalized textile surfaces. *Surfaces and Interfaces*, 2021, **22**, 1–33, doi: 10.1016/j.surfin.2020.100890.
5. ETACHERI, V., DI VALENTIN, C., SCHNEIDER, J., BAHNEMANN, D., PILLAI, S.C. Visible-light activation of TiO₂ photocatalysts: advances in theory and experiments. *Journal of Photochemistry and Photobiology C: Photochemistry Reviews*, 2015, **25**, 1–29, doi: 10.1016/j.jphotochemrev.2015.08.003.
6. GIRISH KUMAR, S., KOTESWARA RAO, K.S.R. Comparison of modification strategies towards enhanced charge carrier separation

- and photocatalytic degradation activity of metal oxide semiconductors (TiO₂, WO₃ and ZnO). *Applied Surface Science*, 2017, **391**, Part B, 124–148, doi: 10.1016/j.apsusc.2016.07.081.
7. GUO, Q., ZHOU, C., MA, Z., YANG, X. Fundamentals of TiO₂ photocatalysis: concepts, mechanisms, and challenges. *Advanced Materials*, 2019, **31**(50), 1–26, doi: 10.1002/adma.201901997.
 8. CARP, O., HUISMAN, C.L., RELLER, A. Photoinduced reactivity of titanium dioxide. *Progress in Solid State Chemistry*, 2004, **32**(1–2), 33–177, doi: 10.1016/j.progsolidstchem.2004.08.001.
 9. RAHIMI, N., PAX, R.A., MacA. GRAY, E. Review of functional titanium oxides. I: TiO₂ and its modifications. *Progress in Solid State Chemistry*, 2016, **44**(3), 86–105, doi: 10.1016/j.progsolidstchem.2016.07.002.
 10. SHEN, R., JIANG, C., XIANG, Q., XIE, J., LI, X. Surface and interface engineering of hierarchical photocatalysts. *Applied Surface Science*, 2019, **471**, 43–87, doi: 10.1016/j.apsusc.2018.11.205.
 11. LI, X., WEI, H., SONG, T., LU, H., WANG, X. A review of the photocatalytic degradation of organic pollutants in water by modified TiO₂. *Water Science & Technology*, 2023, **88**(6), 1495–1507, doi: 10.2166/wst.2023.288.
 12. GONUGUNTLA, S., KAMESH, R., PAL, U., CHATTERJEE, D. Dye sensitization of TiO₂ relevant to photocatalytic hydrogen generation: current research trends and prospects. *Journal of Photochemistry and Photobiology C: Photochemistry Reviews*, 2023, **57**, 1–28, doi: 10.1016/j.jphotochemrev.2023.100621.
 13. TOMAR, N., AGRAWAL, A., DHAKA, S. V., SUROLIA, P.K. Ruthenium complexes based dye-sensitized solar cells: fundamentals and research trends. *Solar Energy*, 2020, **207**, 59–76, doi: 10.1016/j.solener.2020.06.060.
 14. KUSHWAHA, R., SRIVASTAVA, P., BAHADUR, L. Natural pigments from plants used as sensitizers for TiO₂ based dye-sensitized solar cells. *Journal of Energy*, 2013, **2013**(1), 1–8, doi: 10.1155/2013/654953.
 15. JAAFAR, S.N.H., MINGGU, L.J., ARIFIN, K., KASSIM, M.B. WAN, W.R.D. Natural dyes as TiO₂ sensitizers with membranes for photoelectrochemical water splitting: an overview. *Renewable and Sustainable Energy Reviews*, 2017, **78**, 698–709, doi: 10.1016/j.rser.2017.04.118.
 16. DIAZ-URIBE, C., VALLEJO, W., ROMERO, E., VILLAREAL, M., PADILLA, M., HAZBUN, N., MUÑOZ-ACEVEDO, A., SCHOTT, E., ZARATE, X. TiO₂ thin films sensitization with natural dyes extracted from *Bactris guineensis* for photocatalytic applications: experimental and DFT study. *Journal of Saudi Chemical Society*, 2020, **24**(5), 407–416, doi: 10.1016/j.jscs.2020.03.004.
 17. GOULART, S., NIEVES, L.J.J., DAL BÓ, A.G., BERNARDIN, A.M. Sensitization of TiO₂ nanoparticles with natural dyes extracts for photocatalytic activity under visible light. *Dyes and Pigments*, 2020, **182**, 1–6, doi: 10.1016/j.dyepig.2020.108654.
 18. HAGHIGHATZADEH, A. Comparative analysis on optical and photocatalytic properties of chlorophyll/curcumin-sensitized nanoparticles for phenol degradation. *Bulletin of Materials Science*, 2020, **43**, 1–15, doi: 10.1007/s12034-019-2016-9.
 19. VENUMBKA, M.R., AKKALA, N., DURAISAMY, S., SIGAMANI, S., KUMAR POOLA, P., RAO, D.S., MAREPALLY, B.C. Performance of TiO₂, Cu-TiO₂, and N-TiO₂ nanoparticles sensitization with natural dyes for dye-sensitized solar cells. *Materials Today: Proceedings*, 2022, **49**(7), 2747–2751, doi: 10.1016/j.matpr.2021.09.281.
 20. RAHMAWATI, T. Green synthesis of Ag-TiO₂ nanoparticles using turmeric extract and its enhanced photocatalytic activity under visible light. *Colloids and Surfaces A: Physicochemical and Engineering Aspects*, 2023, **665**, 1–14, doi: 10.1016/j.colsurfa.2023.131206.
 21. PRIYADARSINI, K.I. The chemistry of curcumin: from extraction to therapeutic agent. *Molecules*, 2014, **19**(12), 20091–20112, doi: 10.3390/molecules191220091.

22. ABD EL-HADY, M.M., FAROUK, A., SAEED, S.E.-S., ZAGHLOUL, S. Antibacterial and UV protection properties of modified cotton fabric using a curcumin/TiO₂ nanocomposite for medical textile applications. *Polymers*, 2021, **13**(22), 1–14, doi: 10.3390/polym13224027.
23. FULORIA, S., MEHTA, J., CHANDEL, A., SEKAR, M., RANI, N.N.I. M, BEGUM, M. Y., SUBRAMANIYAN, V., CHIDAMBARAM, K., THANGAVELU, L., NORDIN, R., WU, Y.S., SATHASIVAM, K.V., LUM, P.T., MEENAKSHI, D.U., KUMARASAMY, V., AZAD, A.K., FULORIA, N.K. A comprehensive review on the therapeutic potential of *Curcuma longa* Linn. in relation to its major active constituent curcumin. *Frontiers in Pharmacology*, 2022, **13**, 1–27, doi: 10.3389/fphar.2022.820806.
24. UROŠEVIĆ, M., NIKOLIĆ, L., GAJIĆ, I., NIKOLIĆ, V., DINIĆ, A., MILJKOVIĆ, V. Curcumin: biological activities and modern pharmaceutical forms. *Antibiotics*, 2022, **11**(2), 1–27, doi: 10.3390/antibiotics11020135.
25. JIKAH, A.N., EDO, G.I. Turmeric (*Curcuma longa*): an insight into its food applications, phytochemistry and pharmacological properties. *Vegetos (An International Journal of Plant Research & Biotechnology)*, 2024, in press, doi: 10.1007/s42535-024-01038-4.
26. PALASKAR, S.S., KALE, R.D., DESHMUKH, R.R. Application of natural yellow (curcumin) dye on silk to impart multifunctional finishing and validation of dyeing process using BBD model. *Color Research & Application*, 2021, **46**(6), 1301–1312, doi: 10.1002/col.22678.
27. SCHMIDT, M., BIERHALZ, A.C.K., DE AGUIAR, C.R.L. Adsorption, kinetic, and thermodynamic studies of natural curcumin dye on cotton and polyamide fabric and the liberation of its active principle. *The Canadian Journal of Chemical Engineering*, 2024, **102**(10), 1–13, doi: 10.1002/cjce.25277.
28. ABOU-GAMRA, Z.M., AHMED, M.A. Synthesis of mesoporous TiO₂-curcumin nanoparticles for photocatalytic degradation of methylene blue dye. *Journal of Photochemistry and Photobiology, B: Biology*, 2016, **160**, 134–141, doi: 10.1016/j.jphotobiol.2016.03.054.
29. BOKUNIAEVA, A.O., VOROKH, A.S. Estimation of particle size using the Debye equation and the Scherrer formula for polyphasic TiO₂ powder. *Journal of Physics: Conference Series*, 2019, **1410**, 1–7, doi: 10.1088/1742-6596/1410/1/012057.
30. REDDY, K.M., MANORAMA, S.V., REDDY, A.R. Bandgap studies on anatase titanium dioxide nanoparticles. *Materials Chemistry and Physics*, 2003, **78**, 239–245.
31. KARKARE, M.M. The Direct transition and not Indirect transition, is more favourable for Band Gap calculation of Anatase TiO₂ nanoparticles. *International Journal of Scientific & Engineering Research*, 2015, **6**(12), 48–53.
32. SIST EN 13758-1:2002. Textiles - Solar UV protective properties - Part 1: Method of test for apparel fabrics. Geneva : International Organization for Standardization, 12 p.
33. BERGER-SCHUNN, A. Practical color measurement: a primer for the beginner, a reminder for the expert. New York : Wiley, 1994, p. 39.
34. SHAFIQUE, M., MAHR, M.S., YASEEN, M., BHATTI, H.N. CQD/TiO₂ nanocomposite photocatalyst for efficient visible light-driven purification of wastewater containing methyl orange dye. *Materials Chemistry and Physics*, 2022, **278**, 1–14, doi: 10.1016/j.matchemphys.2021.125583.
35. WU, F., LI, X., WANG, Z., GUO, H., WU, L., XIONG, X., WANG, X. A novel method to synthesize anatase TiO₂ nanowires as an anode material for lithium-ion batteries. *Journal of Alloys and Compounds*, 2011, **509**(8), 3711–3715, doi: 10.1016/j.jallcom.2010.12.182.
36. DING, L., YANG, S., LIANG, Z., QIAN, X., CHEN, X., CUI, H., TIAN, J. TiO₂ nanobelts with anatase/rutile heterophase junctions for highly efficient photocatalytic overall water splitting. *Journal of Colloid and Interface Science*, 2020, **567**, 181–189, doi: 10.1016/j.jcis.2020.02.014.

37. TORO, R.G., DIAB, M., DE CARO, T., AL-SHEMY, M., ADEL, A., CASCHERA, D. Study of the effect of titanium dioxide hydrosol on the photocatalytic and mechanical properties of paper sheets. *Materials*, 2020, **13**(6), 1–19, doi: 10.3390/ma13061326.
38. ZHAO, H., KWAK, J.H., ZHANG, Z.C., BROWN, H.M., AREY, B.W., HOLLADAY, J.E. Studying cellulose fiber structure by SEM, XRD, NMR and acid hydrolysis. *Carbohydrate Polymers*, 2007, **68**(2), 235–241, doi: 10.1016/j.carbpol.2006.12.013.
39. AHMAD, M.M., MUSHTAQ, S., AL QAHTANI, H.S., SEDKY, A., ALAM, M.W. Investigation of TiO₂ nanoparticles synthesized by sol-gel method for effectual photodegradation, oxidation and reduction reaction. *Crystals*, 2021, **11**(12), 1–16, doi: 10.3390/cryst11121456.
40. SOCRATES, G. *Infrared and Raman Characteristic Group Frequencies: Tables and Charts*. 3rd edition. New York : Wiley, 2004.
41. TOMŠIČ, B., SIMONČIČ, B., VINCE, J., OREL, B., VILČNIK, A., FIR, M., ŠURCA VUK, A., JOVANOVSKE, V. The use of ATR IR spectroscopy in the study of structural changes of the cellulose fibres. *Tekstilec*, 2007, **50**(1–3), 3–15.
42. ROHMAN, A., DEVI, S., RAMADHANI, D., NUGROHO, A. Analysis of curcumin in *Curcuma longa* and *Curcuma xanthorrhiza* using FTIR spectroscopy and chemometrics. *Research Journal of Medicinal Plant*, 2015, **9**(4), 179–186, doi: 10.3923/RJMP.2015.179.186.
43. SHARMA, S., DHALSAMANT, K., TRIPATHY, P.P., MANEPALLY, R.K. Quality analysis and drying characteristics of turmeric (*Curcuma longa* L.) dried by hot air and direct solar dryers. *LWT*, 2021, **138**, 1–10, doi: 10.1016/j.lwt.2020.110687.
44. BALLESTEROS, J.I., LIM, L.H.V., LAMORENA, R.B. The feasibility of using ATR-FTIR spectroscopy combined with one-class support vector machine in screening turmeric powders. *Vibrational Spectroscopy*, 2024, **130**, 1–7, doi: 10.1016/j.vibspec.2023.103646.
45. LEÓN, A., REUQUEN, P., GARÍN, C., SEGURA, R., VARGAS, P., ZAPATA, P., ORIHUELA, P.A. FTIR and raman characterization of TiO₂ nanoparticles coated with polyethylene glycol as carrier for 2-methoxyestradiol. *Applied Sciences*, 2017, **7**(1), 1–9, doi: 10.3390/app7010049.
46. RASHID, M.M., ZORC, M., SIMONČIČ, B., JERMAN, I., TOMŠIČ, B. In-situ functionalization of cotton fabric by TiO₂: the influence of application routes. *Catalysts*, 2022, **12**(11), 1–17, doi: 10.3390/catal12111330.
47. GUETNI, I., BELAICHE, M., FERDI, C.A., OULHAKEM, O., ALAOUI, K.B., ZAOUI, F., BAHJIJE, L. Novel modified nanophotocatalysts of TiO₂ nanoparticles and TiO₂/Alginate beads with lanthanides [La, Sm, Y] to degrade the Azo dye Orange G under UV-VIS radiation. *Materials Science in Semiconductor Processing*, 2024, **174**, 1–19, doi: 10.1016/j.mssp.2024.108193.
48. TOMŠIČ, B., SAVNIK, N., SHAPKOVA, E., CIMPERMAN, L., ŠOBA, L., GORJANC, M., SIMONČIČ, B. Green in-situ synthesis of TiO₂ in combination with *Curcuma longa* for the tailoring of multifunctional cotton fabric. *Tekstilec*, 2023, **66**(4), 321–338, doi: 10.14502/tekstilec.66.2023075.
49. IVANUŠA, M., KUMER, B., PETROVČIČ, E., ŠTULAR, D., ZORC, M., JERMAN, I., GORJANC, M., TOMŠIČ, B., SIMONČIČ, B. Eco-friendly approach to produce durable multifunctional cotton fibres using TiO₂, ZnO and Ag NPs. *Nanomaterials*, 2022, **12**(8), 1–21, doi: 10.3390/nano12183140.
50. BÖTTCHER, H., MAHLTIG, B., SARSOOR, J., STEGMAIER, T. Qualitative investigations of the photocatalytic dye destruction by TiO₂-coated polyester fabrics. *Journal of Sol-Gel Science and Technology*, 2010, **55**, 177–185, doi: 10.1007/s10971-010-2230-9.
51. CHUMROENPHAT, T., SOMBOONWATTHANAKUL, I., SAENSOUK, S., SIRIAMORN-PUN, S. Changes in curcuminoids and chemical components of turmeric (*Curcuma Longa* L.) under freeze-drying and low-temperature drying methods. *Food Chemistry*, 2021, **339**, 1–9, doi: 10.1016/j.foodchem.2020.128121.

SHORT INSTRUCTIONS FOR AUTHORS OF SCIENTIFIC ARTICLES

Scientific articles categories:

- **Original scientific article** is the first publication of original research results in such a form that the research can be repeated and conclusions verified. Scientific information must be demonstrated in such a way that the results are obtained with the same accuracy or within the limits of experimental errors as stated by the author, and that the accuracy of analyses the results are based on can be verified. An original scientific article is designed according to the IMRAD scheme (Introduction, Methods, Results and Discussion) for experimental research or in a descriptive way for descriptive scientific fields, where observations are given in a simple chronological order.
- **Review article** presents an overview of most recent works in a specific field with the purpose of summarizing, analysing, evaluating or synthesizing information that has already been published. This type of article brings new syntheses, new ideas and theories, and even new scientific examples. No scheme is prescribed for review article.
- **Short scientific article** is original scientific article where some elements of the IMRAD scheme have been omitted. It is a short report about finished original scientific work or work which is still in progress. Letters to the editor of scientific journals and short scientific notes are included in this category as well.

Language: The manuscript of submitted articles should be written in UK English or in Slovene with bilingual Figures and Tables. The authors responsibility to ensure the quality of the language.

Manuscript length: The manuscript should not exceed 30,000 characters without spacing.

Article submission: The texts should be submitted only in their electronic form in the *.doc (or *.docx) and *.pdf formats, where for each author must be given:

- first name and family name
- title
- full institution address
- ORCID ID
- e-mail.

The name of the document should contain the date (year-month-day) and the surname of the corresponding author, e.g. 20140125Novak.docx. The manuscripts proposed for a review need to have their figures and tables included in the text.

Detailed information on the preparation and submission of the manuscript is available on the website:
<https://journals.uni-lj.si/tekstilec/about/submissions>.

Reviewer suggestions

Authors can suggest potential reviewers. Please provide their titles, ORCID IDs, institutions, and e-mail addresses. The proposed referees should not be current collaborators of the co-authors nor should they have published with any of the co-authors of the manuscript within the last three years. The proposed reviewers should be from institutions other than the authors.

Authors may also provide the names of potential reviewers they wish to exclude from reviewing their manuscript during the initial submission process.

Peer-review process

All submitted articles are professionally, terminologically and editorially reviewed in accordance with the general professional and journalistic standards of the journal Tekstilec. All articles are double-blind reviewed by two or more reviewers independent of editorial board.

The review process takes a minimum of two weeks and a maximum of one month. The reviewers' comments are sent to authors for them to complete and correct their manuscripts. If there is no consensus among the reviewers, the editorial board decides on the further procedure. We accept the articles for publication based on a positive decision.

Copyright corrections

The editors are going to send computer printouts for proofreading and correcting. It is the author's responsibility to proofread the article and send corrections as soon as possible. However, no greater changes or amendments to the text are allowed at this point.

Colour print of hard copies

Colour print is performed only when this is necessary from the viewpoint of information comprehension, and upon agreement with the author and the editorial board.

Copyright Notice

Authors who publish with this journal agree to the following terms:

- Authors are confirming that they are the authors of the submitting article, which will be published (print and online) in journal Tekstilec by University of Ljubljana Press / Faculty of Natural Sciences and Engineering, University of Ljubljana, Aškerčeva 12, SI-1000 Ljubljana, Slovenia).
- Author's name will be evident in the article in journal. All decisions regarding layout and distribution of the work are in hands of the publisher.
- Authors guarantee that the work is their own original creation and does not infringe any statutory or common-law copyright or any proprietary right of any third party. In case of claims by third parties, authors commit their self to defend the interests of the publisher, and shall cover any potential costs.
- Authors retain copyright and grant the journal right of first publication with the work simultaneously licensed under a Creative Commons Attribution CC BY 4.0 that allows others to share the work with an acknowledgement of the work's authorship and initial publication in this journal.
- Authors are able to enter into separate, additional contractual arrangements for the non-exclusive distribution of the journal's published version of the work (e.g. post it to an institutional repository or publish it in a book), with an acknowledgement of its initial publication in this journal.
- Authors are permitted and encouraged to post their work online (e.g., in institutional repositories or on their website) prior to and during the submission process, as it can lead to productive exchanges, as well as earlier and greater citation of published work.

Privacy Statement

The personal data entered in this journal site, like names and addresses, will be used exclusively for the stated purposes of this journal and will not be made available for any other purpose or to any other party.

